UNIVERSITI TEKNOLOGI MARA

FABRICATION AND CHARACTERIZATION OF THE HYBRID COMPOSITES OF TIN (SN)-POLYDIMETHYLSILOXANE (PDMS) AGAINST GAMMA RAYS

HANISAH BINTI ZAINAL ABIDIN

MSc

March 2026

UNIVERSITI TEKNOLOGI MARA

FABRICATION AND CHARACTERIZATION OF THE HYBRID COMPOSITES OF TIN (SN)-POLYDIMETHYLSILOXANE (PDMS) AGAINST GAMMA RAYS

HANISAH BINTI ZAINAL ABIDIN

Thesis submitted in fulfilment
of the requirements for the degree of
Master of Science
(Applied Physics)

Faculty of Applied Sciences

March 2026

CONFIRMATION BY PANEL OF EXAMINERS

I certify that a Panel of Examiners has met on 22 December 2025 to conduct the final examination of Hanisah Binti Zainal Abidin on her Masters of Science thesis entitled "Fabrication and Characterization of the Hybrid Composites of Tin (Sn)-Polydimethylsiloxane (PDMS) Against Gamma Rays" in accordance with Universiti Teknologi MARA Act 1976 (Akta 173). The Panel of Examiner recommends that the student be awarded the relevant degree. The Panel of Examiners was as follows:

Hedzlin Zainuddin, PhD
Associate Professor
Faculty of Applied Sciences
Universiti Teknologi MARA
(Chairman)

Mohamad Azhar Mohd Noor, PhD
Senior Lecturer
Faculty of Health Sciences
Universiti Teknologi MARA
(Internal Examiner)

Mohd Idzat Idris, PhD
Associate Professor
Faculty of Science and Technology
Universiti Kebangsaan Malaysia (UKM)
(External Examiner)

PROFESSOR DR HJH ZURAEDA IBRAHIM
Dean
Institute of Postgraduates Studies
Universiti Teknologi MARA

Date: 13 March 2026

AUTHOR'S DECLARATION

I declare that the work in this thesis was carried out in accordance with the regulations of Universiti Teknologi MARA. It is original and is the results of my own work, unless otherwise indicated or acknowledged as referenced work. This thesis has not been submitted to any other academic institution or non-academic institution for any degree or qualification.

I, hereby, acknowledge that I have been supplied with the Academic Rules and Regulations for Post Graduate, Universiti Teknologi MARA, regulating the conduct of my study and research.

Name of Student	Hanisah Binti Zainal Abidin
Student ID. No.	2023650308
Programme	Master of Science (Applied Physics) - AS760
Faculty	Applied Sciences
Thesis Title	Fabrication and characterization of the hybrid composites of tin (Sn)-polydimethylsiloxane (PDMS) against gamma rays
Signature of Student	
Date	March 2026

ABSTRACT

Healthcare workers remain at risk of occupational radiation exposure despite strict safety guidelines and the routine use of personal protective equipment (PPE), with cumulative low-dose exposure linked to increased cancer risk. Although lead-based PPE is highly effective for gamma-ray attenuation, its excessive weight, toxicity, ergonomic burden, and environmental hazards limit long-term usability and safety. The development of lightweight, flexible, and non-toxic alternatives to traditional lead-based radiation shielding materials has gained increasing interest, particularly for medical and industrial applications. This study focuses on the fabrication and evaluation of polydimethylsiloxane (PDMS)-based composite materials reinforced with pure tin and copper tin alloy fillers as potential lead-free shielding solutions. The composites were prepared using a mixing method, followed by curing at an optimized temperature of 100℃ to ensure proper solidification and mold removal. Three groups of samples including pure tin (PT), tin alloy (TA), and pure tin mixed with copper tin alloy (PA) were fabricated and characterized. Field Emission Scanning Electron Microscopy (FESEM) revealed that PT samples exhibited uniform dispersion of tin particles with strong adhesion to the PDMS matrix, while TA and PA samples showed less compact distribution and poor matrix bonding, especially with spherical copper particles. X-ray diffraction (XRD) analysis confirmed the presence of crystalline P-Sn in pure tin samples, CueSns in copper tin alloy composites, and an amorphous pattern in the PDMS matrix, reflecting distinct phase formations influenced by metal composition. Fourier Transform Infrared (FTIR) spectroscopy confirmed no new chemical bonds were formed between the PDMS and metallic fillers, indicating purely physical interactions. Gamma-ray spectroscopy was used to measure shielding properties through key parameters such as Mass Attenuation Coefficient (MAC), Linear Attenuation Coefficient (LAC), Half-Value Layer (HVL), Tenth-Value Layer (TVL), Mean Free Path (MFP), and Radiation Protection Efficiency (RPE) across 122.1-1332.5 keV. The PT6 consistently demonstrated superior performance with the highest RPE (86.92%), MAC (0.84 $cm^2 g^1$) and LAC (3.77 cm"^{1}) values and the lowest HVL (0.18 cm), TVL (0.61 cm), and MFP (0.27 cm) values, indicating enhanced gamma-ray attenuation. The PA6 group performed better than TA6, with intermediate values for RPE (68.87%), MAC (0.38 $cm^2 g^1$), LAC (2.08 cm"^{1}), HVL (0.33 cm), TVL (1.10 cm), and MFP (0.48 cm) values suggesting that incorporating pure tin into copper tin alloy-filled composites can improve overall shielding efficiency. Moreover, PT6 and PA6 has lead equivalent of 0.48cmPb and 0.38 cmPb at 356 keV, respectively. In conclusion, PT6 composites show promising potential as sustainable, efficient, and lead-free radiation shielding materials for low energy radiation, meanwhile mixture of metal (PA6) proved to give better radiation attenuation at high energies radiation, offering improved protection while reducing environmental and health concerns associated with traditional materials.

ACKNOWLEDGEMENT

Firstly, I would like to express my utmost gratitude to Allah S.W.T. for granting me the opportunity to embark on this challenging yet rewarding journey of pursuing my master's degree and for giving me the strength, patience, and perseverance to complete it successfully.

My deepest appreciation goes to my supervisor, Dr. Ainorkhilah Mahmood, for her unwavering support, encouragement, and invaluable guidance throughout my master's research. Her expertise and constructive feedback have been instrumental in shaping my academic growth and ensuring the success of this work. I would also like to extend my heartfelt thanks to Puan Nur Maizatul Azra Mukhtar, Assoc. Prof. Dr. Rafidah Zainon and Cik Nor Aimi Abdul Wahab, whose insights and assistance were vital in navigating through the complexities of my research. Their mentorship has been a cornerstone of my j ourney.

I am profoundly grateful to my father, Zainal Abidin Mohammed for his wisdom, encouragement, and prayers, which have been a constant source of strength. His resilience and dedication have inspired me to persevere in the face of challenges. My mother, deserves special recognition for her endless love, sacrifices, and unwavering belief in me. She has been my anchor, providing me with emotional and moral support throughout this journey. To my beloved husband, Ahmad I'zzat Affandie Ishak, I extend my heartfelt thanks for his patience, understanding, and support. His encouragement and unwavering belief in my abilities have been my greatest motivation. I am immensely thankful to Nurul Syafiqah Roslan, my research buddy, for being a constant source of companionship, collaboration, and encouragement throughout this journey. Her dedication and friendship made the challenges of this research more manageable and memorable.

I am deeply grateful to the Minister of High Education (MoHE) for funding my research study through the Fundamental Research Grants Scheme (FRGS), FRGS/1/2023/STG05/UITM/03/3, which made this research possible. My appreciation also goes to the Institute of Postgraduate Studies (TPSis), Universiti Teknologi MARA, for the conference support fund that enabled me to share my research findings with the academic community.

I would like to acknowledge Universiti Kebangsaan Malaysia (UKM) for providing the facilities and expertise necessary for radiation characterization. Additionally, I am thankful to the Pusat Penyelidikan Sains dan Kejuruteraan (SERC), Universiti Sains Malaysia (USM), for the use of their state-of-the-art FESEM-EDX facilities, which were critical for the analysis in my research. I acknowledge Assoc. Prof. Dr. Ahmad Azmin Mohamad from School of Materials and Mineral Resources Engineering for facilitating XRD analysis. Special thanks to Puan Aishah Zarzali Shah and Universiti Putra Malaysia (UPM) for facilitating the FTIR analysis, an essential component of my study. Lastly, I extend my gratitude to UiTM Cawangan Pulau Pinang, where I conducted my experimental research, and to everyone who contributed directly or indirectly to my academic journey. Your support and encouragement have been invaluable in helping me reach this significant milestone.

TABLE OF CONTENTS

LIST OF TABLES

LIST OF FIGURES

LIST OF SYMBOLS

I	Intensity of transmitted gamma radiation after passing through a material.
I_0	Initial intensity of gamma radiation before encountering the material
w_i	Weight fraction of an element or component in the composite
x	Thickness of the shielding material
Z	Atomic number
Z_{eff}	Effective atomic number
μ	Linear attenuation coefficient
μ_m	Mass attenuation coefficient
μ/ρ	Mass attenuation coefficient
ρ	Density of the shielding material/ composites

LIST OF ABBREVIATIONS

Abbreviations

ALARA	As Low As Reasonably Achievable
EDX	Energy Dispersive X-ray Spectroscopy
FESEM	Field Emission Scanning Electron Microscopy
FTIR	Fourier Transform Infrared Spectroscopy
IAEA	International Atomic Energy Agency
ICRP	International Committee on Radiological Protection
PHPS	Perhydropolysiloxane
PPE	Personal Protective Equipment
PDMS	Polydimethylsiloxane
SEM	Scanning Electron Microscopy
INWORKS	The International Nuclear Workers Study

LIST OF NOMENCLATURE

Nomenclatures

HVL	Half Value Layer
LAC	Linear Attenuation Coefficient
MAC	Mass Attenuation Coefficient
MFP	Mean Free Path
RPE	Radiation Protection Efficiency
RSE	Radiation Shielding Efficiency
TVL	Tenth Value Layer

CHAPTER 1
INTRODUCTION

1.1 Research Background

Effective shielding materials are necessary for protecting individuals working in the environment where radiation sources are used, for example, in healthcare, nuclear energy, and aerospace industries [1], [2], [3]. Both beneficial and risky effects on health have been associated with ionizing radiation. On the positive side, ionizing radiation is useful in treating illnesses, particularly when it comes to radiation therapy for cancer. Furthermore, it is known that ionizing radiation can cause oxidative stress and associated health hazards. An increased chance of cancer, organ damage, and other unfavourable outcomes are examples of adverse impacts; the researchers are especially concerned about increasing radiation exposure [1], [2], [3]. Therefore, putting healthcare workers' safety first is crucial by putting policies like exposure control and ongoing monitoring in place.

Lead's absorption characteristics are high due to its atomic number, and density is equally high (ρ = 11.34 g cm^{-3}, Z = 82) [4], [5]. Consequently, lead is commonly used in the medical field to prevent negative effects and is acknowledged for its effectiveness in attenuating gamma radiation. This makes lead a highly effective material for both Personal Protective Equipment (PPE) and radiation shielding. Even though lead is a good radiation attenuator, wearing lead-based PPE has a number of negative impacts, including ergonomic risks and toxicity. Because of the weight of the lead apron, radiation workers have complained of back pain during extended use of the PPE [4], [6], [7].

Besides, lead is a heavy metal that can be harmful to humans, especially with prolonged exposure. Chronic exposure to lead can result in severe health issues such as neurological damage, kidney dysfunction, and developmental problems, particularly in children. This toxicity makes lead a hazardous material to handle and poses health risks not only to workers who are in close contact with lead but also to the general population [6], [8]. Lead is also hazardous to the environment, and when it is disposed of,

dangerous compounds are released that could affect people's health [8]. Improper handling or disposal of lead waste can lead to environmental contamination, which can persist for years, posing long-term risks to both ecosystems and human health [6]. Therefore, current research highlights how crucial it is to investigate substitute metals for radiation shielding or personal protective equipment.

Given these issues, there is an increasing demand for alternative materials that can provide efficient radiation shielding while lowering the health and environmental risks associated with lead. Researchers have studied a variety of materials, with a focus on those that are non-toxic, lightweight, and environmentally benign. There has been a growing interest in materials based on polymers and metals, which provide flexibility, lower weight, and the possibility for increased safety. Tin, a metal with a relatively high atomic number (Z = 50), has been found as a possible replacement for lead. Tin is not only less hazardous but also lighter and more environmentally friendly than lead, making it a desirable material for radiation shielding applications [9]. The polymer has beneficial properties such as inexpensive, lightweight, non-toxic compared to solely used metal and most importantly, it can integrate with metal to make a superior composite in terms of radiation reduction and mechanical strength. Because of the metal in the polymer matrix, this composite structure may efficiently absorb or disperse the incoming intensity despite appearing lighter [10], [11].

One of the most promising alternatives to lead is a tin-polydimethylsiloxane composite material. Polydimethylsiloxane (PDMS) is recognized for its biocompatibility, flexibility, and ease of processing [12], [13], [14]. While PDMS alone may not provide adequate radiation shielding, it becomes a far more efficient material when coupled with metal fillers such as tin. Tin helps to increase radiation absorption in the composite, while PDMS provides a flexible matrix that enables easy moulding and modification to various applications such as microfluidic and nanofluidic systems, biomodels and organ-on-a-chip platforms, blood analogue materials, electronic components, filtration and pervaporation membranes, sensors, optical and thermal devices, surface coatings, and various biomedical and engineering applications [15], [16], [17], [18]. This combination produces a material that is not only lightweight and

non-toxic, but also highly adaptable, making it suitable for various applications, including medical radiation protection, aerospace, and industrial shielding.

In recent years, the metal-polymer composite has gained popularity as an alternative to lead-based shielding materials due to its lightweight nature, non-toxic composition, and moldability of PDMS, which can be easily formed to meet various requirements. Tin may improve the composite's radiation shielding efficacy, allowing it to absorb high-energy radiation including the scattered one. The versatility of PDMS also enables the development of radiation protection items that are more comfortable and easier to use, such as protective clothes or portable shielding devices [15]. Furthermore, the non-toxic nature of both PDMS and tin makes this composite a far safer option, especially in industries where long-term radiation exposure is a concern.

Only a few studies have examined tin mixed with silicone polymers, despite the fact that numerous investigations have examined metal components such as tungsten [19], iron [20], and bismuth [21] with different type of polymers. Therefore, this study investigated the potential of PDMS-tin composites as a radiation shielding material. This study was intended to develop a material that not only provides effective radiation protection but also addresses the health and environmental concerns associated with conventional lead-based shielding materials. It is anticipated that this research helps the development of safer, more sustainable, and efficient radiation shielding materials, providing an alternative to conventional applications of lead in industries that require radiation protection, thus improving patient health and healthcare.

1.2 Motivation for This Work

The motivation to address the increasing demand for innovative materials that can offer efficient radiation shielding. There is an immediate and continuous demand for lightweight, flexible, and effective shielding materials that go beyond conventional, large, and frequently hazardous solutions in a period where radiation exposure is becoming more widespread in industries like healthcare, aerospace, and nuclear energy. This study concentrating on creating a revolutionary tin-PDMS composite since the potential in polymer-metal composites is well recognized. A promising option for safer,

more adaptable radiation shielding, this combination combines the flexibility and biocompatibility of PDMS with the density and radiation-absorbing qualities of tin.

In addition, the need to create safer working conditions for professionals like radiology technicians and healthcare workers who frequently encounter radiation. This research intends to close a significant gap in the supply of workable radiation shielding solutions by developing a material that not only offers potent radiation attenuation but also maintains mechanical flexibility and ease of manufacture. This study thoroughly assesses this composite using analytical methods, including Field Emission Scanning Electron Microscopy (FESEM), Energy Dispersive X-ray Spectroscopy (EDX), X-ray Diffraction (XRD), Fourier Infrared Spectroscopy (FTIR), and radiation testing using gamma ray, making sure it satisfies both functional and protective needs. This study promotes sustainability, safety, and public health in high-risk radiation conditions in addition to being in line with developments in material science.

1.3 Problem Statement

Despite the safety rules of wearing PPE, healthcare workers globally face ongoing risks from occupational radiation exposure during patient care and in radiation procedure such as radiopharmaceutical, nuclear medicine and radiology procedures (Figure 1.1). Stricter guidelines limit annual radiation exposure to protect workers, yet studies in Malawian hospitals for example revealed concerning levels of monthly exposure for radiographers of 0.247 mSv. The cumulative effects raised significant concern, as even low doses of radiation increased the risk of cancer, notably leukaemia [22]. Radiation exposure may reduce overall lifespan, emphasizing the importance of minimizing occupational exposure in healthcare settings. Therefore, PPE made from lead was commonly utilized due to its effectiveness in attenuating gamma rays, thereby reducing diverse effects [23], [24].

Various effects overshadow the utilization of lead as a radiation attenuator in PPE. These include ergonomic issues, such as back pain reported by workers due to the weight of lead aprons during prolonged use [25]. Furthermore, lead poses environmental risks upon disposal, potentially releasing harmful chemicals that pose a

threat to human health [8]. Additionally, extended radiation exposure on cracked PPE, may lead to radiation leaks and expose radiation workers, patients, and the public to unintended radiation exposure [4], [8]. Additionally, high-toxicity lead dust can cause ingestion and inhalation into the respiratory system and cause lung damage or cancer [1]. Hence, recent research, from the last decade, highlighted the critical need to explore alternative metals or fabricating with other materials such as polymer, glass, or ceramic for radiation shielding or PPE [11], [26], [27]. Therefore, this research has been conducted to assess the efficiency of combining tin metal with PDMS polymer in radiation shielding, mechanical properties and suitability as PPE.

According to the researchers, tin was stated to have the ability to attenuate photon rays and polydimethylsiloxane has favorable characteristics in terms of biocompatibility, flexibility, thermal stability, less toxicity, chemical stability, excellent mechanical properties and shielding ability [9], [28]. Thus, the fabrication of tin powder with PDMS polymer is believed to form a composite that not only can attenuate the radiation but also has high flexibility and strength to be a good PPE. To create the composites, the mixing method was applied where the metal was added to the polymer, and the mixing process was performed.

Figure 1.1 a) Lead Aprons Used At X-ray Department and b) Radiation Worker Wearing Lead Aprons for Radiation Protection during Medical Procedure At Gleneagles Hospital Penang

1.4 Research Objective

The main objective is to study the radiation shielding ability of the hybrid structure of tin and polydimethylsiloxane composite. The research was conducted based on the objectives below:

a) To fabricate the hybrid structure of tin and PDMS polymer with a curing agent by using the mixing method.

b) To analyze the structural and chemical properties of tin/PDMS polymer hybrid composites.

c) To evaluate the effect of radiation absorption performance of composite samples against gamma rays.

1.5 Research Question

i) How can tin and PDMS liquid polymer be effectively utilized to fabricate a solidified PDMS-tin composite?

ii) How does the incorporation of tin into the PDMS liquid polymer affect the structural and chemical properties of the solidified PDMS-tin composite?

iii) Which compositions of tin and PDMS will emerge with high radiation attenuating capabilities?

1.6 Hypothesis

1) Tin powder and PDMS liquid can solidify with the addition of a PDMS curing agent.

2) Tin filler disperses physically and uniformly within the polymer matrix and produces a compact structure of composite.

3) As tin compositions increase, the radiation shielding properties may increase.

1.7 Significance of the Study

The research aims to investigate the radiation protection ability of the tin and PDMS composite using various composition ratios to enhance radiation absorption. The goal is to contribute valuable insights into the development of a composite that not only

offers efficient radiation protection but also addresses concerns related to weight, flexibility, and environmental impact. Aligned with the government's health initiatives and the 12th National Strategic Thrust (RMK12), notably under Thrust 2, which focuses on "Improving the well-being of the people" with the overarching objective of achieving Universal Access to Health Care [29]. This study's findings have the potential to make substantial contributions to the welfare and safety of individuals undergoing procedures involving photon rays. By ensuring protection for both radiation workers and patients from unintended radiation exposure, the research outcomes directly support the government's commitment to enhancing the health and well-being of the population.

1.8 Novelty of This Study

A novel combination of tin fillers embedded within a PDMS matrix was investigated in the present study, marking a significant contribution to the field of radiation shielding materials. While previous studies have predominantly focused on PDMS composites reinforced with metal oxide-based fillers such as lead (II) oxide (PbO) [30], tin (IV) oxide ($Sn0_2$) [9], zinc oxide (ZnO) [31], and bismuth (III) oxide (Bi_20_3) [32], there remains a notable gap in the literature regarding the utilization of metallic tin and copper-tin alloy as functional fillers. The incorporation of these novel metallic fillers not only offers a promising lead-free alternative for X-ray and gamma-ray shielding applications but also has a potentially enhanced attenuation performance, which may be attributed to improved particle interactions, higher density, and uniform dispersion within the polymer matrix.

1.9 Limitation of the Study

The mixture of tin and PDMS was left at room temperature which may cause oxidation might occur. This oxidation might have a negative impact on the sample's performance and reliability. The morphological structural and radiation measurements might be altered as well. Therefore, to minimize oxidation, the samples need to be placed in a closed and monitored environment to minimize the impurities and oxidation process before the analyzation stages.

When cured at a high temperature of 125 °C, the heat caused the composite to mix with the silicon mold, causing it to adhere to the mold surface. This occurrence happened as a result of the interaction between the high temperature and the PDMS matrix, which caused it to soften and bond with the mold, leaving it hard to remove the cured composite without damaging its structure.

As a result, the ideal curing temperature was determined to be 100 °C. This temperature accelerated the solidification of the PDMS, speeding up the curing process while maintaining the composite's integrity. More crucially, at 100 °C, the composite solidified without combining with the silicon mold, allowing for effective removal from the mold without adhesion or damage. This adjusted curing temperature of 100 °C struck a balance between expediting solidification and guaranteeing that the composite could be withdrawn from the mold intact, without adhering to the mold surface.

A notable problem was noted during the making of PDMS-tin composites, particularly at tin filler concentrations of 70% or higher. The problem emerged due to the insufficient amount of PDMS liquid in comparison to the volume of tin powder used. PDMS, a highly viscous polymer, was unable to efficiently distribute excess tin powder at these higher concentrations. This imbalance in the quantity of PDMS and tin resulted in the production of agglomerates, which were tin particle clusters that could not mix smoothly into the polymer matrix. As a result, the composite was unable to establish a uniform distribution of tin within the PDMS, which is critical for the composite's structural stability and performance.

The high viscosity of PDMS triggered this problem. The viscosity of the PDMS increases with larger filler concentrations, making uniform mixing more challenging. The tin powder becomes progressively difficult to incorporate into the PDMS because its viscosity limits the proper flow and dispersion of both the tin particles and the polymer. This causes tin particles to remain unblended, resulting in poor mechanical characteristics and overall ineffective composite production. Therefore, the highest metal that could be achieved and analyzed was standardized at 60%.

Lastly, one observed limitation of gamma spectroscopy is its reduced sensitivity at high photon energies. As the energy of gamma ray's increases, the efficiency of commonly used detectors, such as Nal (TI), tends to decrease significantly. This decline in efficiency results in lower count rates, making it challenging to obtain accurate measurements. Additionally, at high energies, the photopeak-to-Compton ratio typically decreases, which can lead to poor peak definition and difficulty in distinguishing between closely spaced energy peaks. The increase in Compton scattering also contributes to background noise, further complicating spectrum analysis. These factors collectively limit the precision and reliability of gamma spectroscopy in evaluating radiation shielding performance at higher energy levels, particularly when distinguishing subtle differences between composite materials. Therefore, to obtain reliable data, the characterization needs to be performed repeatedly and calculate the average values. Besides, careful calibration of the detector, along with appropriate shielding to reduce background radiation, can also enhance the reliability of the measurements.

Despite the promising outcomes of this study, several other limitations regarding this research must be acknowledged. Firstly, the relatively limited number of samples and their fixed compositions may affect the generalizability of the results. A broader range of filler concentrations or alternative metal combinations could provide a more comprehensive understanding of the composite's shielding performance. Secondly, variations in experimental conditions, such as curing temperature, mold detachment consistency, or sample thickness, may introduce minor discrepancies in measurement accuracy, particularly in gamma attenuation and spectroscopic tests. Lastly, the study is focusing on structural properties, chemical characteristics and radiation shielding parameters without evaluating the mechanical, thermal, or long-term stability of the composites. These factors are suggested being done in future research as the data is needed before determining their practical viability in real-life applications.

1.10 Assumption of the Study

The assumption of the study is used to guide the creation and evaluation of metal-polymer composites for gamma radiation shielding. It was assumed that the composites' observable surface morphology accurately reflected the bulk composite's interior

microstructure in FESEM findings. Additionally, it was believed that the sputter-coating and other preparatory processes did not change the distribution of metal fillers or introduce any notable artifacts. It was assumed that any indications of particle aggregation or dispersion were real physical occurrences caused by the fabrication process.

It was assumed that the elemental composition determined by the EDX matched the actual elemental distribution on the sample surface. it was presumed that the accuracy of the detected spectra was unaffected by any notable elemental overlaps or interferences. Regarding XRD examination, it was believed that every diffraction peak seen came only from the composites' crystalline constituents, like the metal fillers. Since the PDMS matrix is primarily amorphous, it was recognized that it might not yield distinct peaks. Furthermore, any peak broadening was thought to be caused by internal lattice strain or tiny crystallite sizes rather than noise or experimental mistake.

The functional groups in the PDMS matrix and any possible interactions with the tin or copper tin alloy fillers were thought to be accountable for the vibrational bands seen in the FTIR. The interpretation of the spectral data was predicated on the hypothesis that the absorption bands were unaffected by significant environmental pollutants or interfering chemicals. Lastly, it was assumed that the detector system produced precise measurements of transmitted and attenuated gamma rays and that the experimental equipment was appropriately calibrated for Gamma Radiation Spectroscopy. According to accepted theories of photon-matter interaction, the experiment's gamma-ray energy was supposed to interact with the composite materials in a predictable way and calculated into several parameters such as radiation protection efficiency (RPE), linear attenuation coefficient (LAC), mass attenuation coefficient (MAC), half value layer (HVL), tenth value layer (TVL), and mean free path (MFP). Any variation in the results was thought to be caused by the fundamental characteristics of the material rather than by inaccuracies made during the experiment.

These assumptions serve as the study's foundation, guiding experimental design and analysis while guaranteeing that the findings provide useful insights into the development of effective radiation shielding materials.

1.11 Thesis Scope

This research focuses on the development, characterization, and analyzing of metal-polymer composites made of tin (Sn), copper tin alloy (Cu-Sn), and PDMS for gamma radiation shielding applications. A comprehensive set of measurements is used to investigate the effects of material composition, density, and porosity on shielding performance, including RPE, MAC, LAC, HVL, TVL and MFP. The composites' performance is tested using a variety of gamma radiation sources, including Co-57, Ba-133, Cs-137, Mn-54 and Co-60.

The composites are made using different metal concentrations and tested for structural, chemical, and physical properties. FESEM is used to investigate cross-sectional surface morphology, XRD is conducted for structural characterization, whereas FTIR offers information about chemical bonding within materials. Radiation characterization includes calculating LAC and MAC to measure photon interaction capabilities, as well as HVL, TVL, and MFP to determine the material thickness required for effective attenuation. The lead equivalent is also calculated to express the radiation shielding effectiveness of a material by comparing its attenuation capability to an equivalent thickness of lead.

CHAPTER 2
LITERATURE REVIEW

2.1 Introduction

Radiation includes both ionizing and non-ionizing radiation which plays essential roles across various fields from medical imaging and cancer treatment to telecommunications. Ionizing photon rays are widely used in medical diagnostics, treatments, industrial processes, and research because they penetrate matter across various energies ranges [10]. However, their high energy levels also make them potentially hazardous, necessitating careful handling and protective measures. Non-ionizing radiation, which includes radio waves, microwaves, infrared radiation, and UV light, lacks sufficient energy to ionize atoms. While non-ionizing radiation generally poses fewer immediate health risks compared to ionizing radiation, prolonged exposure to certain types, like UV radiation from the sun, can still cause skin damage and increase the risk of cancer [10], [33].

Ionizing radiation and non-ionizing radiation are two (2) categories of electromagnetic waves distinguished by their ability to ionize atoms and molecules. Ionizing radiation (photon), such as X-rays and gamma rays (Table 2.1), carries high energy levels capable of removing tightly bound electrons from atoms, leading to the formation of ions [10]. This property makes ionizing radiation hazardous as it can damage DNA, increase the risk of cancer, and cause acute radiation sickness [2]. Ionizing radiation (particle) includes neutron, alpha, and beta particles. Besides X-rays and gamma rays, neutrons also require proper shielding in building materials and PPE. Meanwhile, alpha and beta particles are low in energy as thin paper sheets can stop the particles effectively [10], [33].

Understanding the properties, hazards, and applications of radiation is crucial for ensuring their safe and effective use in diverse contexts. Proper regulation, protective measures, and ongoing research are essential for maximizing the benefits of radiation while minimizing associated risks to human health and the environment. Thus, the comprehensive understanding of radiation shielding, encompassing both ionizing and

non-ionizing radiation, is vital for advancing technology, healthcare, and scientific research while safeguarding human well-being.

Table 2.1
Photon Energy Levels by Different Sources of Radionuclide [9]

Source	Photon energy (keV)
^{241}Am	60
	80
	160
^{133}Ba	
	223
	356
^{22}Na	511
^{137}Cs	661
^{60}Co	1173.3
	1332.5
^{152}Eu	121.78
	244.69
	344.28
	778.9
	964.13
	1408.01

2.2 Occupational Radiation Exposure

Occupational radiation exposure to healthcare remains a significant concern, despite the utilization of PPE [23]. This exposure is attributed to scattered radiation from patients and instrumentation in the treatment room. As well as from radiopharmaceutical procedures, affecting healthcare workers globally. According to the International Atomic Energy Agency (IAEA), approximately 23 million workers worldwide are occupationally exposed to ionizing radiation, and X-ray was classified as carcinogenic by the International Committee on Radiological Protection (ICRP) [34]. Strict guidelines set the maximum annual effective dose at 1 mSv for the public, while workers regularly exposed to radiation sources must not exceed 20 mSv annually (Table

2.2) [35]. A study conducted in Malawian hospitals revealed that radiographers faced an average monthly dose of 0.247 mSv for the whole body and 0.411 mSv for the skin, emphasizing constant exposure during procedures [22]. Due to its potential cumulative effects, cumulative exposure over a lifetime is a significant concern for radiation workers. Studies indicated an increased risk of cancer from occupational radiation exposure, even at low doses. A specific focus on leukaemia suggested a slightly elevated risk with prolonged exposure to low doses of radiation [36], [37].

Occupational radiation exposure poses significant health risks to professionals working in environments where ionizing radiation is present, such as hospitals, research facilities, and various industrial sectors. The principle of ALARA (As Low As Reasonably Achievable) which is established by ICRP is fundamental in minimizing these risks. It emphasizes the importance of implementing effective radiation safety measures, including optimizing time spent near radiation sources, maintaining distance from such sources, and utilizing appropriate shielding materials, such as lead brick, to absorb harmful radiation during the procedure [38].

A study investigates the correlation between education level and the knowledge and implementation of ALARA principles among radiation professionals in Malaysia. The research involved a survey distributed to various public and private institutions, collecting responses from 78 participants, primarily radiation practitioners such as radiologists and technicians. The findings indicated that only one (1) of the measured variables, which is the time spent near radiation sources, revealed a statistically significant difference based on education level [38], [39], [40]. This suggests that while educational background might not significantly influence overall knowledge and adherence to ALARA principles, it remains critical in shaping awareness and practices related to radiation safety.

The study of occupational exposure to photon rays and mortality from the year 1961 to 2003 found no significant increase in mortality from all causes, all cancers, or any specific cancer among workers exposed to ionizing radiation. Taken together, these studies suggested a potential small excess risk of cancer at low doses and dose rates for nuclear workers, although the evidence remains inconclusive [1]. The evidence was

reported by The International Nuclear Workers Study (INWORKS), which contributed valuable insights and confirmed the association between long-term low-dose radiation exposure and leukemogenesis [36]. However, the exact nature and extent of the cancer risk associated with low-dose radiation exposure remained inconclusive.

Furthermore, many researchers highlighted the significance of low dose ionizing radiation exposure and the associated health risks. For example, the previous study explored genomic instability and DNA damage through various techniques, the findings mentioned that there was a significant dose-response relationship observed for all solid cancers, even at low doses within the 0 to 0.2 Gy range [36]. Plus, the authors also emphasized the need for accurate cumulative effective dose measurements and improved methodologies in assessing occupational radiation exposure in interventional radiologist [36]. Other studies addressed the challenges associated with protective measures, such as lead aprons and thyroid collars. While these tools are essential for shielding healthcare workers from ionizing radiation, a study conducted in Sweden revealed potential discomforts associated with prolonged use. Despite these discomforts, staff recognized the importance of these protective measures in reducing occupational radiation exposure, underlining the need for alternative materials considering the complaints [23], [36], [41].

In a thorough study involving 191,333 workers with an average dose of 6.64 mSv, overall standardized incidence ratios for all cancers were observed. However, there was an increased ratio noted for thyroid cancer and melanoma. Notably, among males, significantly elevated excess relative risks were found for colon, pancreas, and testis cancers. In another study involving 600,000 workers with an average cumulative dose of 19.4 mSv (90% receiving cumulative doses < 50 mSv) from 15 countries, a small risk of cancer at low doses and dose rates was indicated among workers [1]. This suggested that even at relatively low doses and dose rates of ionizing radiation, there was an indication of an increased risk of cancer. Although the average cumulative doses are below 20 mSv (included in the effective dose), the rising concern among radiation workers must be considered by providing effective shielding that can minimize radiation exposure risks.

Table 2.2
Dose Limits for Each Organ

Organ/Tissue	Occupational Limit	Public Limit	References
Lens of the Eye	20 mSv/year (average), 50 mSv (max)	15 mSv/year	[1], [34]
Thyroid	500 mSv/year (historically) - now included in tissue weighting factors	Not specifically stated	[42]
Skin	500 mSv/year	50 mSv/year	
Hands and Feet	500 mSv/year	Not specifically stated	
Gonads (Testes, Ovaries)	20 mSv/year	15 mSv/year	[1], [2], [22], [35], [36], [37]
Bone Marrow (red)	20 mSv/year	15 mSv/year	
Breast, Lung, Colon, Stomach	20 mSv/year	15 mSv/year	

2.3 Interaction of Materials with Photon Rays

The inelastic interaction between photons and materials encompasses three distinct processes including photoelectric effect, Compton scattering, and pair production (Figure 2.1). With photon energies ranging from approximately 10 to 100 keV, the photoelectric effect predominates [10]. When the incoming photon has higher energy than the core electron, it is absorbed by the inner-shell electron, resulting in the ejection of the electron. The remaining energy of the electron is converted into the kinetic energy of the ejected photoelectron. This interaction is significant, particularly at lower photon energies and high Z shielding materials such as lead, bismuth, and tungsten [43], [44], [45].

2.3.1 Photoelectric Effect

The photoelectric effect predominantly occurs at photon energies in the range of approximately 10-100 keV, and its probability increases with increasing atomic number of the shielding material. The photoelectric effect occurs when an incident photon with energy greater than the binding energy of an inner-shell electron is completely absorbed by an atom in the irradiated material. This interaction results in the ejection of a photoelectron, where the excess photon energy is converted into the kinetic energy of the emitted electron in accordance with the conservation of energy [10].

2.3.2 Compton Scattering

Compton scattering, occurring at moderate energy levels between 100 keV and 10 MeV, involves inelastic scattering whereby a photon collides with an outer shell electron, thereby partially diminishing its energy or wavelength. Consequently, both the photon and the electron undergo a change in direction with reduced energy compared to the incident photon. This interaction contributes to the attenuation of radiation capability by dispersing photon rays in various directions. Subsequently, the lower-energy scattered photons are prone to absorption within the shielding material [44], [45], [46].

2.3.3 Pair Production

Pair production converts a photon into an electron-positron pair, absorbing and depleting energy from the incident photon. This process can only occur when the photon energy exceeds 1.022 MeV. In this process, the positron may subsequently annihilate an electron, resulting in the emission of two (2) gamma-ray photons which are lower energy levels compared to original photon rays within an energy range of 511 keV. These annihilation photons further interact with shielding materials by photoelectric effect, Compton scattering, and pair production interaction if the gamma rays emit high in energy levels. Lower energy gamma rays are more likely to be absorbed by the materials. Thus, the interactions progressively diminish the intensity of photon rays and increase the radiation capabilities [44], [45], [47].

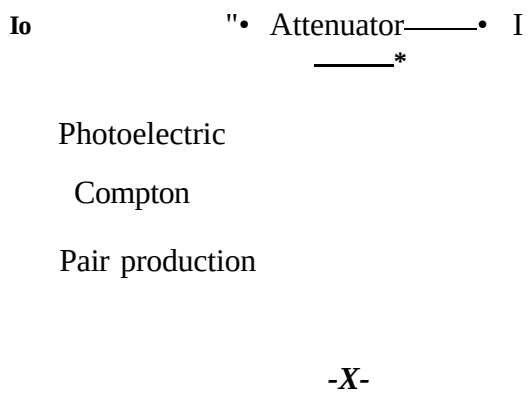

Figure 2.1 Interaction of Radiation Beam with Attenuator

2.4 Radiation Attenuation Properties of the Composites

The ability of a material to reduce the strength of ionizing radiation as it travels through it is known as radiation attenuation. Knowing attenuation characteristics is essential for assessing a material's efficacy in radiation shielding applications. These characteristics include LAC, MAC, RPE, HVL, TVL and MFP. Every characteristic provides information on the composite's interactions with photons across various energies.

A material's ability to decrease radiation as it travels through is measured by LAC. It depends on the material's density, atomic number, and the energy of the radiation. Better radiation blocking is indicated by a greater LAC. The unit of measurement is cm^{-1}. The LAC divided by the density of the composite is the MAC. It enables material comparisons without considering the thickness. It indicates how well a material absorbs radiation based on its composition and is expressed in $cm^2\ g^{-1}$.

The intensity of transmitted gamma rays after passing through a material with thickness can be determined using equations (2.1), (2.2) and (2.3) based on Lambert's Beer Law (Figure 2.2). As photon rays penetrate deeper into materials, the likelihood of interactions with material atoms, such as scattering and absorption, increases. With greater thickness, there is a higher chance of photons being scattered or absorbed, reducing the transmitted radiation intensity [58]:

$$/ = Ioe\text{-}i" \tag{2.1}$$

$$tim = \sim p = X_J\ wi\ O \tag{2.2}$$

where

I	:	Intensity of transmitted ray
Io	:	Intensity of incident ray
		Linear attenuation coefficient of the sample at a specific gamma-ray
x		Thickness of the sample
Um	:	Mass attenuation coefficient
p		Density
w		Weight fraction

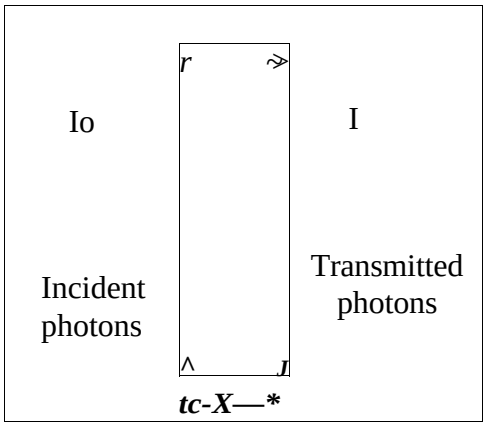

Figure 2.2 Illustration of Beer-Lambert Law

The RPE is a crucial indicator for evaluating a material's gamma radiation shielding capacity. It is defined as the percentage reduction in radiation intensity after passing through the shielding material. A higher RPE number indicates better shielding performance. Among the factors influencing RPE are the material's composition, density, thickness, and incident gamma ray energy. Materials with higher atomic numbers and densities typically have higher RPE values, which improves their radiation shielding capabilities. The intricate relationship can be computed for RPE, representing the composite's ability to block photon ray intensity, by considering density, and thickness, and expressing it through equations (2.4) and (2.5), which are formulated using radiation intensity [48], [49]:

$$RPE = (1 - e\text{-}i'') \times 100 \tag{2.4}$$

$$RPE = \left(1 - \frac{I}{I_0}\right) \times 100 \quad (2.5)$$

Where:

I =Intensity of transmitted ray

Io =Intensity of incident ray

u =LAC of the sample at a specific gamma-ray

x =Thickness of the sample

The HVL signifies the thickness of the composite needed to halve the intensity. A higher HVL value suggests lower effectiveness in attenuating radiation, indicating the requirement for a thicker layer for adequate protection. HVL can be calculated using the LAC of the composite, as shown in equation (2.6) [47], [50], [51], [52]: This pattern emphasizes how crucial it is to choose shielding materials with high atomic numbers since their dense electron fields and higher interaction probabilities might lower the HVL.

With increasing photon energy, TVL, which is the thickness required to lower the gamma ray intensity to a tenth of its initial value also increases equation (2.7). In applications where considerable attenuation is required, the TVL offers an even more distinct description of the shielding material's performance. Higher energy sources emphasize the relationship between material performance, cost, and practicality in shielding design by requiring thicker and denser materials to meet safety regulations.

$$HVL = \quad (2.6)$$

$$TVL = \frac{in(10)}{} \quad (2.7)$$

The MFP measures the average distance a photon travels through a material before encountering an interaction like absorption or scattering can be calculated using equation (2.8). A material's ability to attenuate photons across a shorter distance is indicated by a shorter MFP, which is beneficial in shielding applications. On the other

hand, a longer MFP indicates a lesser shielding efficacy because photons can travel farther before interacting [53], [54].

$$MFP = lJc \qquad (2\_8)$$

Lead equivalent (Pb-eq) is a widely used parameter in radiation shielding studies to compare the attenuation performance of alternative materials with that of conventional lead calculated using equation 2.9. It represents the thickness of lead required to provide the same level of radiation attenuation as a given thickness of a tested material at a specific photon energy. Since lead is the standard reference material for gamma-ray shielding due to its high atomic number and density, The Pb-eq value is derived from the exponential attenuation law and is inherently energy dependent, reflecting changes in dominant photon interaction mechanisms across different energy ranges [10]. Higher Pb-eq values indicate better shielding performance, as a thinner layer of the material can achieve attenuation comparable to that of lead [55].

$$Xpb \ \tilde{\_} \ \frac{Usample}{\sim \ \backslash *\text{-}Pb} \ \hat{} sample \qquad , \ . \ \backslash\hat{}\text{-}'')$$

2.5 Effectivity of the Composites for Radiation Shielding Application

When a material achieves 100% RPE, it means that all incident radiation is totally attenuated, meaning that no detectable radiation is transferred. According to theory, this would be equivalent to a situation in which the photons are completely absorbed, as indicated by both the MAC and the LAC being practically zero [10], [28]. Reporting a 100% RPE that equals zero MAC and LAC in real-world applications is very uncommon, though, and typically indicates either very good shielding under circumstances or measuring equipment limits.

Conditions at which near-total attenuation is observed have been investigated in several studies. For example, at lower photon energy, results close to 100% RPE have been obtained in several studies utilizing high-density, high atomic number materials such as lead or lead-free composites [28], [56]. These situations result in what is essentially a zero MAC and LAC measurement because the attenuation is so thorough

that the transmitted intensity drops below the sensors' detection limit. Such results are usually presented with the disclaimer that the measured "zero" values do not necessarily indicate a complete lack of photon transmission, but rather the experimental setup's sensitivity limitations [57], [58].

Additionally, materials can be developed to achieve near-total attenuation at low energy ranges by increasing thickness or optimizing filler content under carefully monitored laboratory circumstances. Instead of a true zero-transmission situation, reports of 100% RPE in the literature usually mean that the reported attenuation is so high that it surpasses the experimental apparatus's detection capacity. Latest research uses lead-based shields to address near-total gamma attenuation which can be used as standards to compare other materials [59], [60].

100% RPE or equivalently, zero MAC and LAC values are frequently reported in situations when the transmitted radiation is below the detection threshold. Under ideal thickness conditions, this phenomenon is usually seen with lead-based shields, where the high density and atomic number result in incredibly effective photon absorption [61], [62]. These investigations verify that correctly built lead shields can reach near-complete attenuation. These results not only support theoretical hypotheses but also serve as a crucial benchmark for the creation and evaluation of substitute, lead-free radiation shielding materials.

2.6 Overview of Factors Influencing Shielding Efficiency

Several factors influence the shielding efficiency of the materials (Figure 2.3). For instance, high Z numbers such as lead (Z = 82) offered an increase in radiation shielding capability compared to lower Z numbers like zirconium (Z = 40) [30], [63]. Besides, the increase in density of the material also highlights the superior ability in shielding-ability. The material's thickness is also mentioned to be one of the factors that could be manipulated to increase the protective ability [28]. Other than that, the energy level stroked through the materials also influenced the ability of the materials as increased energy level, reduced the ability to attenuate radiation [28], [30], [63].

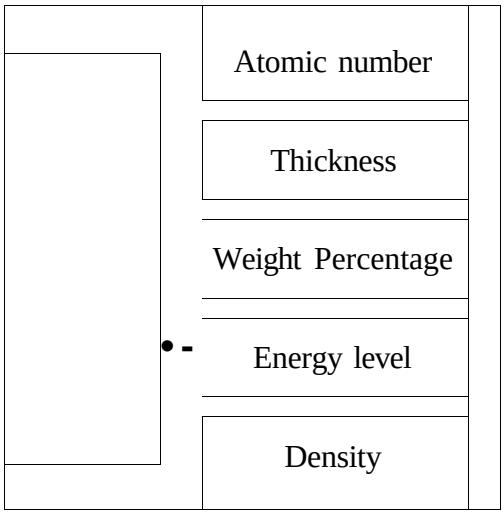

Figure 2.3 Factors Affecting the Shielding Efficiency

The hybridization of metal and polymer structures proved efficient in blocking photon rays. Various factors influence the effectiveness of protecting against photon rays, including the type of metal, atomic number, particle characteristics, and composite thickness [11], [26], [36]. For instance, metals with high Z demonstrated superior shielding abilities against photon rays. Furthermore, blending different metals enhanced the shielding efficacy compared to using a single metal depending on the atomic number of the metal used. Plus, each composite revealed an improvement in radiation protective ability and a decrease in flexibility as the metal weight percentage increased [47], [48]. Additionally, the percentage of radiation reduction decreased as the energy level increased, but an increase in thickness was able to counteract this effect.

The relationship between material thickness and shielding efficacy was reported to be a key factor of radiation attenuation (Table 2.3). Previous research demonstrated an increase in radiation reduction percentage with the escalation of composite thickness. For instance, studies on tungsten carbide/epoxy and tin/epoxy composites portrayed that as the thicknesses rose, radiation reduction percentages improved, reaching 97.88% and 97.00%, respectively (Table 2.4) [28]. The findings are attributed to the photoelectric effect, where increased thickness led to prolonged photon interactions, enhancing absorption and attenuation. Conversely, another study highlighted a decrease in LAC, and MAC with increasing thicknesses, suggesting complexities in photon-material interactions, including Compton scattering [28], [64].

Apart from that, examining the effect of energy levels between 59.51 to 1408 keV on radiation attenuation revealed variations in radiation reduction properties. As the energy level rose from 59.53 to 1332.50 keV, the LAC resulted in an increasing pattern. For instance, 10% macro PbO/HDPE reported LAC from 0.599 to 0.062 keV [61]. The LAC and MAC decreased as energy levels increased, indicating the prevalence of Compton scattering at higher energy levels, where photon rays are not completely shielded. In contrast, lower energy levels favor photoelectric effects, leading to increased LAC. The combination of these interactions may occur, influencing parameters such as HVL and radiation reduction percentage. Understanding these relationships is crucial for designing effective radiation-shielding materials [64], [65].

Lastly, the impact of metal weight percentage that increases the density of composites which affects radiation attenuation was further explored, showing a positive correlation between metal percentage and shielding effectiveness. According to [65], as the metal weight percentage increased, the LAC was reported to increase which is consistent with other findings by other researchers. These research findings indicated enhanced radiation attenuation properties with increased metal weight percentage, as demonstrated by lower HVL and rising LAC and MAC [65]. The expanding distribution of metal on the polymer surface with higher weight percentages enhanced photon interaction, emphasizing the role of structural characteristics in optimizing performance. However, a higher weight percentage does not necessarily guarantee flexibility in applying materials for attenuating photon rays . The density can be calculated using the equation 2.10.

$$Density\ (g\ cm^{d}) = \frac{Mass\ (g)}{Volume\ (cm^{6})} \qquad (2.10)$$

Table 2.3
Overview of the Metal and Polymeric Composites from Previous Studies

		Material State			Mixing		Compression/ [c]Curing/[d]Dried Process			Density (g cm^3)	Dimension			
	?	t :	§3		3		3			I		9 5		9
Tungsten carbide Tungsten carbide cobalt Tungsten carbide bismuth oxide Tungsten carbide barium sulphate Tin powder	Epoxy resin	Powder (1.00-3.00 urn)	Liquid / semi-liquid	Open-mold casting					9:1 9:1 4.5:4.5:1 4.5:4.5:1 9:1			0.7; 1.4	60	**42;**	[28]
Tungsten carbide	Epoxy resin	Powder (40.00-50.00 urn)	Liquid	Mixing		1400		1440		3.100-7.600		0.5 1.0 1.5 2.0			[64]
Iron filings	Polyester resin	Powder (60.00 urn)	Liquid	Mixing					0:10 2:8 3:7 4:6 5:5 6:4	1.252 1.572 1.747 1.965 2.246 2.620		**2.0**	16.13	5.14	[53]
Tungsten	Epoxy resin	Powder (0.60 urn)	Liquid	Mixing		[c]80; 150		240; 60	0:10 3:7 5:5 7:3 8:2	4.59		**3.0**			[66]

Nano Cadmium Oxide (CdO)	High-density polyethylene (HDPE)	Powder (50.00 nm; 0.95 Hm)	[b]Solid	Compression molding	170	15	170	10 20 30 40	10 10	0:10 1:9 2:8 3:7 4:6	0.944 1.039 1.145 1.291 1.452	- 1.110 1.239 1.404 1.573	**0.3**	3.45	55.53	[67]
Tungsten trioxide (W03)	Epoxy resin	[b]Solid (20.00 nm)	Liquid	Mixing			[d]RT	N/A	2880	0:1:9 0.5:1.5:8 1:2:7 2:2:6 2.5:2.5:5		1.180 1.667 1.762 1.868 1.989	**2.0; 4.0**			[54]
Lead oxide (PbO)	Polypropylene (PP)	'owder (0.18 Hm)	Liquid	A pressure molding	195		1750	10 20 30 50	15 15	0:10 1:9 2:8 3:7 5:5	0.902 0.991 1.099 1.236 1.645		0.5	3.14	1.23	[68]
Zirconium oxide ($Zr0_2$)	Epoxy resin	[b]Solid	Liquid	Mixing						[a]0:1.5:9.5 [a]1:1.5:8.5 [a]2:1.5:7.5 [a]3:1.5:6.5 [a]4:1.5:4.5	1.282 1.402 1.548 1.727 1.953					[63]
Bismuth oxide (Bi203)	Recycled poly (vinyl chloride) (PVC)	Powder (NPs)	Pellets	Melt blending; Compression molding	18Q	15	190	20 30	15	0.5:9.5 1.5: 8.5 2.5:7.5 3.5:6.5		1.782 2.887	0.5	112.5	112.5	[69]
Tin oxide (II)	Silicon rubber	Powder (19.00 nm; 9.00	Liquid	Mixing		15				2:8 5:5	1.395 1.905	1.450 1.967				[9]

Tungsten (VI) oxide	Poly (hydroxy ethyl methacrylate-co-styrene) (Poly (HEMA-co-Styrene))	[b]Solid	[b]Solid	Casting	60	-	120	[c]80; 85 [d]100	1440		1.090 1.190 1.310 1.460 1.650 1.890					[65]
ead oxide (PbO)	High-density polyethylene (HDPE)	[b]Solid (10.00 nm; 0.70 urn)		Compression molding technique.	170	50	30	170	15	0:10 1:9 5:5	0.891 0.983 1.507	1.051 1.652	**0.2**	2.62	45.27	[61]
Barium Pyrophosphate (Ba2P207)		powder	Liquid	Mixing						0.5:9.5 1:9 1.5:8.5 2:8 0.5:9.5 1:9 1.5:8.5 2:8	1.260 1.270 1.290 1.329 1.281 1.296 1.325 1.377		1.0	3.14	3.14	[48]

"Zirconium oxides: boron oxides: epoxy resin
[b]Solid= block, pallet or powder
'Curing
"Dried process
RT = room temperature

Table 2.4
Radiation Shielding Properties of Metal-Polymeric Composites from Past Research

		Energy								
		I		I						Eli
Tungsten carbide			Single-Photon Emission Computed Tomography (SPECT) scanner							97.60 48.71 97.88 64.36
Tungsten carbide cobalt										97.29 45.25 97.88 64.94
Tungsten carbide bismuth oxide	Epoxy resin	90		0.70 1.40	140; 364					96.93 41.96 97.85; 58.97
Tungsten carbide barium sulfate										96.09 ;40.23 97.75; 54.04
Tin powder										87.32; 30.85 97.00; 46.91
Tungsten carbide	Epoxy resin	100 90 85 80 75 70 65 60	SPECT scanner	0.50-2.00	140	10.700-4.700 8.900-4.600 8.700-4.600 7.000-4.600 6.200-4.600 4.500-3.900 4.300-3.300 3.900-3.200	1.170-0.890 1.170-0.600 1.420-0.750 1.370-0.700 1.240-0.600 1.180-0.500 1.260-0.500 1.250-0.490	0.06-0.14 0.07-0.15 0.07-0.15 0.09-0.15 0.11-0.15 0.15-0.17 0.16-0.21 0.17-0.21	0.09-0.21 0.11-0.21 0.11-0.21 0.14-0.21 0.16-0.21 0.22-0.25 0.23-0.30 0.25-0.31	

Iron filings	Polyester resin	0 20 30 40 50 60	High-purity germanium detector (HPGe)	2.00		0.06-1.33	0.245-0.075 0.622 0.873 1.187 1.591 2.129-0.142				1.11-7.82 0.44-5.64	21.79-30.53 18.48-25.96 16.78-23.60 15.06-21.21 13.30-18.75 11.51-16.24	1.61-11.28 0.63-8.14	[a]82.57 [a]24.00 [a]18.80 [a]17.72
Tungsten	Epoxy resin	0 30 50 70		3.00		1.33; 1.17					9.17 6.65 5.07 3.37 2.53	N/A		
Nano Cadmium Oxide (CdO)	High density Polyethylene (HDPE)	10 20 30 40		0.30	60-1408			0.692-0.060 1.188-0.059 1.669-0.057 2.195-0.056	*0.798-0.065 *1.375-0.064 *1.938-0.063 *2.562-0.062	0.97-11.17 0.51-10.26 0.32-9.34 0.22-8.50	*0.78-9.68 *0.41-8.71 *0.25-7.83 *0.17-7.10			
* Tungsten trioxide (W03)	Epoxy resin	0 5 10 20 25	HPGe	2.00; 4.00		0.06	0.250 0.510 1.010 1.570 2.210	0.210 0.310 0.580 0.840 1.110		2.76 1.35 0.68 0.44 0.31				63.41 87.17 98.26 99.82 99.99

Lead oxide (PbO)	Polypropylene (PP)	0 10 20 30 50	Gamma-ray spectrometer	0.50		0.06-1.41	0.171-0.053 0.608-0.057 1.156-0.063 1.818-0.070 3.889-0.0907	[d]0.173-0.052 0.628-0.059 1.178-0.065 1.871-0.072 3.927-0.093	N/A		N/A				
Zirconium oxide (Zr02)	Epoxy resin	0 10 20 30 40	HPGe			0.06-1.33	[b]0.259;0.108 0.109 0.124 0.133 [b]2.978;0.146		-		[c]2.60;6.69;8.79 0.92 0.70 0.33 [c]0.23, 4.58, 6.10	-	3.73-13.53 0.33-9.41		98.43 99.75
* Bismuth oxide (Bi2Q3)	Recycled poly (vinyl chloride) (PVC)	5 15 25 35	Nal (Tl) scintillation detector	0.50	121-1408				0.466 - 0.044 1.018-0.052 1.655-0.071 2.530 - 0.075		1.4207-11.974 0.88458-10.463 0.50647-9.0990 0.26379-7.8696	5.44-39.78 3.57-35.42 2.32-29.82 0.88-26.14	1.99-17.28 1.29-15.62 0.87-13.38 0.38-11.35		
Tin oxide (II)	Silicon rubber	20 50	Nal (TI) cylindrical detector	0.05	60-1408				1.169-0.054 2.588-0.054	* 1.428-0.058 *3.187-0.060					
Tungsten (VI) oxide	Poly (hydro xyethyl methacrylate-co-styrene) (Poly(HEMA-co-Styrene))	0 10 20 30 40 50			662-1332		0.099 - 0.069 0.106-0.075 0.121 -0.080 0.135-0.088 0.151-0.093 0.170-0.109						10.10-14.50 9.40-13.30 8.30-12.50 7.40-11.40 6.60-10.80 5.90-9.20	7.00 22.00 36.00 52.00 72.00	9.00-11.00 15.00-18.00 27.00-33.00 35.00-37.00 57.00-58.00

Lead oxide (PbO)	High-density polyethylene (HD-PE)	0 10 50	HPGe	0.20	60-1333	0.170-0.056 0.599-0.062 3.684-0.097	*0.705-0.068 *4.488-0.111	0.190-0.063 0.609-0.063 2.445-0.064	*0.1-0.065 *2.717-0.067
Barium Pyrophosphate ($Ba_2P_20_7$)	Polyester resin	5 10 15 20	HPGe	1.00	60-1408			0.420-0.058 0.620-0.056 0.844-0.054 0.990-0.053	••0.405-0.056 ••0.613-0.056 ••0.804-0.055 ••0.981-0.055
Barium Zirconate ($BaZrQ_3$)	Polyester resin	5 10 15 20	HPGe	1.00	60-1408			0.456-0.057 0.681-0.055 0.907-0.053 1.103-0.058	••0.413-0.056 ••0.628-0.056 ••0.824-0.055 ••1.006-0.055

80.20

83.52

" RSE for 30% metal weight across different energies
[b] 0.060 & 0.662 MeV respectively
[c] 0.060, 0.663 & 1.173 MeV respectively
[d] Simulation results
* Nanoparticle results

2.6.1 Relationship Between Atomic Number of Metal and Radiation Attenuation

Each metal employed in these studies has its atomic number (Z), which can influence radiation protection. The inclusion of a metal with a high Z into the polymer matrix could enhance both its ability to attenuate photon rays and mechanical performance. In studies conducted by [69] and [61], bismuth oxide (E^Cb) and PbO were employed with 35% and 50% of metal weights, respectively. According to [69], the MAC values were recorded at 2.530 to 0.075 cm^2 g^{-1} covering energy levels of 121 to 1408 keV meanwhile [61] stated the MACs were 2.445 to 0.064 cm^2 g^{-1} at energy levels of 60 to 1333 keV. Notably, the higher Z of bismuth has increased the MAC values, thus confirming the superior effectiveness of bismuth compared to lead [61], [69].

Study from [67] and [9] highlight the use of 20% cadmium oxide (CdO) and tin oxide (SnCh) at the same energy level (60 keV), with the MAC values of 1.375 and 1.428 cm^2 g^{-1}, respectively. Both studies demonstrated that at lower photon energy levels, materials with higher atomic numbers exhibit better photon attenuation due to the dominance of the photoelectric effect. These findings also indicated that the slightly higher atomic number of tin has played a role in its efficacy of blocking photon rays. However, at the energy level of 1408 keV for CdO and Sn02, the MAC decreased to 0.064 and 0.058 cm^2 g^{-1}, respectively. As energy increases, the photoelectric effect becomes less significant, and Compton scattering becomes the dominant interaction [9], [70].

Because tin has an atomic number of 50 and cadmium has an atomic number of 48, Sn02 contributes more atomic numbers than CdO. However, the atomic number is not the only factor that affects these oxides' attenuation qualities; density, electron configuration, and the material's interaction with photon energy are other important considerations. Due to the stronger photoelectric effect caused by tin's slightly higher atomic number than cadmium, Sn02 often shows better photon attenuation at lower energies [9], [67].

A comparison between two (2) other studies has revealed that a higher Z would lead to greater efficiency in attenuating photon rays. [65] and [63] reported the use of

tungsten and zirconium, respectively, each contributing 40% by weight. The LAC at 0.662 MeV for tungsten reported at 0.151 cm^{-1} and 0.146 cm^{-1} for zirconium [63], [65]. Tungsten showed a superior shielding ability against photon rays compared to zirconium. Thus, maximum shielding protection can be efficiently achieved with high Z, even when fabricated in lower weight percentages. Interestingly, despite zirconium having a lower Z compared to tungsten, it appeared to be almost comparable to tungsten in terms of efficiency as the mixture of epoxy/zirconium was mixed with another metal, barium. This observation implied that the mixture of these two (2) metals has enhanced the protective properties of the composites [63], [65].

2.6.2 Relationship Between Material Thickness and Shielding Efficacy

Previous research has reported that the radiation reduction percentage would increase in relation to an escalation in the thickness of the composites. For example, [29] explored tungsten carbide/epoxy resin composites with thicknesses of 0.7 and 1.4 cm. The results indicated that when the thickness was increased from 0.7 to 1.4 cm, the radiation reduction percentage rose increased from 97.60% to 97.88%. Similarly, in the case of tin/epoxy resin composites, radiation reduction was increased from 87.32% to 97.00% with an increase in thickness. These findings showed that tin, despite having a lower atomic number than tungsten, offered a comparable radiation reduction percentage when its thickness was increased [28], [64]

In specific terms, the increase in radiation reduction percentage emphasized that photon rays were absorbed by the atoms of the materials in a phenomenon known as the photoelectric effect. The thickness of the materials also played a crucial role, as an increase in thickness correlated with an elevation in the percentage of radiation reduction. This could likely be attributed to the prolonged photon interactions within the material, resulting in increased absorption and attenuation. Thus, the highest radiation reduction percentage can be achieved by increasing the thickness of the composites [28], [64].

In another study, [64] stated that the LAC was decreased from 10.7 to 4.7 cm^{-1}, while the MAC was decreased from 1.17 to 0.89 cm^2 g^{-1} when the thickness

of the composite was increased from 0.5 to 2.0 cm. This decreasing pattern could be attributed to the complexity of the interaction between photon rays and the materials. The reduction in LAC and MAC values with increasing thickness illustrated multiple interactions including Compton scattering, where the photon rays were not entirely diminished but scattered in different directions. The effectiveness of the materials became significant as the photon rays traversed through the rising thickness. Remarkably, the materials served as a barrier that blocked the photon rays, even though there was a reduction in both LAC and MAC [28], [64].

2.6.3 Effect of Metal Weight Percentage on Radiation Attenuation

According to [66], an increase in the percentage of metal in the composite can be associated with enhanced radiation attenuation properties. They reported that HVL values for composites with 70% and 80% of tungsten/epoxy were 2.53 and 3.37 cm, respectively. A low HVL value would indicate an increased effectiveness of the material in reducing radiation intensity by half. Additional research findings have consistently indicated a positive correlation between radiation shielding effectiveness and the weight percentage of metals, as shown in Figure 2.4 [54], [63], [68].

Furthermore, when comparing different metal concentrations, the study reveals that composites with 50% metal content exhibit significantly higher LAC values than those with only 20% metal content. This suggests that increasing the filler concentration enhances attenuation efficiency due to the higher availability of interacting atoms within the material. However, even at lower concentrations, the tin-filled composite demonstrates considerable attenuation capabilities, particularly at intermediate and high photon energies, making it a promising alternative for lead-free radiation shielding applications. These findings highlight the influence of metal composition and concentration on photon attenuation performance, reinforcing the need for material optimization in radiation shielding applications [9].

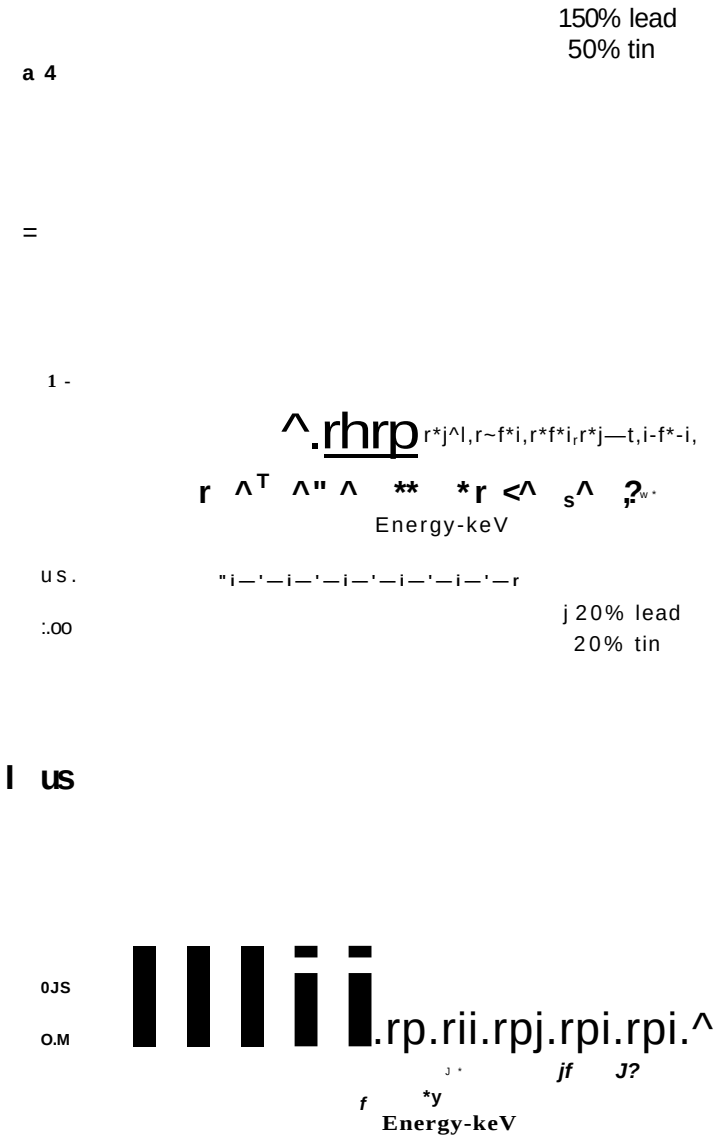

Figure 2.4 LAC Pattern Against Energy Level [9]

Other studies have also highlighted a rising trend in LAC and MAC values, and reductions in HVL values when the weight percentage of metals was increased [64]. The distribution of metal particles on the polymer surface expanded, thus enhancing the surface area. This expansion raised the likelihood of photon interaction with the material's surface, which emphasized the importance of structural characteristics in optimising the overall performance of the composites. Nevertheless, increased weight percentage did not necessarily mean that the materials were flexible enough to be applied for attenuating photon rays.

2.6.4 Effect of Energy Level of Gamma Ray on Radiation Attenuation

The energy levels that are used to examine the shielding effectiveness of the reported composites vary between low to high energy gamma ray**.** Radiation shielding efficiency was recorded by previous studies using several parameters, such as the LAC, MAC, HVL, and radiation reduction percentage. Based on the study from [53] using the composites made of 60% of iron fillings with polyester resin, the LAC reported decreased from 2.129 to 0.142 cm^{-1} when the energy level was increased from 0.06 to 1.33 MeV [61]. These findings were consistent with other study using 50% of tin oxide mixed with silicone rubber (Table 2.4) which portrayed a similar pattern of the MAC decreasing from 2.588 to 0.054 cm^2 g^{-1} when the energy level was increased from 60 to 1408 keV [9].

Specifically, the LAC of lead- and tin-filled composites follows a comparable trend, where attenuation is more pronounced at lower energies and decreases as photon energy increases [9]. The graph in Figure 2.4 illustrates that at low photon energies, lead-filled composites exhibit superior attenuation compared to tin-filled composites, which aligns with the fact that lead has a higher atomic number and density, enhancing its ability to absorb photons through the photoelectric effect. However, as photon energy increases, the difference in attenuation between lead and tin narrows, with both materials showing similar LAC values at higher energy levels. This pattern indicates a shift in the dominant interaction mechanism from photoelectric absorption to Compton scattering, where atomic number plays a lesser role in determining shielding efficiency.

It was concluded that the energy level of the materials has influenced these parameters. When the energy level was increased, the values of LAC, MAC, and radiation reduction percentage were decreased, which could be due to interactions resulting in pair production, where photon rays were not absorbed completely. The preferred interaction between photon rays and atoms of the composite materials at lower energy levels was photoelectric effects. In this interaction, the entire energy of the photon is absorbed by the inner shell of the atom, resulting in increased LAC values. Noticeably, a combination of interactions may also occur throughout the process [64], [65].

2.6.5 Effect of Multiple Metals Fabricated into a Polymer Matrix

According to the research conducted by [28] and [48] the incorporation of more than one (1) metal into a polymer could enhance the ability of composites to attenuate photon rays. Both studies reported that metals with higher Z were able to increase the density and ability of composites to diminish photon rays. The MAC for 20% of Ba2P2O7 and BaZrO3 was recorded as 0.990 and 1.1033 cm^2 g^{-1} at an energy level of 59.5 keV, respectively. Additionally, at the same energy level, the RPE was reported as 80.20% and 83.52%, respectively, indicating the successful fabrication of metals and polymers [28], [48].

Previous study has also revealed the RPE for the composition of WC/Bi2O3/epoxy resin at 96.93% compared to the RPE for WC/BaSO4/epoxy resin at 96.09% [28]. Although the composites in the study by [48] were thicker (1.0 cm), their RPE values appeared to be lower compared to the study by [28] which employed a thinner (0.7 cm). These findings described the correlation between the Z and radiation attenuation, which indicated that an increase in thickness did not necessarily produce composites with better attenuation properties and other factors must be considered as well [28], [48].

The study introduced 25% of ZrO2/B2O3 to epoxy, resulting in 0.109 cm^{-1} of LAC at 0.060 MeV with a density of 1.402 g cm^{-3} [63]. Although zirconium was a common element in the studies by [63] and [48], the additional metals and their compositions, have affected the ability of these materials to protect against radiation. [48] reported that the density of 20% of metal compositions has resulted in a composite with a density of 1.377 g cm^{-3} and despite the low density, its radiation-blocking efficiency was higher. These findings confirmed the importance of using metals with a high Z for effective radiation shielding applications.

On the contrary, findings from the study by [71] showed that the incorporation of two metals did not necessarily result in better shielding efficiency. In this study, a mixture of polyester and boron yielded 1.3226 cm^2 g^{-1}, while polyester integrated with molybdenum resulted in 1.6391 cm^2 g^{-1}. These outcomes may be attributed to the Z of the metals, as boron (Z = 5) has a significantly lower Z compared to molybdenum

(Z = 42). Hence, the integration of multiple metal fillers may enhance shielding efficiency, especially if the metals used have higher Z [71].

2.7 Lead As a Shielding Material

Conventional radiation protection PPE such as lead aprons, thyroid collars, gonad shields, protective gloves, leaded eyewear and shielding wall concrete for the treatment room is widely used to minimize exposure to ionizing radiation in medical and industrial environments. These protective garments are constructed using lead or lead-equivalent materials, typically ranging from 0.25 mm to 0.5 mm [39], [40], [72]. The shielding efficiency of this PPE is closely tied to the energy of incoming photons. At lower photon energies (30 to 70 keV), most PPE items can attenuate up to 97 to 99% of scattered X-ray radiation [24], [72]. However, at higher photon energies (100 to 150 keV), the attenuation efficiency decreases, often ranging between 50 to 70%, depending on the material thickness and quality [24], [72].

Lead aprons with a 0.5 mm equivalence are commonly used during fluoroscopic and diagnostic imaging procedures, offering high attenuation against scattered X-rays generated from machines operating at 70 to 100 kVp, corresponding to photon energies typically in the 30 to 60 keV range [24]. Thyroid collars, which protect the highly radiosensitive thyroid gland, can reduce radiation doses to the neck by up to 8.5 times when properly fitted [42]. Gonad shields serve a vital role in protecting reproductive organs from direct and scattered radiation, particularly in pediatric and reproductive-age patients [60].

In addition to full-body and neck protection, PPE also extends to the eyes and hands. Leaded eyewear with 0.75 mm equivalence can reduce eye lens dose by 1.6 to 4.5 times, an essential protection against radiation-induced cataracts, especially in high-exposure roles such as interventional radiology [34]. Lead gloves, though offering somewhat reduced dexterity, are effective in minimizing hand exposure and have been shown to attenuate up to 80% of radiation under specific clinical conditions [73].

Lead is commonly used as a shielding material against photon rays. Lead is known for its toxicity, is heavyweight, and is prone to fracture easily. The toxicity of lead causes environmental pollution and affects human health [9], [70]. To address the ergonomic limitations of lead, newer PPE products incorporate lead-free shielding materials such as bismuth, tungsten, antimony, and tin. These alternatives offer similar protection at low photon energies while significantly reducing weight and toxicity concerns. However, their attenuation performance may decline more rapidly at higher energies compared to standard lead-based PPE.

For instance, exposure to lead may affect humans through a peripheral and central nervous system or haemoglobin synthesis. Multiple health issues were addressed by research when exposed to the lead including neuromuscular disorder, hearing problems, encephalopathy, delayed growth, permanent brain death, anaemia, abnormal spermatogenesis, damaged body tissues, and more. Considering the disadvantages of lead as a shielding material, alternative metals that are comparable to lead in terms of shielding ability should be investigated [33].

2.8 The Potential of Tin-PDMS Composite As Lead-Free Absorber

Researchers are looking for alternative materials as a result of increasing concerns about the health and environmental issues linked with lead-based radiation shielding [38]. With an optimal combination of radiation attenuation effectiveness, lightweight characteristics, and fabrication flexibility, metal-polymeric composites have become a practical alternative. These composites reduce the toxicity and handling challenges of traditional lead-based materials while improving shielding efficacy by combining metallic fillers with polymer matrices [6], [7].

Many metal-polymer combinations have been studied, with a focus on composites that have high photon attenuation capabilities with excellent mechanical integrity. This section explores specifically tin and polymer composites as shielding materials and evaluates their viability as viable and efficient substitutes for radiation protection applications.

2.8.1 Past Research Findings on Tin As the Filler for Composites

Past studies revealed the promising potential of these composites in shielding against photon rays. In a study by [28] a composite comprising 90% tin powder embedded in epoxy resin achieved remarkable RPE of 97.00% and 46.91% at 140 keV and 664 keV, respectively, with a thickness of 1.4 cm. Similarly, [9], [74] showcased the efficiency of a composite incorporating 50% tin oxide into silicon rubber for attenuating photon rays. The MAC results across various energy levels indicated notable improvements, with values ranging from 3.187 to 0.060 cm^3 g^1 at a thickness of 0.05 cm, compared to 20% tin oxide with values of 1.428 to 0.058 cm^3 g^{-1}[9], [74]. These findings highlight the positive correlation between increased metal weight compositions and enhanced attenuation capabilities.

A research was performed by fabricating polypropylene with tin microparticles with specific compositions. The findings revealed the LAC values at 30% and 50% tin content were 8.35 and 10.67 cm''^1 respectively which concluded the higher shielding efficiency for higher metal content [75]. The findings were also confirmed by the calculation of the required thickness needed to shield 99% of the X-ray which was calculated as 0.55 cm and 0.43 cm across 30 keV for 30% and 50% tin filler respectively [75]. As the metal filler increased, thinner composites might be able to attenuate the photon rays. However, the mechanical results using the breaking elongation test for 30% tin content appeared to be higher (27.95%) compared to 50% tin content (22.89%) [75]. The results concluded that, as the metal fillers increased, the flexibility decreased.

In addition, the studies also concluded that 30% metal content is an optimal metal weight percentage, as exceeding 30% metal content may lead to a reduction in mechanical properties flexibility. These findings signified the practical potential of metal-polymer composites in photon ray protection. Nevertheless, the detailed exploration of mechanical and chemical properties using tin remains inconclusive. Thus, to ensure a balanced integration that optimizes both attenuation capability and mechanical integrity, further study needs to be conducted before the implementation of the materials as shielding materials.

2.8.2 Safe and Effective Radiation Shielding Using Tin As Potential Wearables

Tin is recognized for its relatively low toxicity compared to other heavy metals, making it an excellent candidate or potential material in radiation shielding. The study by [76] has demonstrated tin's crucial role in various binary alloys used for radiation shielding, such as Pb-Sn50 and Sn-Zn50. The Sn-Bi50 alloy was highly effective for gamma-ray shielding, while the Pb-Zn50 alloy excelled in neutron shielding, highlighting tin's role in enhancing the structural, mechanical, and nuclear shielding properties of these alloys.

In another study, a superior X-ray radiation shielding platform was developed using polyaniline reinforced with graphene oxide, decorated with a tungsten-bismuth-tin complex. Tin (II) chloride (SnCb) was instrumental in this process, decorating graphene oxide flakes alongside tungstic acid (H2WO4) and bismuth sulfite (Bi2(S03)3) to form a highly efficient interconnected absorber for X-ray radiation attenuation. This innovative, lead-free shielding system suggested the potential material replacing lead in the healthcare system and demonstrated enhanced X-ray protection in the 30-60 kVp range. The inclusion of tin in the shield's composition significantly improved its attenuation efficiency, making it a promising candidate for lightweight, non-toxic X-ray shielding applications. The integration of Tin within the design underscores its importance in boosting the performance and safety of radiation shielding systems [77].

These studies indirectly underscore the importance of tin in developing effective, safe, and environmentally friendly radiation shielding materials. Its application in wearable photon ray shielding through tin added into PDMS composites offers a unique combination in terms of flexibility, durability, and safety.

2.8.3 Polysiloxane As the Matrix for Composites

Polysiloxane or silicone is generally known for its stable and versatile nature as a polymer, which maintains its structural integrity even when subjected to elevated temperatures ranging from -55 to 300 °C, revealing its thermal stability properties [16], [17]. Due to these characteristics, coupled with its easy and cost-effective

manufacturing, silicone rubber finds applications in diverse fields, including its use in radioprotective measures during radiological diagnosis. Significantly, the versatility of silicone is notable, as it can be easily moulded into different shapes and forms [16], [17]. This characteristic facilitates the creation of the potential of flexible gamma-ray shields, enabling the material to be formed into various surfaces and structures [15], [17]. This characteristic enhances its effectiveness in delivering flexible radiation shielding.

Silicon polymers have diverse compositions, including polydimethylsilicone, polymethylhydrosiloxane, perhydropolysiloxane, PDMS, and more. Previous research investigated the efficiency in shielding application for various silicon polymers [14]. The authors mentioned that each silicon polymer exhibited distinct effectiveness in shielding against photon rays. For instance, perhydropolysiloxane (PHPS) was reported as the highest MAC compared to other silicon polymers which explained the superior ability of PHPS in shielding against photon rays (Table 2.5). Furthermore, another study conducted by [78] concluded the superior mechanical properties of PHPS (D1033), with reported hardness and elastic modulus values of 0.09 and 0.4 GPa, respectively. These high values suggest the excellent durability of the material as its needs to be applied a certain high force to induce deformation or stretching [14].

Additionally, PDMS gained attention in several studies due to its notable characteristics such as less toxic, lightweight, resistant to biodegradation, flexibility, chemical stability, and excellent mechanical properties. A lower MAC value was reported for PDMS compared to PHPS but higher compared to other polymers like High-density polyethylene (HDPE). Young's modulus for PDMS was recorded at approximately 2 MPa which is considered lower than PHPS. Although low Young's modulus value reflected easy deformation as the material was applied to stress, it also suggested the flexibility and elasticity of the polymer in comparison to PHPS [61], [74], [79].

Table 2.5
Comparison Between PHPS and PDMS Properties.

Properties	Polymer		References
	PHPS	PDMS	
Chemical composition	H_3SiN	C_2H_6OSi	[14], [80]
Melting point (°C)	-	-49.9 to-40	[17]
Young Modulus	D2850: 10.76 GPa D2250: 3.59 GPa	360-870 kPa	[17]
Hardness	D2850: 2.05 GPa D2250: 0.64 GPa	41-43 [shore A]	[17]
Tensile strength (Mpa)		2.24-6.7	[17]
MAC (cm^3 g^{-1})	0.919-0.055	0.661-0.054	[14]
Curing agent	Amine catalyst (Diethylethanolamine) tetrabutylammonium chloride (TBAC)	Crosslinking: Dimethyl methylhydrogen siloxane Inhibitor; tetramethyl tetravinyl cyclotetrasiloxane Sylgard 184 from Dow Corning (trimethyl)pentamethylcyclopen tadienylplatinum(IV)	[15], [16], [81], [82]

Moreover, the compatibility of silicone with metal filler represented a significant advantage in enhancing gamma-ray shielding and mechanical properties. The research by [13] explored the incorporation of radiation-absorbing materials such as tungsten and nano titanium oxide (TiCh) fabricated into silicone matrix and reported silicone's ability to integrate with various fillers. The study also illustrated the surface morphology of the composites, and the uniform distribution of metal fillers within the silicone matrix, which demanded effective shielding properties and increased mechanical properties [13]. Thus, silicon polymers can be used in various applications considering the uniqueness and characteristics of each silicon polymer.

2.8.4 Past Research Findings on Structural Properties of PDMS-Based Composites

Successful fabrication can be observed using a scanning electron microscope (SEM), FESEM and other similar instrumentation. A smooth distribution of the metal within the polymer matrix would indicate an effective adhesion and integration between the metal and the polymer. The researcher found that smaller particles were distributed

better within a polymer compared to larger particles. However, an increase in the percentage of small metal particles would lead to agglomeration [38]. The presence of agglomeration suggests a potential decrease in the efficiency of a material in reducing radiation. Thus, agglomeration needs to be minimized to optimize the effectiveness of the test materials in attenuating photon rays [19], [83], [84].

According to the reviewed papers, the techniques used to produce these composites involved mixing or blending the metals and polymers for a specific time and temperature. These steps would be followed by compression or casting techniques to shape the composites into sheets, blocks, or bricks. To assess the structural integrity and distribution of metals within the polymer matrixes post-fabrication, SEM was used. The distribution and adhesion of metals within the polymer matrixes can be evaluated. Remarkably, a metal filler with a higher Z appears brighter within the polymer matrix, as shown in Figure 2.5a. Meanwhile, the reduction in porosity and distribution of the metal oxide particles throughout the polymer matrix, suggest effective embedding and minimal agglomeration (see Figure 2.5b). The strong material integrity implied an increase in the interaction between photon rays and the composite particles, which consequently increased its blocking efficiency [9], [69], [85].

A critical aspect that was investigated in this literature review was related to the comparative analysis between nano and microparticles within a polymer matrix. Nanoparticles often exhibit homogeneous dispersion and effective embedding in a polymer matrix, thus enhancing their integration. In contrast, microparticles have displayed a less favorable structure, characterized by insufficient coverage and detachment of the metals from the matrix, which indicated weaker integration [9], [67], [69]. Additionally, the LAC values for the nanoparticles revealed superior effectiveness in shielding against photon rays. The LAC values for 50% of micro-tin oxide and 50% of nano-tin oxide are 2.588 and 3.187 cm^{-1}, respectively, across 59.51 keV energy level [67]. Therefore, the utilization of metal nanoparticles was preferred to maximize the effectiveness against radiation [9], [67], [69] .

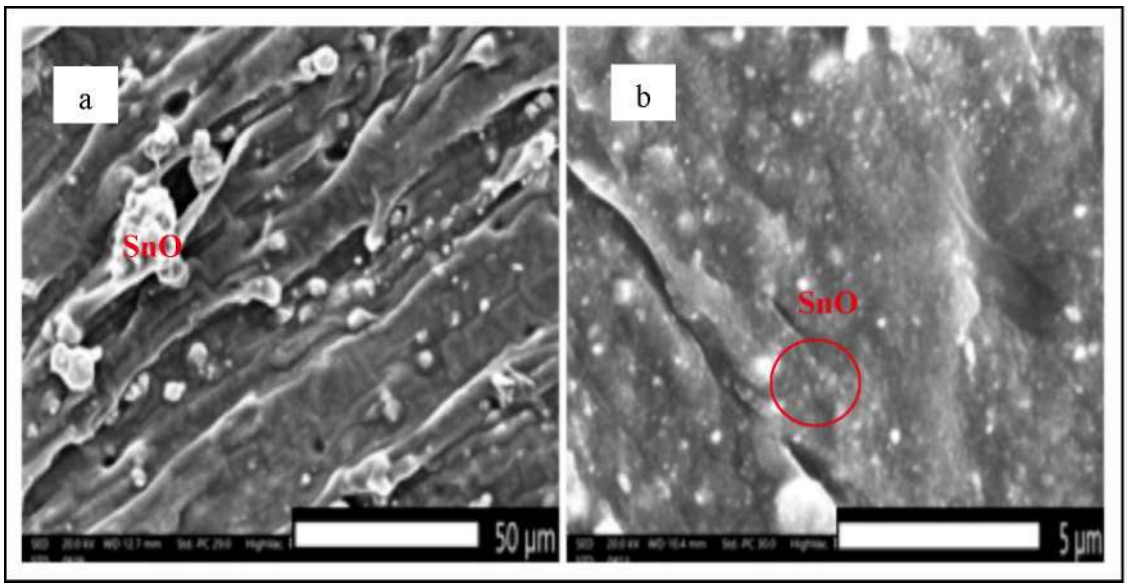

Figure 2.5 SEM Images of a) 50% of Micro-Tin Oxide/Silicon Rubber and b) 50% of Nano-Tin Oxide/Silicon Rubber [11]

50% micro-sized PbO/PDMS composite's structural properties are displayed in the SEM image Figure 2.6a. The micro PbO particles are dispersed throughout the PDMS matrix and are observably big and irregular in shape. Their distribution, however, is uneven, with observable agglomeration in different areas. Inhomogeneous material qualities may result from this uneven distribution. These big particles pop out, giving the composite a rather rough surface that could compromise its mechanical integrity [70]. Furthermore, the particle-matrix interface is less integrated, which could indicate a decrease in strength that could lead to defects or stress concentrations when subjected to mechanical stress.

On the other hand, the 50% nano-sized PbO/PDMS composite is shown in the SEM picture in Figure 2.6b. In this case, the PDMS matrix contains much smaller and more evenly distributed nano PbO particles. Better homogeneity and fewer surface flaws are indicated by the significantly smoother surface morphology that results from this more compressed distribution [70]. Better interaction and bonding with the PDMS matrix are made possible by the nanoparticles' larger surface area, which may improve their mechanical strength and radiation shielding capabilities.

In summary, the structure of the nano PbO/PDMS composite is better than that of the micro PbO/PDMS version. Better dispersion, a smoother, more consistent surface,

and a stronger interfacial bond with the polymer matrix are all provided by the nanoscale filler. These characteristics imply that, in terms of both structural integrity and functional qualities, nano PbO-filled composites may perform better than their micro-filled counterparts.

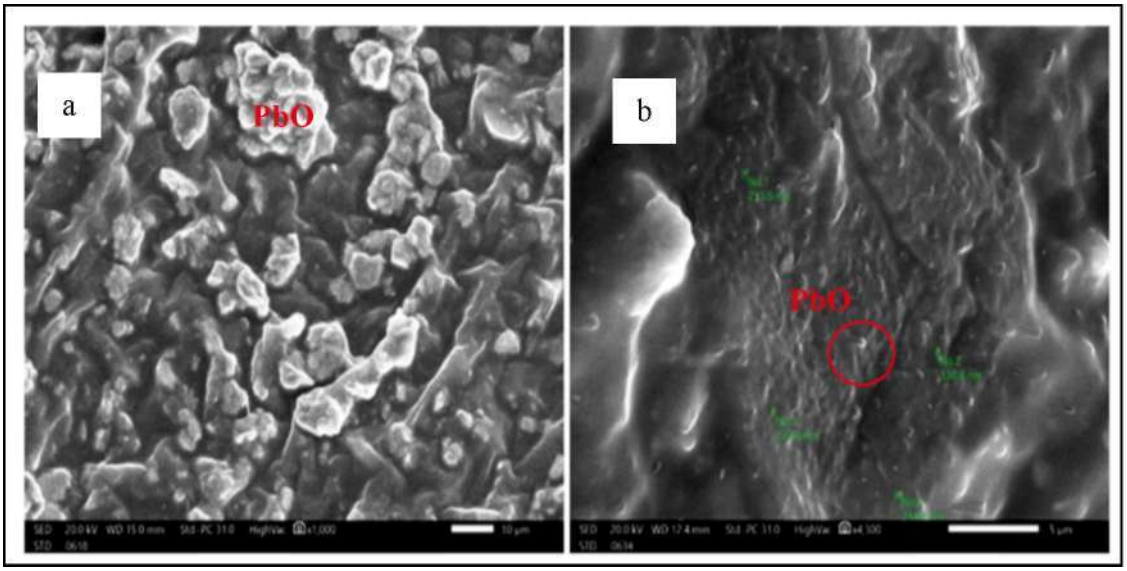

Figure 2.6 SEM Images of (a) 50% Micro PbO/PDMS and (b) 50% Nano PbO/PDMS [70]

Utilizing XRD analysis, which offers information on crystallinity, amorphous nature, and sample homogeneity, the internal arrangement and structural characteristics of materials were examined. Significant findings were obtained from the XRD study of recycled polyvinyl chloride (r-PVC), bismuth oxide nanoparticles, and a combination of r-PVC and bismuth oxide nanocomposites ranging the scattering angle range of 10° to 80° (Figure 2.7). A wide peak at about 24° was visible in the r-PVC XRD pattern, with smaller, less noticeable peaks at 29.22°, 38.21°, 49.87°, and 56.61°. In line with earlier research, these characteristics show that the r-PVC polymer matrix is amorphous. The polymer backbone's additives and impurities are responsible for the presence of a noticeable peak at 32.65° and weaker peaks above 40°. The amorphous structure is confirmed by these observations [69].

Bismuth oxide nanoparticles' XRD pattern showed clear, strong peaks at 27.94°, 33.70°, and 35.86°, which are indicative of the a-phase bismuth oxide and monoclinic structure. Pure a-phase bismuth oxide production is confirmed by these values, which are following Joint Committee on Powder Diffraction Standards (JCPDS) No. 76-1730

[69]. Both r-PVC and bismuth oxide peaks were present in the XRD patterns for the nanocomposites containing 5% and 35% bismuth oxide nanoparticles at the predicted locations. This demonstrates that the nanofiller was successfully incorporated into the polymer matrix. Additionally, the intensity of the peaks varied with the weight fraction of bismuth oxide, demonstrating a link between filler content and the composite's structural features. The XRD patterns showed that the materials maintained their amorphous nature even after bismuth oxide was added in amounts up to 35%. This persistence of amorphous properties points to the nanofiller's efficient combination and uniform dispersion within the polymer matrix [69].

In summary. The study by [69] reported that the diffraction peaks of the composites closely resembled the peaks of individual r-PVC and Bi_2O_3. The presence of well-defined and sharp peaks highlighted the representative of each integrated component. Conversely, the absence of sharp peaks or the emergence of new peaks suggested potential chemical interactions or effective dispersion of the metal fillers in the polymer matrix. Another study further reported a significant result of the incorporation of PbO and HDPE, whereby the peaks, that represented HDPE, were evident in the XRD patterns for both samples with 10% and 50% of PbO [61]. Previous researchers have used XRD to evaluate the integration of the composites, thus offering crucial information on their structural details [61], [69].

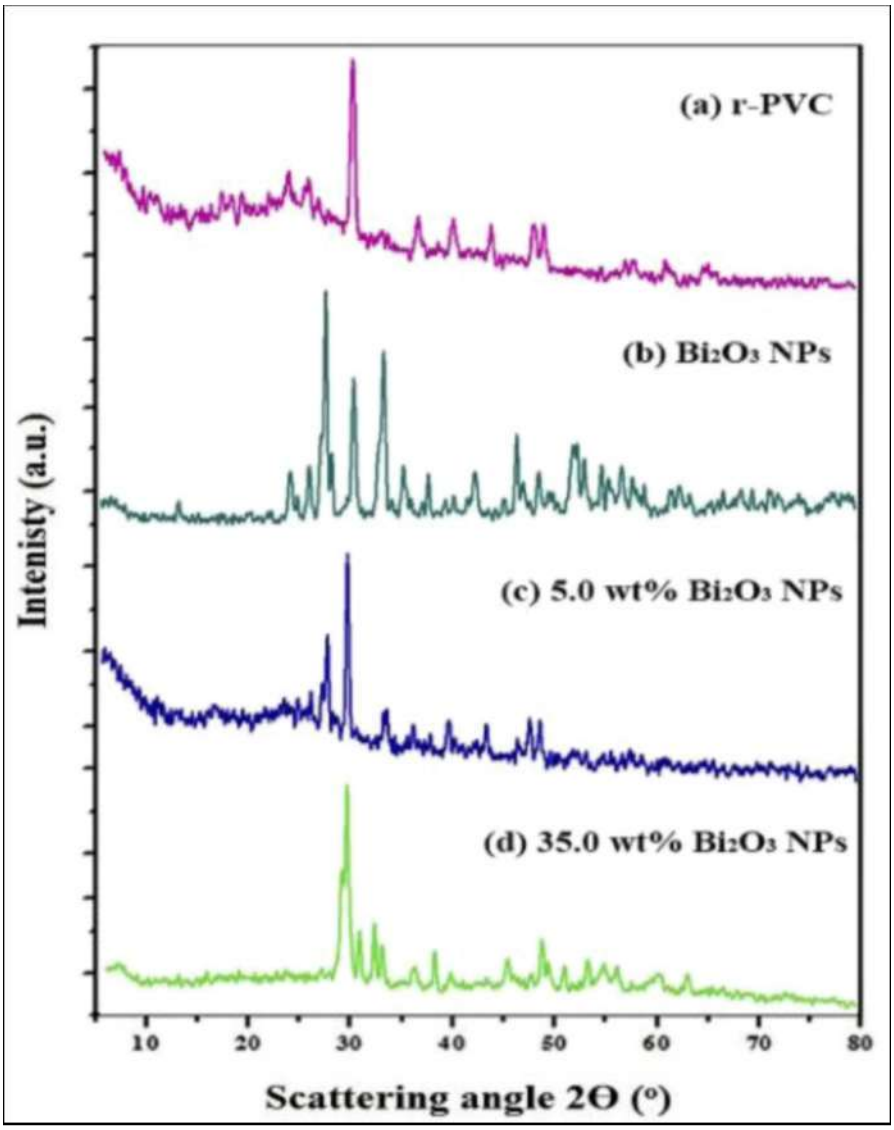

Figure 2.7 XRD Pattern of (a) r-PVC, (b) Bismuth Oxide Nanofillers, (c)R-PVC Mixed with 5% Bismuth Oxide Nanoparticles and (d) R-PVC Mixed with 35% Bismuth Nanoparticles [69]

2.8.5 Past Research Findings on Chemical Properties of the PDMS-Based Composites

The studies regarding FTIR analysis were conducted to identify the molecular bonding within the composites by taking the frequency range of 400 to 4000 cm^{-1} at room temperature. The characteristic bending and rocking peaks can be determined based on the FTIR spectra in Figure 2.8.

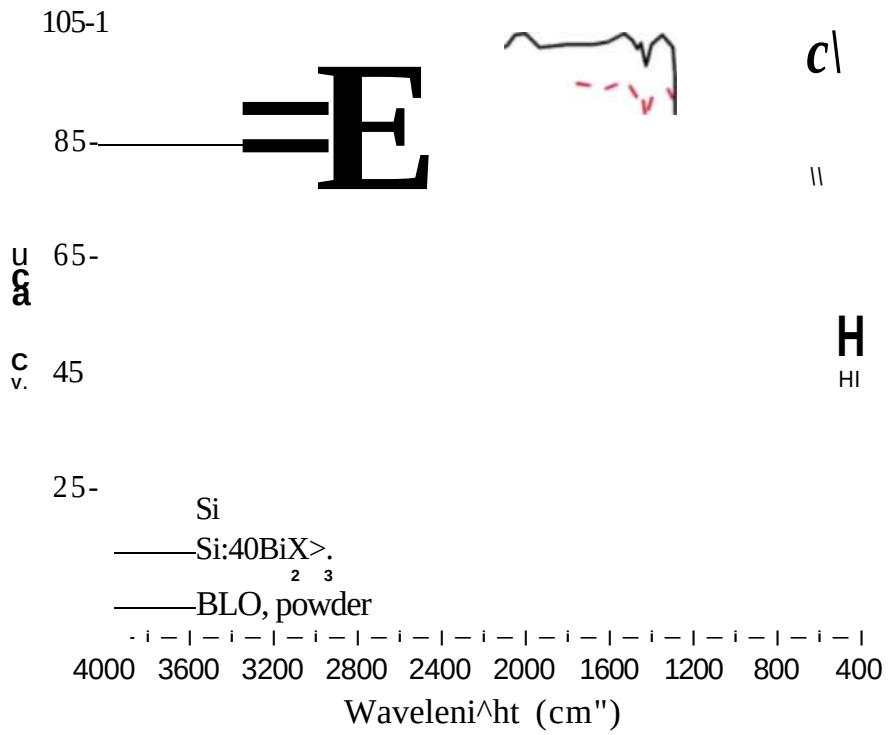

Figure 2.8 FTIR Spectrum of Silicon, Silicon Mixed with Bismuth Oxide and Bismuth Oxide Powder [86]

Significant data regarding the structure and interactions of polydimethylsiloxane, bismuth oxide powder, and the polydimethylsiloxane-bismuth oxide composite with 40% bismuth oxide content may be observed in the FTIR spectra. The outcomes demonstrate that bismuth oxide particles were successfully incorporated into the silicon-based matrix while preserving the polydimethylsiloxane's structural integrity [86]. The peak detected at about 1411 cm^{-1} is ascribed to the bending vibrations of water molecules that are absorbed from the natural surroundings. This characteristic is consistent across all samples, suggesting that ambient humidity affects both the bismuth oxide-containing composite and pure polydimethylsiloxane. This result demonstrates the effect of ambient moisture on the materials and is consistent with earlier findings.

The structural components of pure polydimethylsiloxane are confirmed by distinctive peaks in its spectrum. The silicon-methyl (Si-CFb) group's bending vibrations are represented by the peak at about 1262 cm^{-1}, while its rocking vibrations are represented by the peak at about 780 cm^{-1}. Furthermore, the silicon-oxygen-silicon (Si-O-Si) stretching bond, a crucial component of the siloxane backbone, is shown by

the peak at 1006 cm^{-1}. These peaks are still visible in the bismuth oxide-containing composite, indicating that the addition of bismuth oxide particles does not alter the polydimethylsiloxane matrix's basic structure [86].

Pure polydimethylsiloxane lacks a distinctive peak at around 410 cm^{-1}, which is found in both the bismuth oxide powder and the polydimethylsiloxane-bismuth oxide composite. The metal-oxygen bond, a property of bismuth oxide, is represented by this peak. This peak's existence in the composite revealed the successful integration of bismuth oxide into the silicon matrix. This integration is essential for improving the material's performance, especially in applications that call for better qualities like mechanical reinforcement or radiation shielding [69], [86].

To sum up, the FTIR study shows that bismuth oxide was successfully incorporated into the polydimethylsiloxane matrix. The successful blending of the two (2) materials is demonstrated by the retention of important structural characteristics of polydimethylsiloxane as well as distinctive spectrum contributions from bismuth oxide [86]. Therefore, these findings suggest that PDMS can create an excellent matrix for the integration of metals including tin.

2.8.6 Past Research Findings on Radiation Properties of PDMS-Based Metal Composites

The following Table 2.6 summarizes the radiation shielding properties of four different metal oxides mixed with PDMS which are lead oxide (PbO), tin oxide (SnCh), zinc oxide (ZnO), and bismuth (III) oxide (E^Cb), as analyzed in various studies. These composites were evaluated based on their radiation attenuation performance in terms of MAC, LAC, RPE, HVL, TVL, and MFP. Table 2.6 highlights the trends in each property as the concentration of these materials increases. Understanding the behavior of these materials in radiation shielding applications is crucial for the development of effective and safer alternatives to traditional shielding materials like lead.

The study on PbO reinforced PDMS composites demonstrates that the radiation shielding properties of these materials improve significantly with the increase in PbO

concentration. Both the MAC and LAC increase as PbO is added, highlighting enhanced radiation attenuation. The RPE also improves with nano-PbO composites, showing superior performance in shielding gamma radiation compared to micro-sized PbO. Furthermore, the HVL and TVL values decrease with increasing PbO concentration, signifying that less material is required to attenuate radiation. The MFP also shortens, indicating more frequent interactions between gamma photons and the composite. Nano-PbO exhibits a better performance than its micro-sized counterpart, with higher shielding capabilities across all metrics [70].

Table 2.6
Summarization Radiation Attenuation Properties of PDMS-Based Composites as the Metal Content Increase

-2 o ft **e o**	O	<	**3**			PH	**S** 1) **Pi**
PbO/ PDMS	Significant increase	Significant increase	Significant increase	Decrease	Decrease	Decrease	[70]
S11O2/ PDMS	Increase	Increase	Increase	Decrease	Decrease	Decrease	[9]
ZnO/ PDMS	Increase	Increase	Increase	Decrease	Decrease	Decrease	[83]
B12O3/ PDMS	Increase	Increase	Increase	Decrease	Decrease	Decrease	[32]
PDMS	Moderate efficiency compared toPHPS	Moderate efficiency compared toPHPS	Moderate efficiency compared toPHPS	Thicker layers for significant shielding	Thicker layers for significant shielding	Thicker layers for significant shielding	[14]

Sn02 reinforced PDMS composites follow a similar trend. As the concentration of nano-Sn02 increases, the MAC and LAC improve, indicating a better ability to attenuate gamma radiation. The RPE for nano-Sn02 composites is superior, particularly when compared to micro-Sn02 composites. Like PbO composites, the HVL and TVL decrease as Sn02 content rises, showcasing the material's effectiveness at lower thicknesses. The MFP also decreases with the increasing concentration of Sn02 metals, further reinforcing the composites with higher composition of nanoparticle leads to better radiation protection. Although Sn02 composites perform well, especially with nanoparticles, they do not surpass PbO composites in terms of overall shielding performance [9].

For ZnO reinforced PDMS composites, the MAC and LAC increase with ZnO content, and nano-ZnO outperforms micro-ZnO composites in terms of radiation attenuation. RPE values are higher for nano-ZnO composites, showing improved protection efficiency. Notably, ZnO composites exhibit the most rapid decrease in HVL and TVL, suggesting that ZnO nanoparticles provide an exceptionally fast and efficient reduction in radiation intensity. The MFP for nano-ZnO composites also shortens as the concentration increases, which is consistent with the trend observed in other nanoparticle-reinforced composites [31]. Despite this, ZnO composites are more efficient in terms of shielding at lower material concentrations compared to PbO or Sn02 composites.

Finally, the study on Bi203 reinforced PDMS composites reveals the highest performance across all radiation shielding metrics. The MAC, LAC, and RPE all show significant improvements with increasing Bi203 content, with nano-Bi203 showing superior radiation attenuation properties compared to its micro-sized counterpart. HVL and TVL values decrease rapidly, indicating that Bi203 composites are particularly efficient at lower thicknesses. The MFP also decreases with increasing Bi203 content, reflecting the material's effectiveness in photon interactions [32]. Bi203 composites are the most effective at providing radiation shielding, outperforming PbO, Sn02, and ZnO composites in most cases.

All four (4) composites including PbO, Sn02, ZnO, and Bi203 show promising results for radiation shielding, Bi203 reinforced PDMS composites stand out as the best overall performers, offering superior shielding properties across all key metrics. ZnO composites are the most efficient in terms of rapid attenuation and lower material usage. PbO and Sn02 composites also offer excellent performance, with nano-sized particles consistently outperforming micro-sized ones. However, Bi203 composites provide the most balanced solution in terms of both shielding effectiveness and material cost, making them ideal for radiation protection applications.

In conclusion, PDMS performs effectively as a matrix material for composites that provide radiation shielding. Its adaptability and versatility to include different metal fillers greatly increase the material's radiation attenuating efficiency. The benefits of

PDMS-based composites in maximizing radiation protection properties are highlighted by the comparative study of various composites reinforced with fillers like PbO, SnO2, ZnO, and Bi2O3 [9], [31], [32], [70]. The important parameters, such as MAC, LAC, HVL, TVL, and MFP, show that PDMS composites can be customized to provide better shielding for particular radiation types and intensities. PDMS is a promising material in the development of advanced, efficient, and adaptable radiation shielding solutions.

CHAPTER 3
RESEARCH METHODOLOGY

3.1 Introduction

The methodology is categorized into four (4) stages. The first stage is the preparation of tin/PDMS composites by adding tin filler (density = 7.31 g cm^{-3}) into the PDMS elastomer liquid containing dimethyl siloxane; dimethylvinylsiloxy-terminated, dimethylvinylated and trimethylated silica, ethylbenzene with curing agent containing siloxanes and silicones di-Me, Me hydrogen, dimethylsiloxane dimethylMnylsioxy-terminated, dimethylvinylated and trimethylated silica (Figure 3.1). The next stage is the morphological and structural characterization where the composites' structure has been analyzed for mineral composition and chemical bonding of the materials. After that, the third stage is radiation characterization where the composite is assessed for radiation shielding abilities. The last step is data processing and analysis where all the data has been calculated and analyzed to obtain parameters that can be used for comparison and understanding. The summarization of the laboratory work is described in the workflow (Figure 3.2).

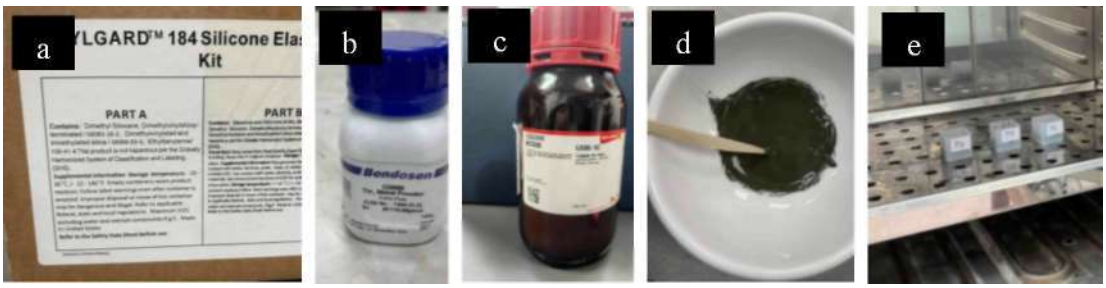

Figure 3.1a) Poly dimethylsiloxane Kit, b) Pure Tin Powder, c) Copper Tin Alloy, d) Mixture of Metal and Polymer and e) Heating Process in Oven at 100 °C

3.2 Stage I: Preparation of Tin and PDMS Composite Samples

In this stage, two (2) kinds of composites have been prepared using mixing methods, the control and the polymer-metal composite sheets. The mixture was poured into the mold and undergo a solidification process.

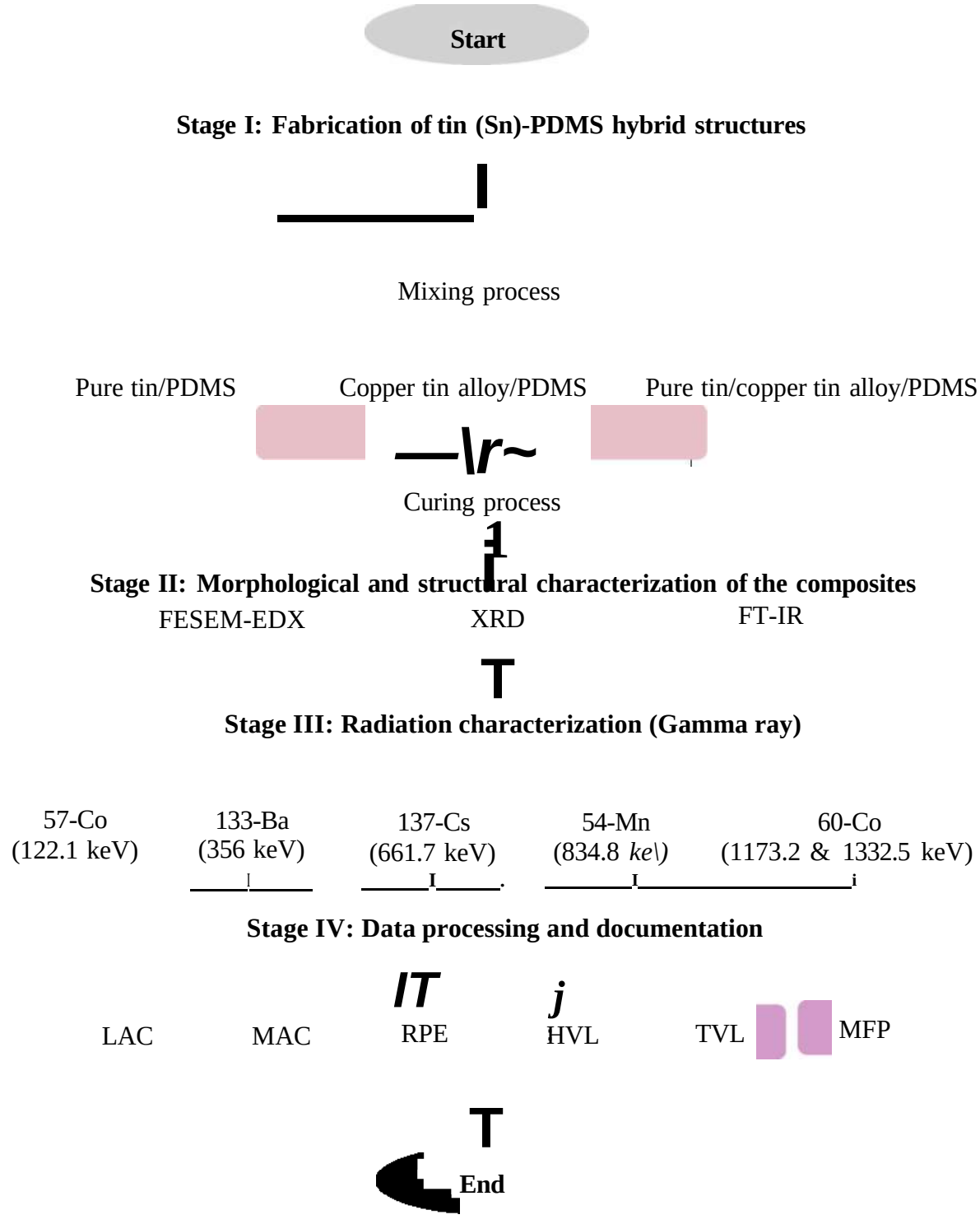

Figure 3.2 Flowchart of Research Methodology

3.2.1 Raw Materials

Tin metal powder, copper tin alloy powder, and PDMS polymer were the raw materials used in this investigation. Progressive Scientific Sdn. Bhd. provided the tin powder, while Sigma Aldrich provided the copper tin alloy. HardwareMISE Sdn. Bhd. provided PDMS, a viscous liquid polymer (3500 cP, 1.103 g cm^{-3}). To create radiation shielding composites, all powders were utilized as fillers. High-purity (99.99%) solid lead and tin plates were used as reference shielding materials for the comparative study. Lead had a density of 11.34 g cm^{-3} and a melting point of 327.5 °C, whereas tin had a melting point of 231.9 °C and a density of 7.31 g cm^{-3}. Both plates were acquired from Shandong Zhongqing Metal Materials Group Co., Ltd (Table 3.1).

Table 3.1
Material Properties of Metal and Polymer Used in This Study

Properties	**Tin metal**	**Copper tin alloy**	**PDMS polymer**	**Lead plate**	**Tin plate**
Symbol	Sn	$Cu_{84}Sn_5$	C_2H_6OSi	Pb	Sn
Form	Powder	Powder	Liquid	Solid	Solid
Particle size (APS)	8 µm	74 µm	-	-	-
Manufacturer/ Supplier	Progressive Scientific Sdn. Bhd.	Sigma Aldrich	HardwareMISE Sdn. Bhd.	Shandong Zhongqing Metal Materials Group Co.,Ltd	Shandong Zhongqing Metal Materials Group Co.,Ltd
Density (g cm^{-3})	7.31	8.8	1.103	11.34	7.31
Liquid viscosity	-	-	3500 cP	-	-
Purity (%)	99.8	-	-	99.99	99.99
Melting point	231.9 ℃	-	-	327.5 ℃	231.9 ℃

3.2.2 Control Preparation

The standard commercial lead plate, tin plate, and 100% fabricated PDMS composites were used as the control sample. To prepare the 100% fabricated-PDMS composite, the PDMS elastomer and curing agent were mixed at 10 parts of PDMS elastomer (density = 1.11 g cm^{-3}) with 1 part of curing agent (density = 1.03 g cm^{-3}). This fabricated PDMS control sample was fabricated at 0.5 cm thickness and was cured for 35 minutes at 100 °C to form a solidified composite. The commercial lead plate and tin plate were purchased from Shandong Zhongqing Metal Materials Group Co., Ltd at a specific thickness of 0.5 cm.

3.2.3 Mixing Process of Sample

A 5.0 mm thick tin-PDMS-based composite sheet was fabricated by composing tin powder and PDMS liquid polymer at different composition ratios. The composite was prepared by adding tin powder as filler at 10%, 20%, 30%, 40%, 50%, and 60% into the polymer matrix. The PDMS polymer functions as a binder to the tin powder. Table 3.2 shows the composition ratio of the composite and its label.

In the composite preparation, the tin powder has been weighed in the ceramic bowl according to the calculation based on the equation 2.9 in section 2.6. The PDMS liquid and curing agent were added to the tin powder ceramic bowl. Both ingredients were manually stirred for 60 seconds to ensure the powder could be dispersed evenly throughout the polymer matrix (Figure 3.3). The mixture was poured into the mould with the dimensions of 2 cm x 2 cm x 0.5 cm. The preparation and initial curing process occurred at room temperature. The initial curing process was done in a glass-vacuum desiccator to degas the air before being cured in a dry oven at 100 ^{o}C for 35 minutes. After that, the sample was left at room temperature for 30 minutes to cool down before being taken out from the mould and put into the closed container.

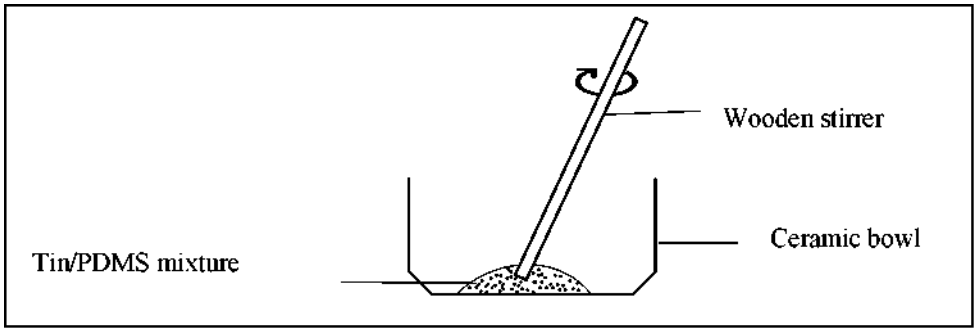

Figure 3.3 Illustration of Mixing Process of Tin/PDMS Composite

3.2.4 Curing Process

In the field of polymers and composites, curing involves the chemical reaction that transforms liquid or semi-liquid polymer into solid, hardened materials. This process is often initiated by heat, catalysts, or additives, leading to the formation of a stable and durable structure. In this experiment, the curing agent was used to expedite the solidification process. The sample underwent an initial curing process at room

temperature in a vacuum desiccator to degas the air for about 30 minutes and proceeded to curing at 100 °C for 35 minutes to enhance the composites' structure and minimize the curing time. Then, the composite was taken out from the mold and put into closed containers before characterization (Table 3.2).

Table 3.2
Label and Ratio for Each Composite in This Study

Sample label	Ratio (Metal :Polymer)
Control	
C(100%PDMS)	0:10
CT (99.99% tin)	10:0
CL (99.99% lead)	10:0
Pure tin/PDMS	
PT1	1:9
PT2	2:8
PT3	3:7
PT4	4:6
PT5	5:5
PT6	6:4
Copper tin alloy/PDMS	
TA1	1:9
TA2	2:8
TA3	3:7
TA4	4:6
TA5	5:5
TA6	6:4
Pure tin/copper tin alloy/PDMS	
PA1	1:9
PA2	2:8
PA3	3:7
PA4	4:6
PA5	5:5
PA6	6:4

3.2.5 Density Measurement

The density of the fabricated composites was determined using both theoretical and experimental approaches. The theoretical density was calculated using the rule of mixtures by considering the known densities and weight fractions of each constituent material based on the equation 2.9 in section 2.6. The experimental density was determined by measuring the mass of each fabricated sample using an analytical

balance, while the volume was obtained from the measured geometrical dimensions of the samples. The experimental density was then calculated using the same equation as theoretical density.

3.3 Stage II: Morphological and Structural Characterization

Stage II includes the morphological and structural characterization, which was conducted to study the surface morphology and mineral composition of the tin/PDMS hybrid polymer structures. Physical properties like mass, volume, and density were determined in the physical-mechanical laboratory at UiTM Cawangan Pulau Pinang. Morphological studies of the samples' cross-sectional using FESEM, and elemental analysis using EDX. The FESEM/EDX analysis was conducted using facilities at Usains Biomics Laboratory Testing Services Sdn Bhd, Universiti Sains Malaysia. The composite samples were subjected to XRD analysis at School of Materials and Mineral Resources Engineering.

3.3.1 Field Emission Scanning Electron Microscopy (FESEM)

FESEM is a crucial tool in analysing the morphological and structural properties of the composites, offering high-resolution imaging of material surfaces with nanoscale precision (Figure 3.4). Operating on the principle of scanning a focused electron beam using a field emission gun across the specimen, FESEM captures signals and is used to create detailed images showcasing the topography, composition, and elemental distribution of the sample. By offering 3D imaging capabilities and enabling the study of nanoscale features, FESEM facilitates a comprehensive understanding of material properties [9], [70].

The microstructural characterization of the tin-PDMS composites was conducted using an Extreme High-Resolution Field Emission Scanning Electron Microscope (XHR-FESEM), Model FEI Verios 460L. To observe the internal morphology, each sample (Table 3.3) was carefully cut to expose the cross-sectional region, enabling detailed analysis of the filler distribution and interfacial interactions within the composite (Figure 3.5).

Before imaging, the samples were coated with a thin layer of gold using a sputter coater. This conductive layer minimizes charging effects and improves image clarity, which is essential since both PDMS, and tin are non-conductive materials. FESEM analysis was performed at five magnifications: 100×, 500×, 1000×, 5000×, and 10,000×. These magnifications were selected to examine both macro- and micro-level structural features, including filler dispersion, porosity, and the interface between the tin particles and the PDMS matrix. Imaging was carried out on three different spots per sample to ensure representative and reliable observations.

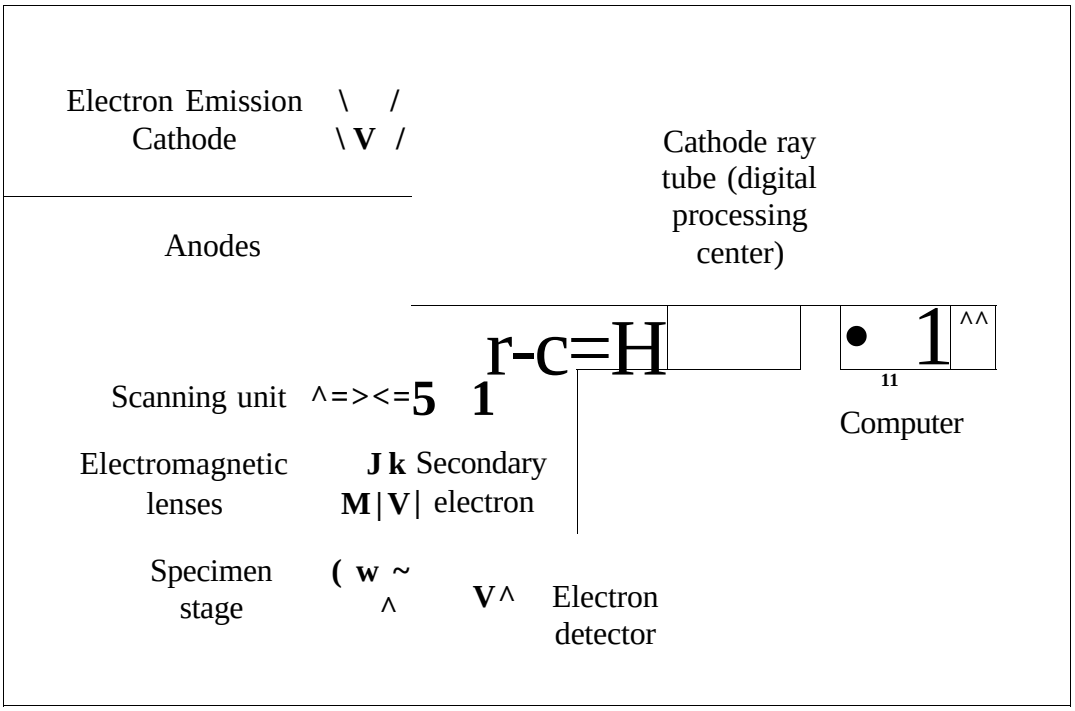

Figure 3.4 Illustration of FESEM Process

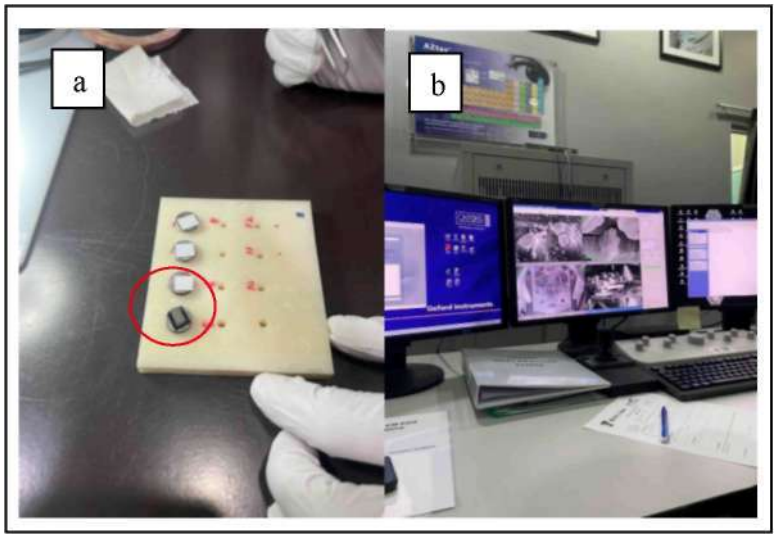

Figure 3.5 a) Cross-Sectional Surface of the Composites and b) FESEM Monitor

Table 3.3
Overview of Composites Samples with Varying Metal Filler Concentrations

Composite	**Control PDMS**	**10% metal**	**20% metal**	**30% metal**	**40% metal**	**50% metal**	**60% metal**
Label	Control	PT1	PT2	PT3	PT4	PT5	PT6
Pure tin/PDMS		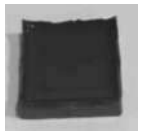					
Label	Control	TA1	TA2	TA3	TA4	TA5	TA6
Copper in alloy/PDMS							
Label	Control	PA1	PA2	PA3	PA4	PA5	PA6
Pure tin/copper tin alloy/PDMS	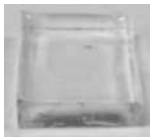						

3.3.2 Energy-Dispersive X-ray Spectroscopy (EDX)

EDX is a chemical analysis used to reveal the presence of elements in the specimens. The generated graph describes the x-axis (energy of X-ray) and y-axis (concentration) (Figure 3.6). The peak height indicates the quantification of each element concentration in the samples meanwhile the position of the peaks helps to identify the elements [28], [87]. Elemental analysis of the tin-PDMS composite was performed using Energy-Dispersive X-ray Spectroscopy (EDX) integrated with the FEI Verios 460L XHR-FESEM system. The cross-sectional samples, previously gold-coated for FESEM imaging, were used for EDX analysis to identify and confirm the elemental composition and distribution within the composite.

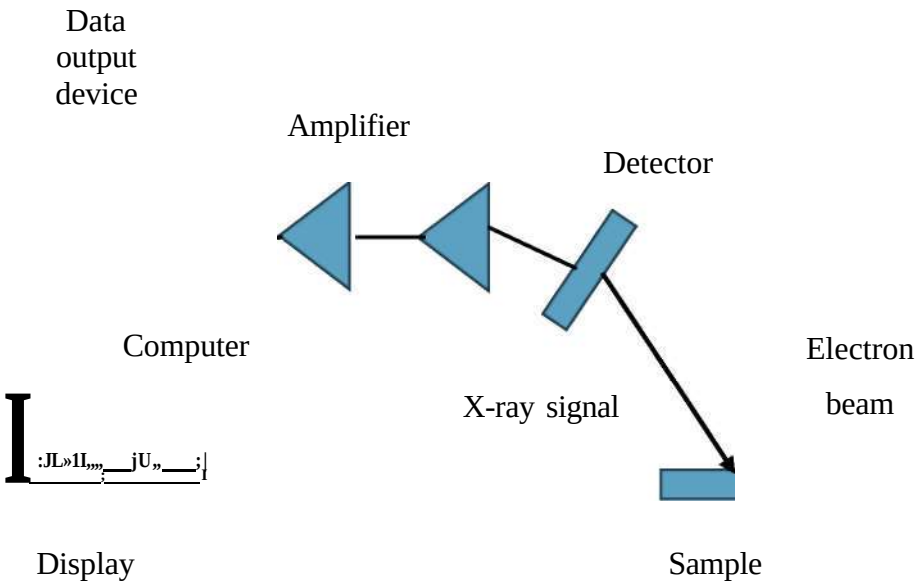

Figure 3.6 Schematic Diagram of EDX Data Processing

3.3.3 X-Ray Diffraction (XRD)

XRD is a test used to characterize the physical properties of the materials by assessing the degree of the composite's crystallinity within the metal/polymer structure (Figure 3.7). In this research, one of the structural analyses was performed using X-ray diffraction (XRD, Bruker AXS D8) with CuKa radiation X = 1.5406 A). XRD involves directing X-rays onto a crystalline sample, resulting in the scattering of X-rays by the

crystal lattice. The diffracted X-rays generate a diffraction pattern, which is then analyzed to reveal information about the arrangement of atoms within the crystal structure. The test also provides insights into the complexity of metal and polymer interaction and integration. For instance, if the peak reveals a different unknown phase, the foreign atoms are likely to present [69].

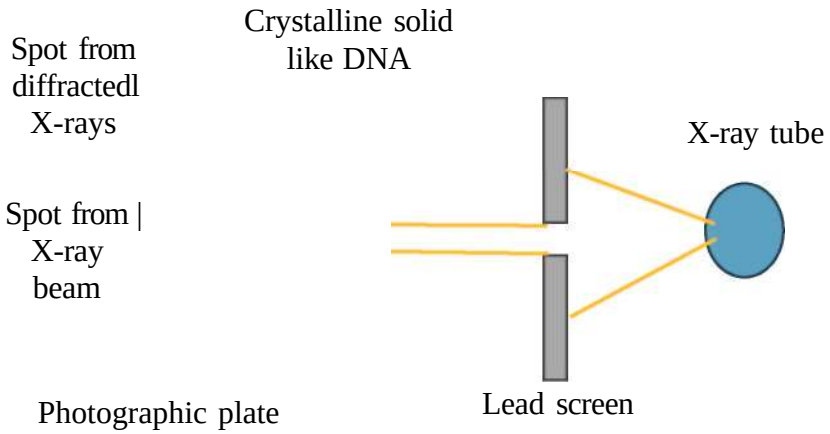

Figure 3.7 Schematic Diagram of XRD

3.3.4 Fourier Transform Infrared (FTIR)

The chemical interactions and functional groups discovered in the tin-PDMS composites were examined using FTIR (Figure 3.8). A PerkinElmer Spectrum 100 series FTIR spectrometer, which operates in the wavenumber range of 4000 to 400 cm^{-1}, was used to perform the analysis. At room temperature, all measurements were made. This spectrum range includes any possible shifts or extra peaks resulting from interactions with tin filler particles, as well as the distinctive vibrations of important functional groups like Si-O-Si, Si-CFb, and C-H, which are normally present in polydimethylsiloxane [32], [88].

FTIR analysis is used in this study to find any structural alterations or interactions between the added tin particles and the PDMS matrix. Peak intensity, position, or new peak formation changes reveal if physical or chemical interactions are occurring and how they might impact the structural and functional characteristics of the composite [48], [86]. This research used the FTIR with brand PerkinElmer, model Spectrum 100

series with a 4000-400 cm^{-1} wavenumber to acquire molecular vibration data on samples at room temperature.

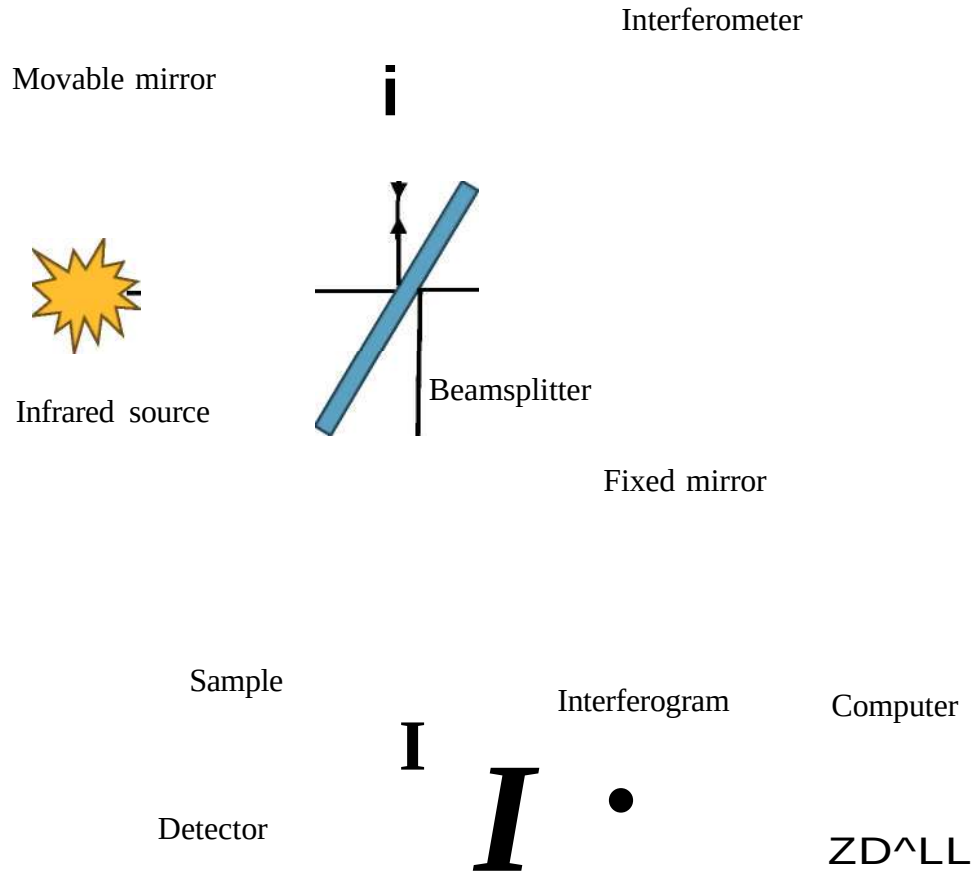

Figure 3.8 Schematic Diagram of FTIR Analysis Process

3.4 Stage III: Radiation Characterization

In stage III, the fabricated composite sheets have proceeded to radiation characterization using gamma rays as illustrated in Figure 3.9. The process was conducted at the Nuclear Science Laboratory, Faculty of Science and Technology, Universiti Kebangsaan Malaysia (Figure 3.10). In this stage, the composite sheets are positioned between the photon source and the detector, allowing for the measurement and data recording of radiation count activity for 60 seconds that penetrates through the composite material. The penetrated rays exhibit the balance of the amount of radiation that has been absorbed and attenuated in the composite. The calibration is performed before conducting the procedure using Co-60 (1173.2 and 1332.5 keV).

Gamma-ray is produced through different sources of radionuclides such as Manganese-54 (^{54}Mn), Cesium-137 (^{137}Cs), Cobalt-60 (^{60}Co), Cobalt-57 (^{57}Co) and Barium-133 (^{133}Ba). Each source emits different energy levels that will be struck to the sample and measured by gamma spectrometer. Table 3.4 shows all five (5) radionuclides with six (6) gamma energy were used in this study to assess the radiation attenuation and shielding performance of the Tin-PDMS composites.

Table 3.4
Gamma Ray Energies Used for Radiation Characterization

Source	Photon energy (keV)	Half-life
^{57}Co	122.1	271.8 days
^{133}Ba	356	10.51 years
^{137}Cs	661	30.17 years
^{54}Mn	834.8	312.2 days
^{60}Co	1173.3	5.271 years
	1332.5	

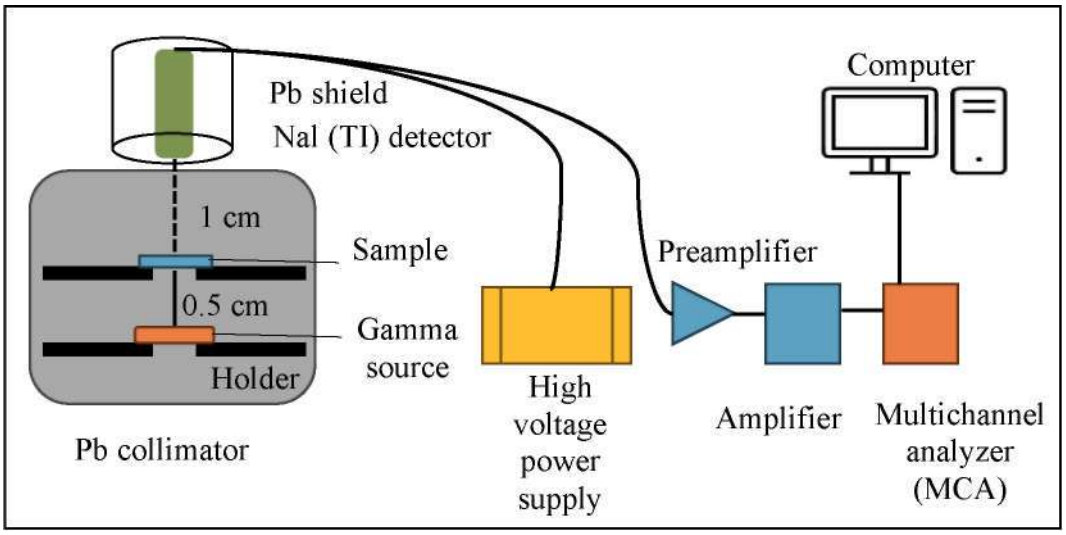

Figure 3.9 Illustration of Set Up for Gamma Characterization Using Gamma Spectroscopy

Figure 3.10 a) Radionuclide Sources b) The Multichannel Analyzer (MCA) Interface and c) The Experimental Set Up

3.5 Stage IV: Data Analysis and Documentation

The relevant equations from section 2.4 were used to calculate the LAC, MAC, RPE, HVL, TVL, and MFP of the composite. The results obtained were compared with established commercial lead (Pb) standards to verify the shielding efficiency of the composites [13], [14], [89]. The lead equivalent for optimized samples was calculated using equation 2.9 in section 2.4. This comprehensive scientific methodology ensures a thorough investigation of the polymer-metal composite sheets, their structural and radiation properties, and their potential as radiation shielding.

CHAPTER 4
RESULTS AND DISCUSSION

4.1 Introduction

FESEM-EDX, XRD, FTIR, and gamma-ray spectroscopy were used in this study to thoroughly characterize the fabricated PDMS-based composite materials. Important information about the metal fillers' surface shape and dispersion behaviour within the PDMS matrix was revealed by the FESEM investigation. Composites comprising copper tin alloy displayed spherical copper particles that peel off from the PDMS matrix, indicating lower integration between metal and polymer. Pure tin particles showed a more uniform distribution and strong adhesion with the polymer. Further structural characterization was done using XRD to obtain the crystalline phases present within the material.

With the distinctive peaks of PDMS preserved and slight shifts or intensity variations indicating potential physical interactions between the polymer chains and filler particles, FTIR study verified the successful integration of metal fillers into the PDMS matrix. The radiation shielding performance of the composites was assessed using gamma-ray spectroscopy, with particular attention focused on important parameters like LAC, MAC, RPE, HVL TVL, and MFP. The findings indicated that the shielding properties of the composites were improved by adding more metal filler, especially tin. The potential of tin-PDMS composites as potential lead-free substitutes for low-energy gamma-ray shielding applications was confirmed by the enhanced attenuation characteristics of the investigated samples with increased metal contents

4.2 Physical Properties for Each Composite

The physical characteristics of the produced composite samples, including both theoretical and experimental values, are compiled in this section. With slight changes in thickness, each composite was created with set dimensions of 2.0 cm × 2.0 cm × 0.5 cm. The experimentally determined thickness, mass, and consequent density are shown

in Table 4.1 together with the theoretical mass and density subjected to 0.5 cm thickness.

Table 4.1
Data of Physical Properties for Each Composite

Samples	Thickness (cm)	Mass (g)		Density (g cm^{-3})	
		Theoretical	Experimental	Theoretical	Experimental
C	0.5	2.21	2	1.103	1.0250
CL	0.5	22.68	21.87	11.340	10.940
CT	0.5	14.62	15.14	7.310	7.570
PT1	0.46	3.45	3.15	1.724	1.607
PT2	0.52	4.68	4.23	2.344	2.066
PT3	0.52	5.93	5.83	2.965	2.915
PT4	0.51	7.17	6.79	3.586	3.395
PT5	0.49	8.41	8	4.207	4.000
PT6	0.54	9.65	9.35	4.827	4.500
TA1	0.49	3.75	3.5	1.873	1.786
TA2	0.49	5.28	4.91	2.642	2.455
TA3	0.51	6.82	6.47	3.412	3.235
TA4	0.52	8.36	8.04	4.182	3.941
TA5	0.52	9.9	9.54	4.952	4.770
TA6	0.53	11.44	11.23	5.721	5.505
PA1	0.49	3.69	3.58	1.843	1.827
PA2	0.47	5.16	4.94	2.583	2.520
PA3	0.54	6.64	7.3	3.323	3.578
PA4	0.51	8.12	7.6	4.063	3.800
PA5	0.52	9.6	9.19	4.803	4.595
PA6	0.56	11.08	11.55	5.542	5.553

The data shows theoretical and actual values for thickness, mass, and density for various composite samples made of PDMS reinforced with different types and amounts of metal fillers. The control samples (C, CL, and CT) serve as benchmarks. Sample C, made of pure PDMS, shows a low density due to the absence of metal fillers, with only a slight discrepancy between theoretical and experimental values, likely due to minor air entrapment or curing [90], [91]. In contrast, CL and CT show perfect agreement between theoretical and experimental values, indicating a well-prepared and uniform composite with minimal experimental error. These findings support the accuracy of the fabrication process and theoretical computations.

For the PT and TA series, a clear trend of increasing density is observed as the metal content increases from 10% to 60%. In all cases, the experimental density is slightly lower than the theoretical value. For example, PT6 shows a theoretical density of 4.827 g cm^{-3} compared to an experimental value of 4.5 g cm^{-3}. These discrepancies could be due to the curing process that reduced the mass of PDMS, or air bubbles entrapped within composites at higher tin concentrations. Agglomeration of tin particles at high filler content might also contribute to non-uniform distribution, which affects the actual density [30], [56].

The PA series, which combines both pure tin and copper tin alloy in the PDMS matrix, exhibits more variation compared to the PT and TA series. While most PA samples also show experimental densities slightly below theoretical values, PA3 stands out with a higher experimental mass and density than the calculated theoretical value. This points to a potential overfilling that occurred during manufacturing or an uneven dispersion of metal fillers that produced a denser area in the sample. The other samples in this group continue the general trend of slightly lower experimental values, pointing to potential sedimentation or poor distribution particularly due to the presence of multiple types of metal fillers [45], [76], [92].

In addition to these physical properties, the developed innovative composites offer ergonomic and environmental advantages. They are significantly lighter than conventional lead and free from heavy metal toxicity, addressing the potential comfort for long-term wear and concerns regarding disposal and environmental safety. The flexibility and moldability of PDMS further enable the design of custom-fit or layered shielding structures that could be modified into garments, equipment casings, or structural barriers.

In summary, the overall data show a consistent trend of increasing density with rising metal content across all sample series. The experimental densities are generally close to the theoretical values, indicating a good fabrication process. However, minor discrepancies, most likely due to air entrapment, agglomeration, or inhomogeneous dispersion suggest that improvements in mixing and curing methods could enhance composite uniformity.

4.3 Morphology Structure Analysis Using FESEM

Figures 4.1, 4.2, 4.3 and 4.4 illustrate the cross-sectional FESEM micrograph image of the control PDMS composite and PDMS consisting of homogenously distributed tin fillers with different weight percentage ratios.

Several studies have stated that the polymer could be cured at room temperature and fastened up using UV light [93], [94]. The challenge of this study concerns the weak integration between metal and polymer matrix as no heating process has been done, and the process takes time to fully cure. As the curing process takes time, the sedimentation of metal filler occurred which may cause improper distribution of metal filler within the polymer matrix. Thus, poor integration between polymer and metal powder may cause peeling off of metal from polymer, which is reflected by the weak bond between them both and inefficient composites as shielding materials.

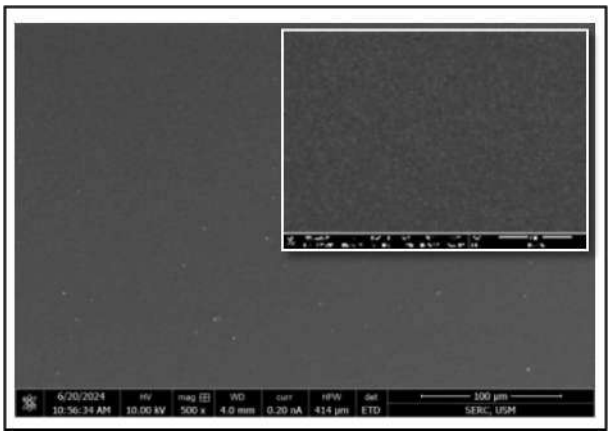

Figure 4.1 Control PDMS with No Metal Particles Seen

According to the FESEM analysis, the distinct morphological differences among the three (3) composite groups: PT, TA, and PA. The dispersion, adhesion, and overall structural integrity of the metal fillers within the PDMS matrix varied depending on the type and concentration of the fillers. In the PT composites, the particles appeared well-dispersed and uniformly integrated within the PDMS matrix. The composite exhibited a relatively stable structure, with minimal phase separation or agglomeration signs. As the filler concentration increased, a greater number of metal particles were observed, yet the uniformity remained consistent which suggests that PT maintains strong interfacial adhesion with PDMS. The smooth and continuous morphology further indicates effective wetting and bonding between PT and the polymer matrix, allowing

for homogenous dispersion [4], [5]. The curing temperature was optimal as the metal particles appeared well distributed with the PDMS matrices without any sedimentation.

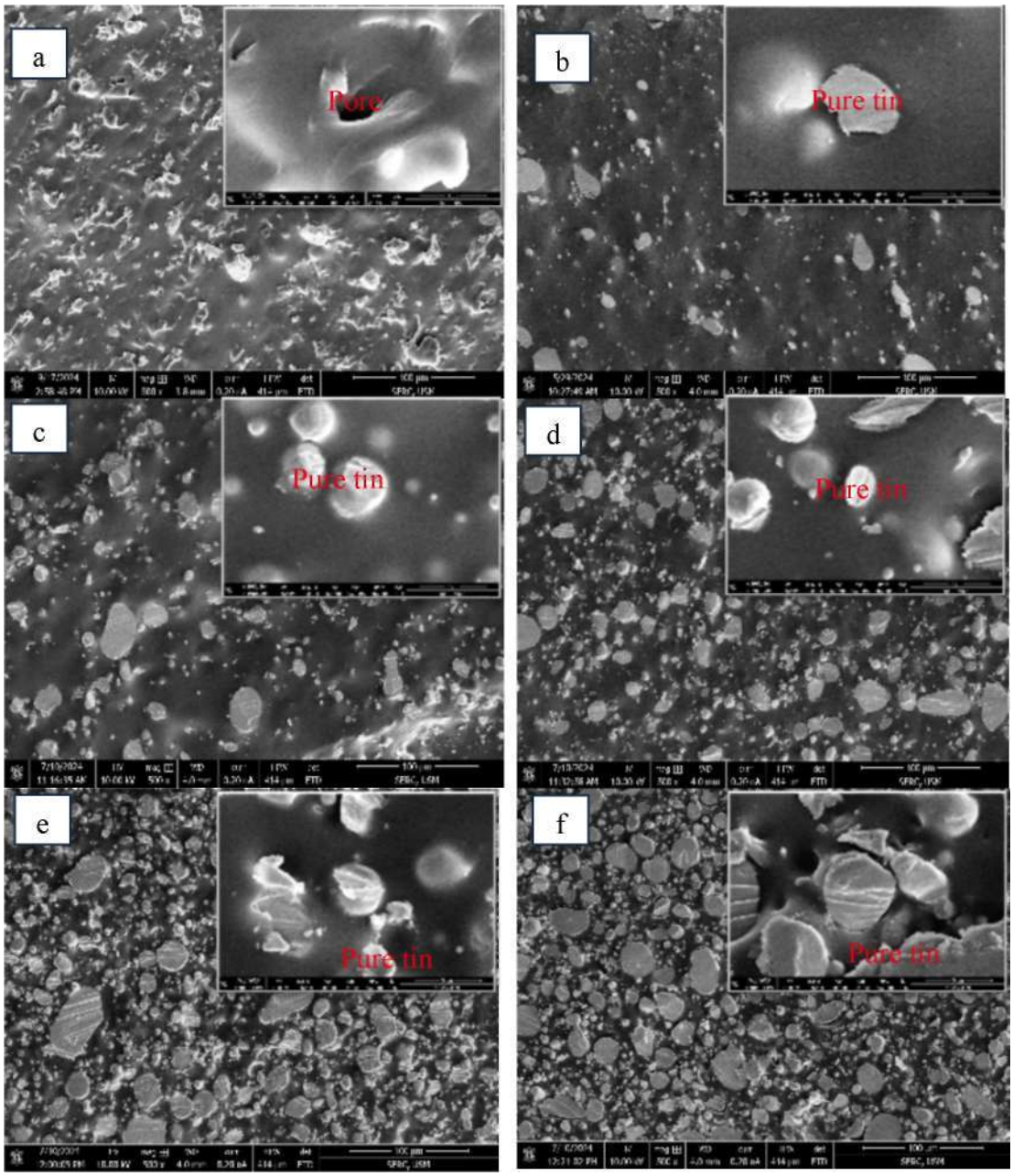

Figure 4.2 FESEM images of PT Samples at Two (2) Different Magnifications. The Larger Background Images Show Surface Morphology at 500× Magnification, While the Smaller Inset Boxes Display Higher-Resolution Images at 10 000× Magnification for Each Sample: (a) PT1, (b) PT2, (c) PT3, (d) PT4, (e) PT5, and (f) PT6.

Conversely, the TA composites exhibited poor adhesion with PDMS. FESEM images showed that the particles were predominantly spherical and less integrated into the polymer matrix, often appearing detached. This detachment was particularly evident in samples with higher filler concentrations, as seen in Figure 4.3f, where peeling of

metal regions was observed when the sample was cut. The gap can be seen at 10 000× magnification in Figure 4.3d, suggesting the peel-off of the copper particles that cause pores within the composite.

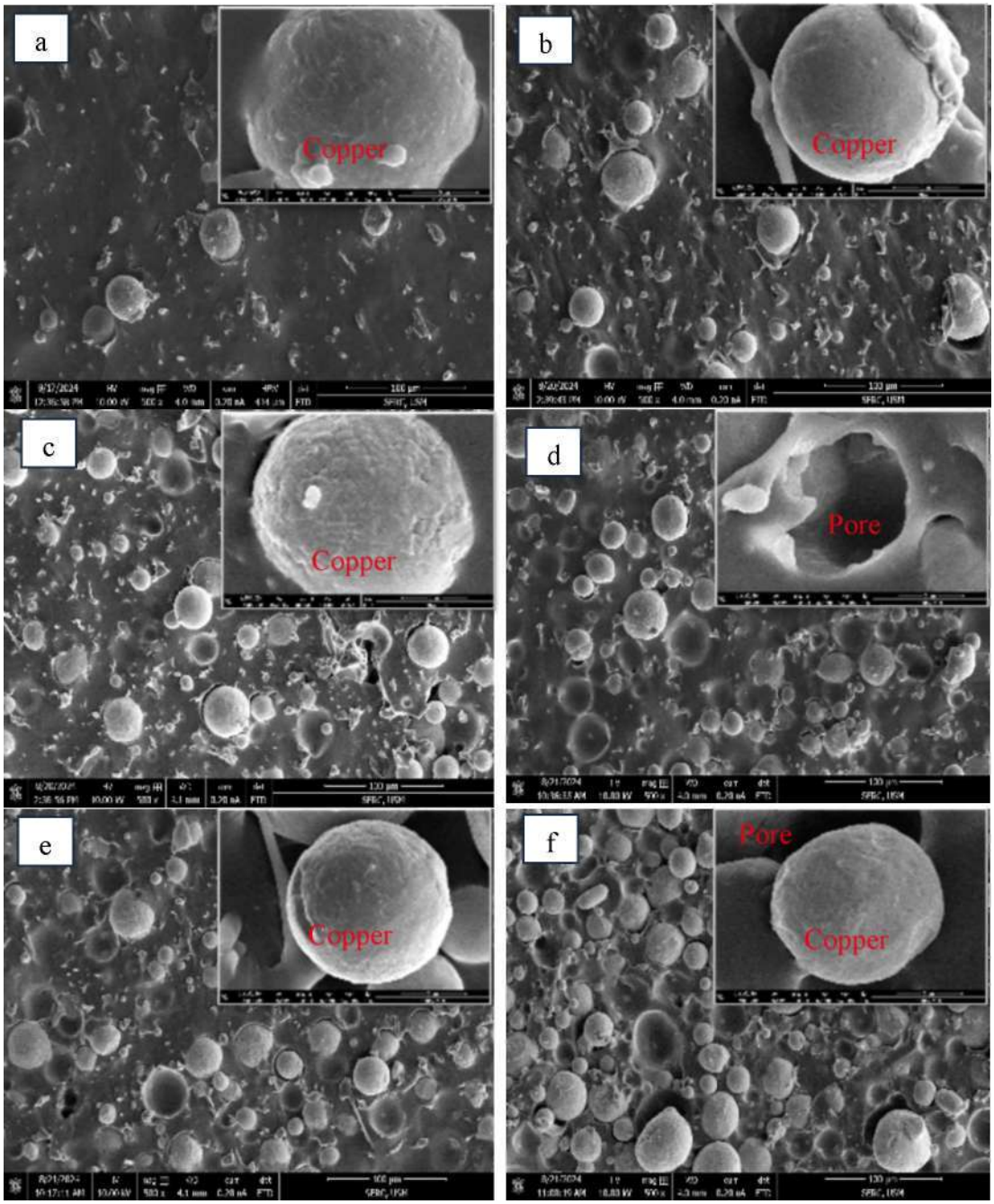

Figure 4.3 FESEM Images of TA Composites at Two (2) Different Magnifications.The Larger Background Images Represent Surface Morphology at 500× magnification, While The Smaller Inset Boxes Display High-Resolution Images at 10 000× Magnification for Each Sample: (a) TA1, (b) TA2, (c) TA3, (d) TA4, (e) TA5, and (f) TA6.

The weak bonding between TA and PDMS could be attributed to differences in the particle morphology. The spherical shape of copper tin alloy particles likely reduced mechanical interlocking, further contributing to detachment issues. The increasing metal content in these composites intensified the instability, further separating the metal filler from the matrix [95].

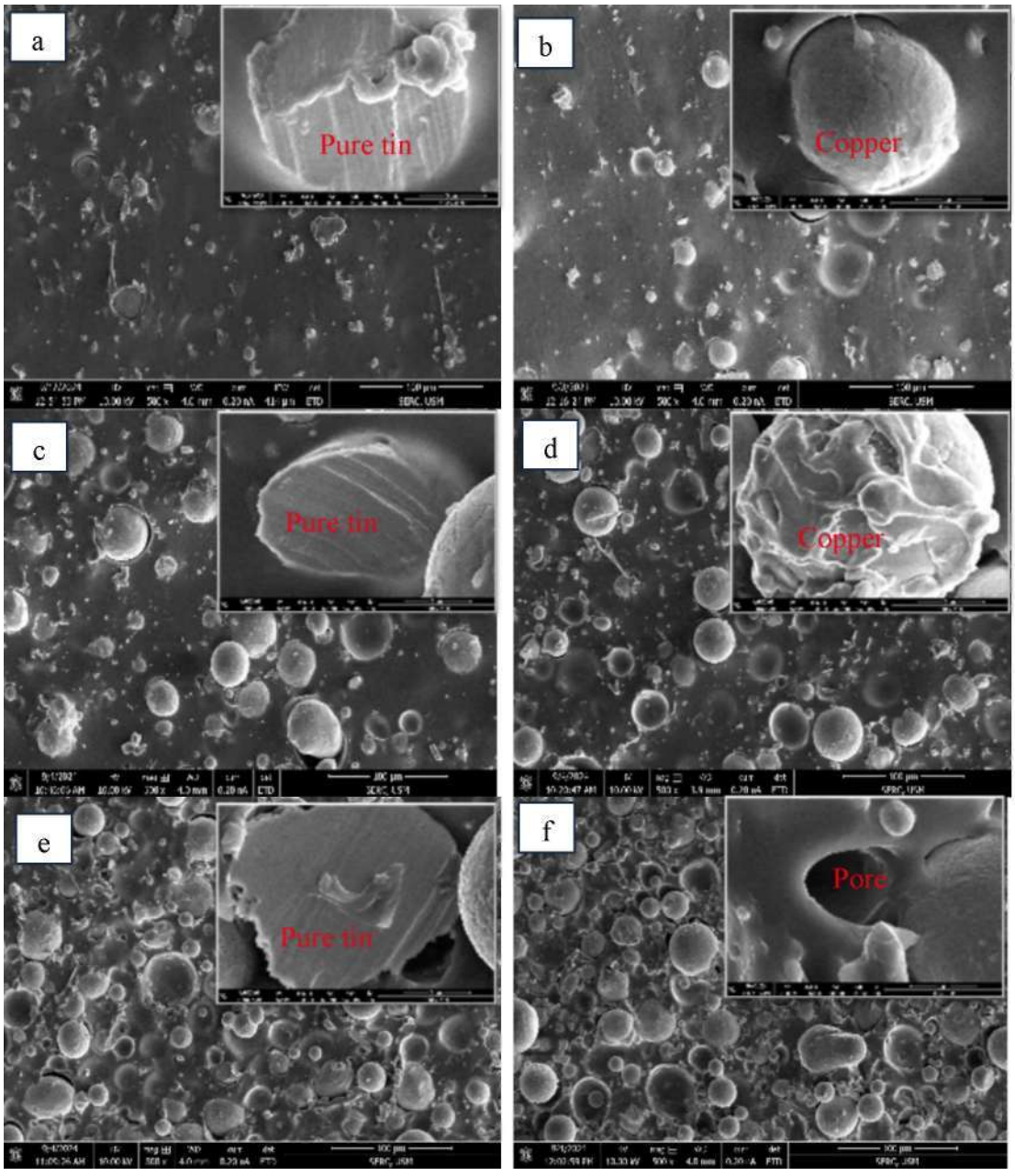

Figure 4.4 FESEM Images of PA Composite Samples Captured at Two (2) Magnifications. The Main Images Illustrate the Overall Surface Morphology at 500× Magnification, While the Inset Boxes Provide Detailed Views at 10,000× Magnification for Each Sample: (a) PA1, (b) PA2, (c) PA3, (d) PA4, (e) PA5, and (f) PA6.

The PA composites exhibited a combination of both behaviors. While pure tin particles remained well-integrated, the presence of copper tin alloy resulted in partial detachment, indicating a compromise in overall bonding strength. The observed gaps within the cross-sectional composites can be seen lower compared to TA samples, likely due to the combination of two (2) different metal particles. The varying interactions between the two metal fillers suggest that pure tin contributes to maintaining structural integrity, whereas copper tin alloy weakens the composite's stability [56], [96]. This highlights the importance of filler compatibility with the polymer matrix in determining the mechanical properties of the final material.

The observed trends from all three (3) different series emphasize that as the metal fillers increase, the particles can be seen compact within the cross-sectional area. Overall, the findings suggest that pure tin is highly compatible with PDMS, forming a stable and uniform composite, while copper exhibits weak adhesion and detachment, particularly at higher concentrations. The PA composites demonstrate an intermediate behavior, reinforcing the importance of interfacial interactions in composite fabrication. Future studies should focus on improving copper tin alloy compatibility with PDMS through surface modifications and optimized processing techniques to enhance overall composite performance.

4.4 Elemental Composition Analysis Using EDX Analysis

The elemental composition analysis of PT, TA, and PA composites highlights distinct trends in the distribution of key elements as the metal filler content increases in Table 4.2. Additionally, the control sample, which consists solely of the polymer matrix without metal fillers, serves as a reference for comparison.

The oxygen content decreases as the metal filler increases in a composite material, likely due to the relatively low proportion of PDMS as the amount of metal filler increases. Since the polymer matrix often contains oxygen in its chemical structure, a higher metal content would reduce the overall oxygen content in the composite. Other than that, tin might have a propensity to react with oxygen, forming stable metal oxides. If these oxides form and are isolated from the bulk composite, the overall oxygen content measured within the composite could appear lower [97], [98].

Since silicon and carbon come from the polymer matrix, the control composite naturally has the highest silicon (39.86%) and carbon (28.80%) contents. Significant amounts of oxygen (27.39%) are also found, which is normal given the polymer structure. Crucially, the control sample contains no detectable tin, indicating that it is entirely composed of the polymer and does not include any metal.

Table 4.2
Elemental Composition (Weight %) in the Tin-PDMS Composite from EDX Analysis.

lements (wt%)

Composites	C	O	Si	Cu	Sn
C	28.80	27.39	39.86	3.95	0.00
PT1	19.31	22.51	31.01	12.67	14.49
PT2	25.14	30.36	28.77	2.30	13.43
PT3	19.75	27.48	28.66	3.63	20.48
PT4	18.16	27.52	28.69	3.55	22.07
PT5	15.44	28.20	19.83	4.45	32.07
PT6	7.52	19.97	10.93	4.12	57.45
TA1	22.77	19.49	29.71	25.61	2.42
TA2	24.02	20.80	30.82	22.35	2.01
TA3	19.70	15.26	24.89	35.25	4.90
TA4	21.44	19.07	26.91	28.18	4.41
TA5	19.05	16.00	24.08	35.73	5.14
TA6	15.39	10.91	15.37	51.45	6.88
PA1	22.76	23.73	32.97	12.76	7.78
PA2	21.37	22.91	32.92	18.47	4.34
PA3	18.23	17.00	21.96	35.49	7.31
PA4	16.22	14.19	18.98	40.79	9.83
PA5	19.78	18.18	23.93	28.18	9.92
PA6	17.44	15.48	18.10	36.15	12.83

A potential reason for the presence of traceable copper (3.95%) in the control PDMS sample is the impurities traced by EDX. Minor metallic impurities may be caused by the synthesis and handling circumstances, and metal traces may be present in commercially available PDMS formulations. Besides, there are several possible causes for this unexpected copper composition. Contamination from the environment is one possibility which may be from contaminated surfaces, water, or air in laboratory settings. The PDMS samples may have unintentionally absorbed trace amounts of copper if they had been subjected to such circumstances during handling, storage, or preparation. Additionally, if the beam interacts with or is scattered by adjacent areas,

using copper tape for attachment during FESEM or EDX examination may aid in copper detection. Instrumental artifacts can come into play; analytical instruments such as EDX can lead to elemental overlap or false-positive findings due to background noise, incorrect calibration, or cross-contamination from previously examined samples [99], [100], [101]. From PT1 (14.49%) to PT6 (57.45%), the tin content gradually rises in PT composites, which use pure tin as the filler. This rise is accompanied by a drop in the percentages of carbon and silicon, confirming the effects of ratio between the polymer matrix and tin filler. All PT samples have comparatively constant oxygen levels. Since the pure tin utilized is 99.99% tin, the trace amounts of copper found are probably the result of instrument sensitivity of the impurities in the metal powder used. This implies that copper's presence in PT composites is minimal and has little effect on the material's characteristics.

The copper content in TA composites, which contain a copper tin alloy, increases significantly, going from 25.61% in TA1 to 51.45% in TA6. Copper is the predominant metallic component in these composites, as seen by the comparatively low tin content, which ranges from 2.42% to 6.88%. Like PT composites, the amounts of silicon and carbon decrease as the metal content rises, indicating increasing the metal filler within the polymer matrix. There are few oxidation consequences since the oxygen concentration fluctuates only a little but stays within a constant range [97], [102], [103].

PA composites exhibit a more evenly distributed dispersion of metal components since they contain both copper and tin as fillers. Copper ranges from 12.76% to 40.79%, whereas tin concentration rises from PA1 (7.78%) to PA6 (12.83%). Although copper is more prevalent, the trend shows that both metals make substantial contributions to the composite structure. Carbon and silicon levels drop as the metal filler concentration rises, just like in PT and TA composites. The oxygen content stays comparatively constant, indicating that oxidation is not a major factor in changing the composition. PA group reveals relatively high concentration of tin likely due to the mixture of two (2) different fillers (pure tin and copper tin alloy).

Overall, the trend shows that while oxygen levels are constant across all composites, the addition of metal fillers causes a steady drop in the silicon and carbon components

of the polymer matrix. Because of tin's high Z and density, the PT composites with the highest tin concentration should improve photon attenuation. Without any metallic fillers, the control sample serves as a representation of the baseline composition. It demonstrates that the addition of tin and copper is the direct cause of any changes in elemental composition. These results highlight the importance of optimizing the metal-to-polymer ratio to achieve the desired outcome in radiation shielding applications.

4.5 XRD Analysis of PDMS-Based Composites

The XRD patterns of the control samples such as CT and C and the fabricated, PT6, TA6, and PA6 are presented in Figure 4.5. The diffraction data were recorded over the 29 range of 10° to 90°, enabling the identification of crystalline phases and assessment of the degree of crystallinity in each sample.

The pure tin sample, composed solely of 99.99% pure tin, displays sharp, high-intensity peaks at multiple 29 positions, notably around 30.6°, 32°, 44°, 55°, and 65°, corresponding to the characteristic reflections of metallic tin (Sn), which typically crystallizes in a tetragonal structure (JCPDS card no. 04-0673) P-Sn phase. These prominent peaks confirm the highly crystalline nature of pure tin, serving as a reference for evaluating the diffraction behavior of the composite samples [104], [105], [106].

In contrast, the PDMS sample in curve b, representing the PDMS polymer matrix without any metal reinforcement, reveals a broad, low-intensity hump in the region of approximately 10° to 25° 29, indicating an amorphous structure. This behavior is typical for PDMS, which lacks a regular and long-range crystalline order. The absence of sharp diffraction peaks is typical of polymeric materials like PDMS, which consist of flexible siloxane chains that do not form periodic lattice structures detectable by XRD [105], [106]. These findings further confirm that any observed diffraction peaks in the composite samples are attributed solely to the presence of crystalline metal fillers.

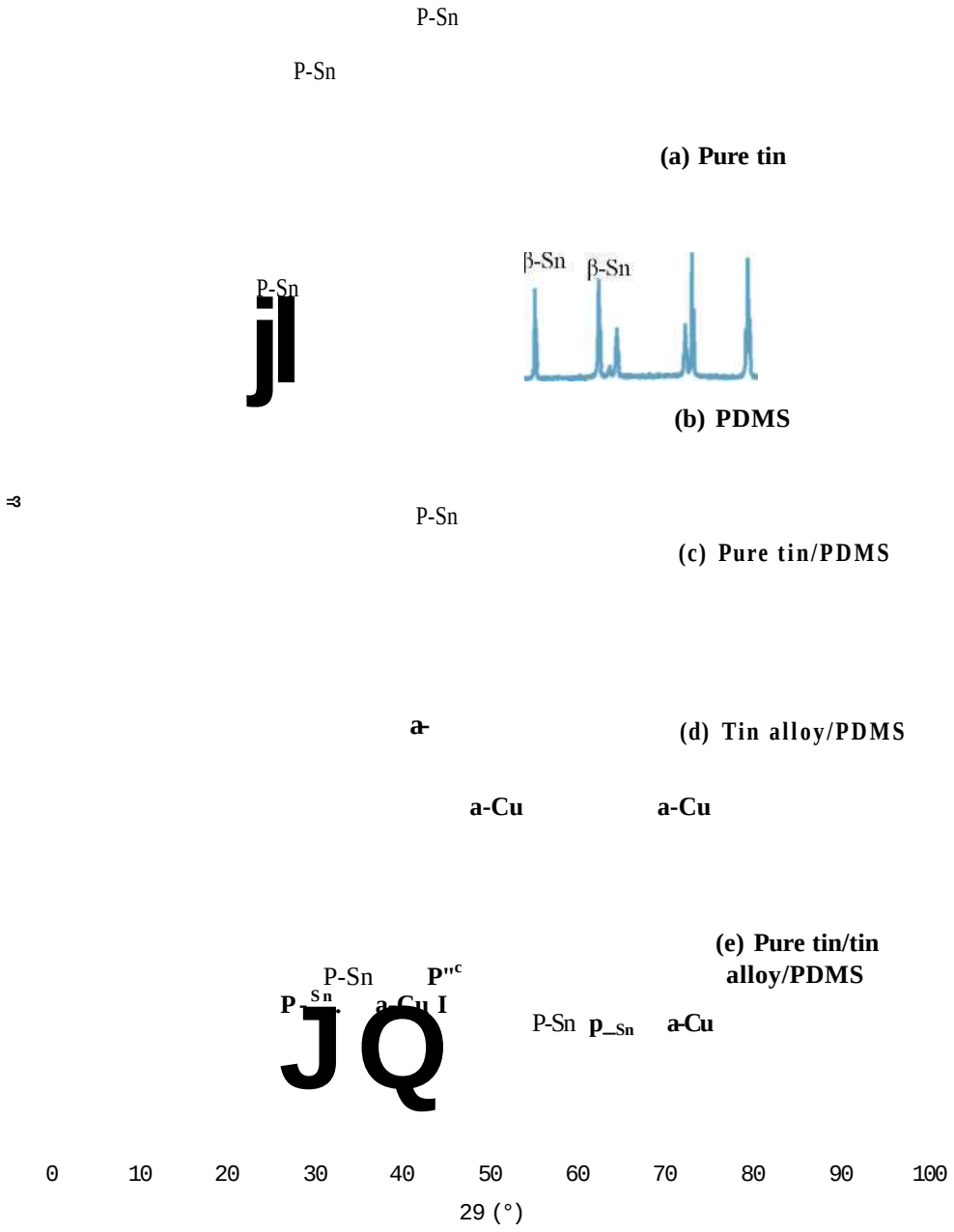

Figure 4.5 XRD Patterns of The Prepared Composites

The PT sample (curve c) exhibits several tin-related peaks, though at reduced intensities compared to CT. This attenuation can be attributed to the integration effect of the polymer, which disperses the crystalline phase. Nonetheless, the presence of sharp peaks confirms that the tin remains crystalline and well-distributed within the PDMS. The presence of P-phase of tin (P-Sn). was confirmed by the same diffraction peaks as CT, though with slightly reduced intensity due to dispersion in the PDMS matrix. PT sample reveals distinct and sharp diffraction peaks corresponding to P-Sn.

These peaks are consistent with the tetragonal structure of metallic tin (JCPDS 04-0673), with characteristic reflections observed at approximately 30.6°, 32.0°, 43.8°, 55.8°, 63.2°, and 65.8°, which correspond to the (200), (101), (220), (211), (301), and (112) crystallographic planes of P-Sn, the thermodynamically stable tetragonal form of metallic tin at room temperature [107], [108]. These reflections indicate that the tin particles retain their crystalline nature within the polymeric matrix.

The XRD pattern of the TA sample (curve d) exhibits prominent reflections corresponding to the a-Cu phase (JCPDS 04-0836), indicating the presence of a face-centered cubic structure typically associated with copper-rich regions [109]. Peaks observed near 43.3°, 50.4°, and 74.1° 20 can be indexed to the (111), (200), and (220) planes of a-Cu, respectively. Additional peaks, particularly those around 30.5°, 42.8°, and 43.5°, are attributed to the hexagonal intermetallic phase CueSns (JCPDS 45-1488), formed due to interactions between Cu and Sn during alloying. In some cases, minor traces of Cu3Sn may also be inferred from reflections near 32.0° and 50.9°, although their intensity is relatively weak, suggesting limited formation [109]. Overall, the XRD analysis confirms the successful incorporation of copper tin alloy in crystalline form within the amorphous PDMS matrix.

The PA sample (curve e) shows a diffraction pattern that features peaks from both tin and copper tin alloy phases. The peak intensity is intermediate between PT and TA6, reflecting the dual-phase composition. The presence of multiple crystalline domains suggests a heterogeneous distribution of tin and alloy particles, and the overall peak pattern supports the coexistence of distinct metallic phases without significant interference or amorphization. The PA sample combined P-Sn and Cu-rich alloy phases, resulting in a complex XRD pattern with overlapping reflections from P-Sn, a-Cu, and intermetallic compounds such as CueSns [108], [110]. This confirms the coexistence of multiple crystalline domains in the PDMS matrix, consistent with the mixed-metal composition. In the PA composite, the intensity of P-Sn peaks is slightly diminished due to the presence of the copper tin alloy and the distribution within the PDMS matrix. In contrast, the TA sample, which lacks pure tin, does not exhibit P-Sn reflections, supporting the structural integrity of the alloy system without free tin phases.

The copper tin alloy used in TA and PA composites has a composition of QmSns, representing a copper-rich region of the Cu-Sn phase diagram. According to phase identification via XRD, the dominant phase is a-Cu, where a small amount of Sn is dissolved in the Cu lattice, forming a substitute solid solution. This is confirmed by the presence of characteristic copper peaks at 29 ~ 43.3°, 50.4°, and 74.1°, matching JCPDS card no. 04-0836 [109], [111]. Minor contributions from Cu3Sn intermetallic may also be present if any localized phase separation occurred during curing, though these are not expected to dominate at this composition. The identification of these phases supports the hypothesis that the alloy remains crystalline and stable within the PDMS matrix.

Overall, the XRD analysis demonstrates that all representative metal-containing composites (PT, PA, TA) retain their crystalline structure despite being embedded within the PDMS matrix. These findings confirm that increasing the complexity of metal composition (alloy and single metal) and its interaction with the polymer matrix influences the crystallographic characteristics of the composites, which may in turn affect their radiation shielding performance.

4.6 FTIR Analysis of Composites

The FTIR spectral data for four (4) different samples designated as control, PT6, TA6, and PA6 are shown in the graph in Figure 4.6. Wavenumbers (cm^{-1}) are shown by the x-axis, which runs from 0 to 4500, while absorbance intensity is indicated by the y-axis, which scales from 0 to 1.2. Investigating how these different materials absorb infrared light is the aim of this study since it can provide insight into their molecular makeup, chemical interactions, and overall structure. The spectrum's peaks demonstrate the effects of various infrared light wavelengths on the materials, which correspond to various molecular vibrations, such as bond stretching or bending [69], [87].

All of the samples exhibit different absorption peaks, particularly in the 500 to 1500 cm^{-1} region. These peaks are typically recognized as the vibrational modes of the polymer backbone and associated metal compounds. The Si-O-Si stretching vibrations in PDMS are specifically represented by the peaks around 1000 to 1200 cm^{-1};

interactions with the polymer matrix caused by metals result in slight changes in peak strength or shifts in peak intensity.

The control spectrum has distinctive peaks in the Si-0 and Si-CH3 areas that are consistent with pure PDMS [69], [86]. The transmittance is higher in the 1500 to 3500 cm"[1] range, indicating a slight absorption by the pure polymer matrix. However, because the PT6 sample has pure tin embedded in PDMS, it shows a shift in the spectra, especially in the 500 to 1500 cm"[1] range. This indicates that tin's interaction with the PDMS matrix affects the peak positions and intensities. Although the TA6 spectrum's peak intensities differ, its transmittance behaviour is similar to that of PT6. The copper tin alloy produces additional vibrational modes, perhaps due to interactions between the metal and the PDMS matrix.

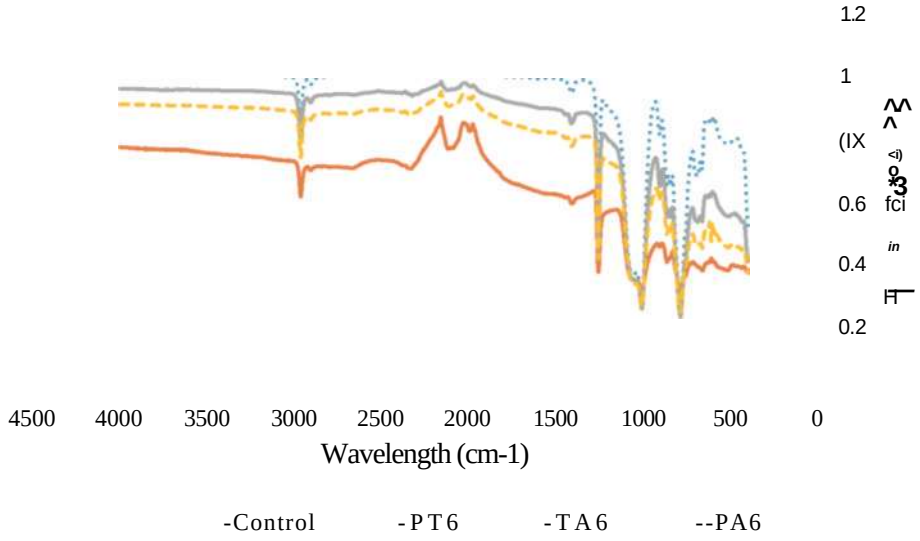

Figure 4.6 FTIR Spectra of Representative of Each Set (at 60%) and Control Sample

Because sample PA6 contains both copper tin alloy and pure tin in PDMS, it displays the most complex spectrum. Significant differences exist in peak intensities and shifts compared to the respective PT6 and TA6 samples. This demonstrates how the synergistic effects of the two metals cooperating in the PDMS matrix alter the transmittance properties. Over the whole spectrum, the control shows the highest transmittance trends, as would be expected for a pure polymer. In contrast, the transmittance of the metal-containing samples (PT6, TA6, and PA6) is reduced,

especially in the 500 to 2000 cm^{-1} range, indicating that the metals' presence and interactions with PDMS have increased absorption [61], [86], [112].

The FTIR spectra show that the addition of pure tin and copper tin alloy significantly alters the transmittance characteristics of the PDMS matrix. These spectrum fluctuations, which indicate differences in the chemical interactions within the matrix, may be related to the potential shielding properties of these composites. Each formulation (PT6, TA6, and PA6) exhibits distinct spectral properties, indicating that their effectiveness for radiation shielding or absorption applications may vary [31], [86], [87].

PT6, represented by the orange line, has the lowest absorbance throughout the spectrum, particularly in the 1000 to 2000 wavenumber range. Pure tin mixed with PDMS may have fewer active chemical connections, such as weaker C-H or Si-0 interactions typical of PDMS-based materials, as indicated by the comparatively low intensity of its peaks, which also suggests a simpler molecular structure. A simpler material composition could be indicated by the decreased absorbance, which could make PT6 less reactive or have fewer intricate interactions with other materials [31], [86].

The highest absorption is seen in the grey line, which stands for TA6 (copper tin alloy with PDMS). The more prominent peaks observed in 1000 to 1500, and 2000 to 2500 cm^{-1} reflect stronger molecular vibrations and more complex interactions between the copper tin alloy and the PDMS matrix. Higher absorbance suggests stronger or more numerous connections, such as metallic interactions between copper and tin atoms or covalent bonds with the polymer. These connections aid in the creation of a denser molecular structure, which may enhance mechanical strength or chemical resistance in applications requiring stronger materials [61], [86].

The yellow line, which represents PA6, shows an intermediate absorption between PT6 and TA6. Its absorption profile suggests a mix of pure tin and copper tin alloy characteristics. The absorbance is stronger than that of PT6, indicating the presence of additional or stronger bonds due to the alloy component, even if it is weaker than TA6,

indicating the effect of the pure tin in its structure. These components most likely combine to create a hybrid structure that balances the properties of pure tin, such as lower reactivity and fewer bonds, with the strength of the copper tin alloy [61].

Because of its simpler molecular structure and fewer active bonds, PT6 has the lowest absorbance, whereas PA6 has a balanced absorbance, suggesting that it combines the characteristics of both materials to provide a balance between simplicity and complexity. The highest absorbance is found in TA6, indicating a more intricate molecular structure with more active chemical interactions. This could have to do with the copper tin alloy's ability to increase the material's overall bonding strength through greater metallic and covalent contacts [86].

In conclusion, the bonding and molecular structures of PT6, TA6, and PA6 exhibit significant differences in their FTIR spectra that suggest the physical interaction between the metal and polymer. TA6 is notable for having a greater absorbance, indicating a more complex composition, whereas PT6 shows weaker interactions. PA6 offers a compromise by containing elements of both pure tin and copper tin alloy. When selecting materials for various industries based on desired properties like mechanical strength, flexibility, or chemical resistance, it is crucial to understand these differences.

4.6.1 FTIR Analysis of Each Sample Groups

The FTIR spectra of the control sample and PT, TA, and PA groups (Figure 4.7) reveal the presence of characteristic functional groups associated with the PDMS matrix, along with variations induced by increasing metal filler content. All samples exhibit prominent absorption bands in the fingerprint region (400-1500 cm^{-1}), corresponding to the stretching and bending vibrations of Si-O-Si, Si-CFb, and C-H bonds, confirming that the fundamental chemical structure of PDMS is preserved across all composite formulations.

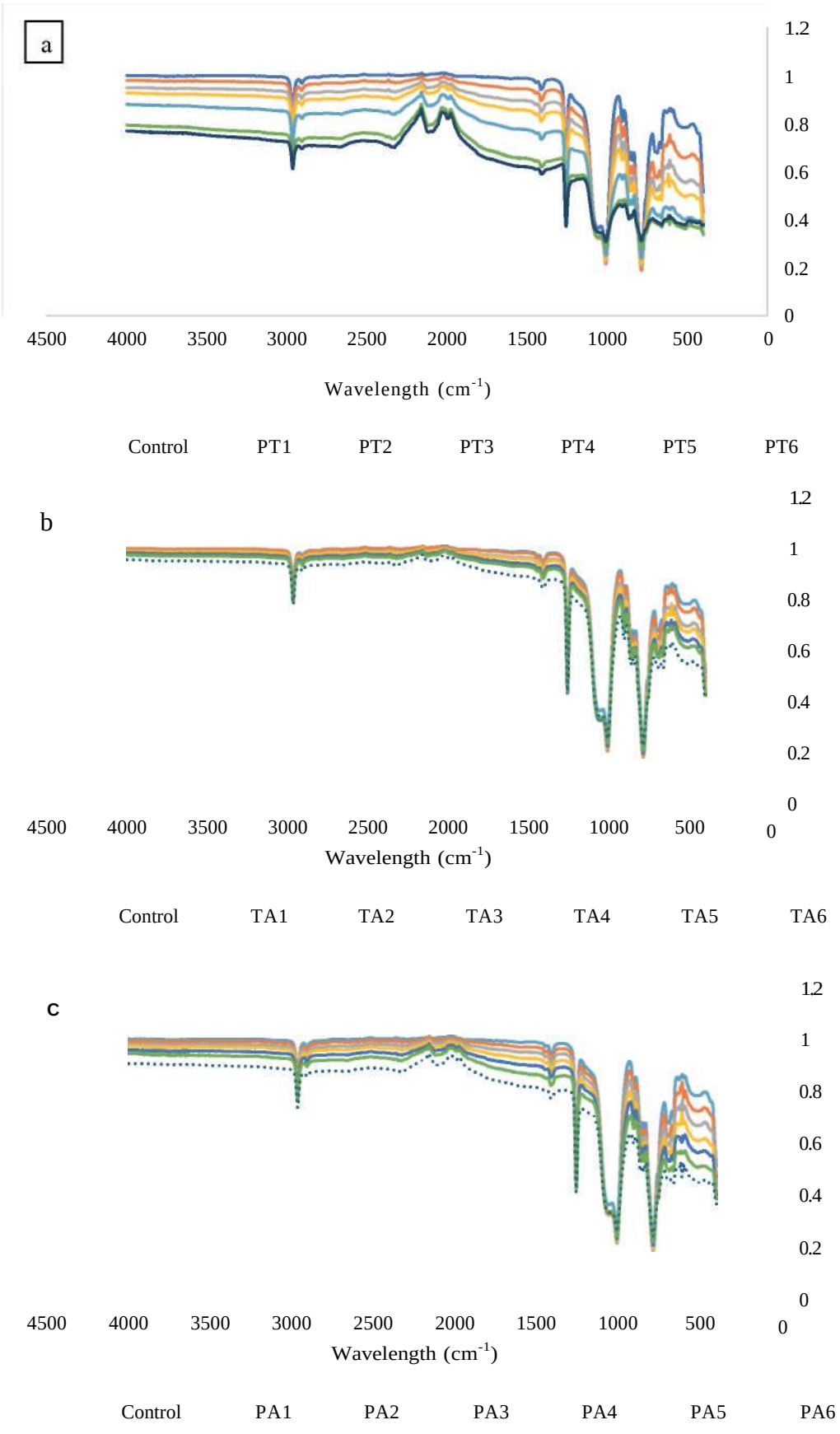

Figure 4.7 FTIR Spectra of (a) PT, (b) TA and (c) PA group

A strong absorption band observed around 1000-1100 cm^{-1} is attributed to the asymmetric stretching of the Si-O-Si siloxane backbone, while bands in the 850-1250 cm^{-1} range are associated with Si-CHa stretching and bending vibrations [113]. Variations in the intensity of these peaks with increasing metal filler concentration suggest interactions between the metal particles and the PDMS matrix, which may influence the flexibility, stability, and local bonding environment of the polymer network.

In the mid-infrared region (1500-3000 cm^{-1}), the spectra remain largely consistent for all samples, indicating that the C-H stretching vibrations and the polymer backbone are not significantly altered by the incorporation of metal fillers. Peaks observed in the 2900-3000 cm^{-1} range correspond to symmetric and asymmetric stretching of CH_3 groups, reflecting the hydrophobic nature of PDMS, while a weak band near 3000 cm^{-1} associated with O-H stretching shows a slight decrease in intensity with increasing filler content [32], [113]. This reduction suggests potential interactions between metal fillers and oxygen-containing functional groups, possibly leading to limited interfacial bonding or changes in moisture affinity. Additionally, modifications in peak intensity below 800 $cirr^{1}$ indicate changes in PDMS bending modes, further supporting the presence of close interactions between the metal fillers and the polymer matrix.

Overall, the gradual decrease in transmittance with increasing metal concentration for PT, TA, and PA composites indicates enhanced absorption and stronger filler-matrix interactions, while the preservation of key PDMS functional groups confirms that the composites maintain their fundamental chemical structure, supporting their suitability for radiation shielding applications.

4.7 Radiation Characterization

Characterization of gamma-ray radiation provides important information about a material's shielding capability. Many significant parameters, including the MAC, LAC, RPE, HVL, TVL, MFP and lead equivalent are used to measure the interaction between gamma rays and the composites using formulas stated in section 2.6.

4.7.1 Evaluation of Mass Attenuation Coefficient (MAC) for Composite Performance

The MAC is an essential parameter when assessing a material's ability to shield radiation. By considering the attenuation capability concerning the material's density, MAC offers a more intrinsic measure of shielding efficacy than the LAC which is dependent on the physical thickness of a material [14], [113], [114]. As photon energy rises, the MAC values of the examined samples clearly show a declining trend (Table 4.3 and Figure 4.8), which is consistent with the behaviour predicted by photon interaction processes as mentioned in section 2.3. Compton scattering takes over as the main interaction mechanism at higher photon energies, resulting in decreased attenuation efficiency, whereas the photoelectric effect predominates at lower photon energies, producing high MAC values.

The control PDMS sample (C) exhibits low practical radiation shielding capability due to its low atomic number composition; however, its MAC values appear relatively high at certain energies. This apparent behavior arises from the density-normalized nature of MAC, where materials with very low density, such as PDMS, may exhibit inflated MAC values when the linear attenuation coefficient is divided by a small density value. Consequently, a higher MAC value for PDMS does not reflect superior shielding effectiveness but rather represents attenuation per unit mass rather than per unit thickness [115].

The MAC values for CL are infinite (GO) at 122.1 keV, indicating full photon absorption at these energies as previously mentioned in section 2.5. An infinite MAC value was reported because complete attenuation of the incident photons was observed at this energy, resulting in zero transmitted photon intensity. Since MAC is calculated using the logarithmic ratio of incident to transmitted intensity, a transmitted intensity approaching zero leads to a mathematically undefined or infinite MAC value. Physically, this indicates that the lead shielding thickness used in this study was sufficient to fully absorb the incoming photons at 122.1 keV, primarily due to the dominance of the photoelectric effect at low photon energies and the high atomic number of lead [30], [56]. This highlights the limitation of MAC when complete

attenuation occurs and reinforces the importance of considering additional shielding parameters.

The CT sample has a peak of 0.95 cm^2 g''^1 at 122.1 keV, demonstrating significantly more attenuation capability than CL at these low energies. The MAC values, however, progressively decrease with increasing energy, reaching a final value of 0.04 cm^2 g''^1 at 1332.5 keV, reflecting reduced attenuation efficiency at higher energies where Compton scattering dominates. While tin-based composites exhibit enhanced attenuation performance at low photon energies, their effectiveness decreases relative to lead at higher energies, as mentioned in section 2.3.1 [9].

Table 4.3
MAC Values of All Composites Across Different Gamma Ray Energies

	MAC (cm^2 g^1)					
amples	122.1 keV	356 keV	661.7 keV	834.8 keV	1173.2 keV	1332.51
C	0.11	0.24	0.06	0.04	0.02	0.20
CL	00	0.24	0.10	0.08	0.06	0.07
CT	0.95	0.09	0.07	0.07	0.04	0.04
PT1	0.47	0.05	0.05	0.07	0.03	0.14
PT2	0.67	0.04	0.07	0.09	0.02	0.13
PT3	0.62	0.05	0.06	0.07	0.03	0.09
PT4	0.80	0.06	0.07	0.08	0.04	0.09
PT5	0.82	0.09	0.06	0.07	0.04	0.11
PT6	0.84	0.08	0.06	0.08	0.05	0.09
TA1	0.19	0.02	0.05	0.09	0.11	0.09
TA2	0.27	0.06	0.05	0.08	0.09	0.11
TA3	0.29	0.05	0.06	0.08	0.08	0.10
TA4	0.30	0.06	0.05	0.07	0.09	0.13
TA5	0.26	0.07	0.06	0.07	0.07	0.12
TA6	0.28	0.07	0.06	0.07	0.12	0.11
PA1	0.26	0.04	0.03	0.13	0.05	0.25
PA2	0.35	0.05	0.06	0.10	0.08	0.15
PA3	0.31	0.04	0.05	0.06	0.06	0.11
PA4	0.39	0.06	0.06	0.08	0.07	0.15
PA5	0.35	0.07	0.06	0.07	0.11	0.14
PA6	0.38	0.09	0.06	0.06	0.11	0.14

The MAC values in the PT series (PT1 to PT6) show a similar pattern, with the maximum attenuation occurring in PT4, PT5, and PT6. The excellent shielding capability of PT6 is confirmed by its MAC of 0.84 cm^2 g^{-1} at 122.1 keV. The MAC values, however, decrease with increasing energy, peaking at 0.09 cm^2 g^{-1} at 1332.5 keV. The changes within the PT series indicate that attenuation efficiency can be greatly increased by adjusting the composition of the material or by increasing the tin content [74], [116]. This suggests that the composites' high tin content effectively absorbs low-energy photons, demonstrating their consistent performance in attenuating both low and moderate energy gamma rays. These results were comparable to the theories whereas the metal fillers increased, the MAC values will increase as mentioned in section 2.6.

In contrast to the PT series, the TA series (TA1 to TA6) exhibits modest attenuation performance. TA6 has the highest MAC values of all these samples with 0.28 cm^2 g^{-1} at 122.1 keV. These values, however, are still less than those found for PT4 to PT6, indicating that the TA samples' composition might have fewer high-Z components or structural features that restrict attenuation efficiency. While TA6 is good at attenuating lower-energy photons, its ability to block high-energy gamma radiation is rather restricted, as evidenced by its MAC of 0.11 cm^2 g^{-1} at 1332.5 keV, which is lower than that of PT6 and CT.

The PA series (PA1 to PA6) shows a similar pattern, with PA6 having the highest MAC values in its group. At 122.1 keV, the MAC for PA6 is 0.38 cm^2 g^{-1}. With a MAC of 0.14 cm^2 g^{-1} at 1332.5 keV, PA6 is among the best-performing samples at high energies. This implies that, in comparison to other PA and TA samples, PA6 might offer superior attenuation for higher-energy gamma rays. On the other hand, especially at higher photon energies, PA1 and PA2 have the lowest MAC values in the PA series.

By comparing all the composites, at higher gamma-ray energies (1173.2 keV and 1332.5 keV), although the overall MAC values decrease across all samples due to the increased penetration capability of higher-energy photons, the TA and PA series, particularly TA6 and PA6, exhibit relatively higher attenuation. These samples show improved performance at higher energy levels, most likely as a result of mixed metal fillers' synergistic effects or optimized composite structures as stated in section 2.6.1.

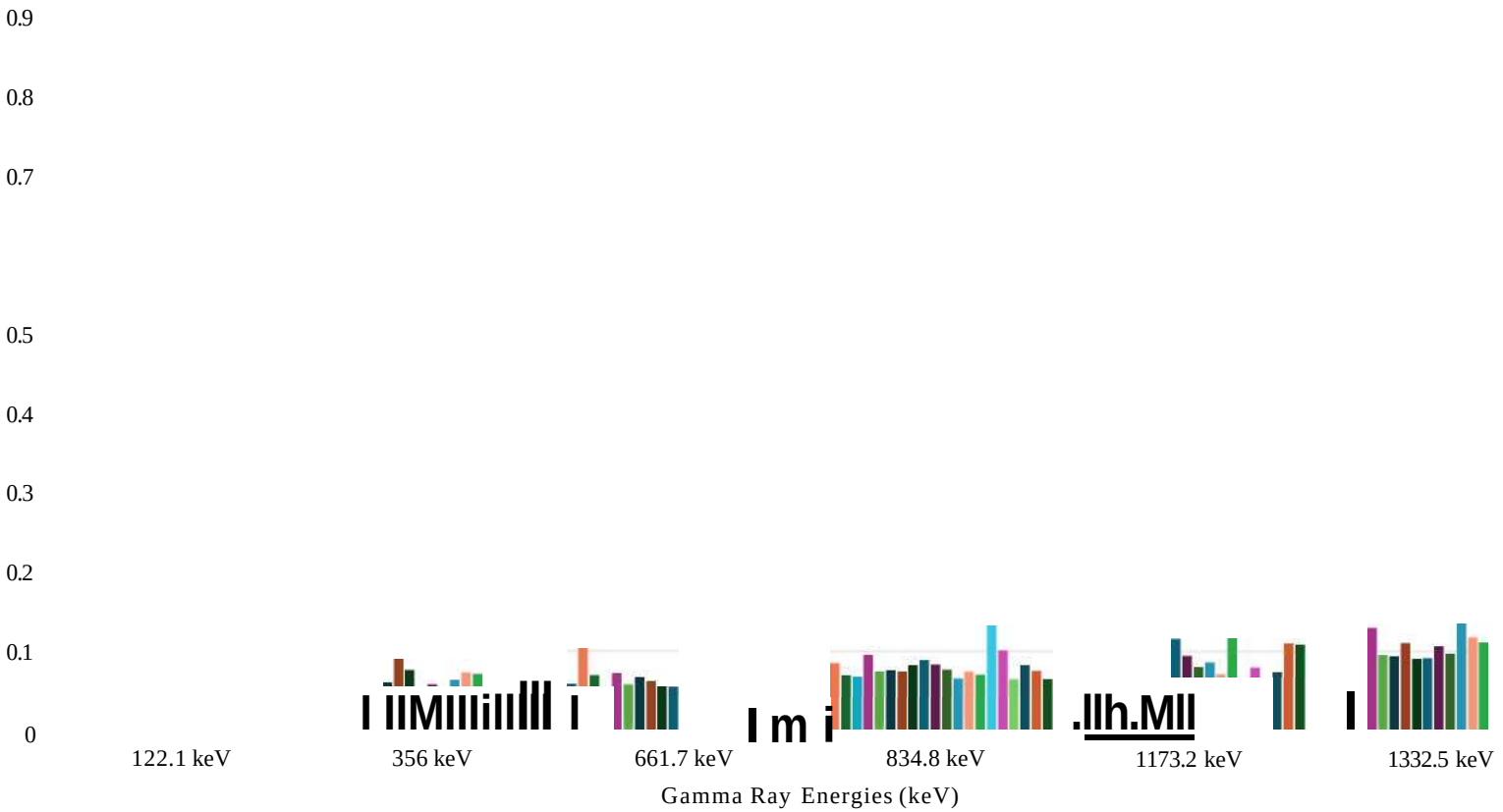

Figure 4.8 Bar Graph of MAC Values Against Composites

The PT series, particularly PT4, PT5, and PT6, have the highest attenuation capability. However, TA6 and PA6 perform more effectively for higher energy gamma rays, suggesting that composite formulations with mixed fillers could enhance attenuation across a wider range of energies. As photon energy increases, attenuation efficiency falls, suggesting these materials could be effective lead-free radiation shielding substitutes.

Despite thorough calibration of the experimental setup including energy calibration, background correction, and detector efficiency normalization, an increase in the attenuation coefficient was observed at higher gamma-ray energies, specifically at 1332.5 keV. This result appears inconsistent with the expected trend, which typically shows a decreased value in attenuation as photon energy increases. Several possible explanations, both physical and experimental, may account for this deviation. This pattern is consistent with the study that showed a slight increment throughout the energy levels, likely due to the particle distribution within the materials that interact with the photon rays [117].

A key factor influencing this behavior is the composition of the composite material, particularly the presence of high atomic number additives. Although the same composite formulation was used throughout the experiment, if it incorporates metal fillers, it is plausible that increased attenuation at higher energies is a consequence of the onset of pair production. Pair production is a photon interaction process that becomes significant at photon energies exceeding 1.022 MeV and is highly dependent on atomic number [10]. As such, composites containing high-Z elements may demonstrate an upward trend in attenuation coefficients at energies above this threshold due to the increased cross-section for pair production.

In addition to compositional effects, the observed increase may also result from complex radiation and matter interactions within the composite. For thicker or high-Z composites, secondary effects such as photon build-up and internal scattering can alter the effective attenuation behavior [10]. These phenomena become more prominent at higher energies, where photon penetration is greater and multiple scattering is more likely to occur. Such effects are not adequately captured by simplified exponential

attenuation models and may require computational techniques, such as Monte Carlo simulations (e.g., MCNP or GEANT4), to accurately predict the radiation transport behavior within the composite [118], [119].

Geometrical factors in the experimental setup may also contribute to the anomaly. At high photon energies, Compton scattering dominates, and scattered photons may reach the detector if the system lacks sufficient collimation or shielding. Misalignments in the source-sample-detector arrangement, or partial coverage of the incident beam by the sample, can lead to underestimation of the true attenuation. These geometric considerations are particularly relevant for high-energy gamma photons, which are more likely to undergo small angle scattering [120].

Furthermore, the calculation method for the MAC may introduce numerical error, especially when the transmitted intensity closely approaches the incident intensity. The logarithmic relationship in equations 2.1, 2.2 and 2.3 is sensitive to small differences between I and Io, making the attenuation coefficient prone to overestimation when attenuation is minimal, as is typical at higher photon energies [57]. Therefore, the rise in attenuation at high gamma-ray energies observed in the composite sample may result from a combination of pair production effects, internal scattering mechanisms, experimental geometry, and calculation sensitivity. Each of these factors must be carefully considered to accurately interpret high-energy attenuation behavior in radiation shielding materials. Increased Compton scattering, cumulative interactions, and improved material homogeneity in PA6 are the potential causes of the modest improvement in radiation shielding performance at 1173.2 keV and 1332.5 keV. Small elevates values of radiation performance at high energy are common in multi-element composites where scattering predominates, even though attenuation normally decreases with energy.

Overall, the present findings indicate that the mass attenuation coefficient (MAC) alone is not a fully reliable parameter for assessing radiation shielding performance, particularly when comparing materials with significantly different densities. Low-density materials, such as PDMS-based composites, may exhibit comparatively high MAC values due to density normalization, despite their limited practical shielding

capability, whereas high-density materials, such as lead, may display reduced or mathematically infinite MAC values under conditions of complete photon attenuation. Therefore, MAC should not be used as a standalone parameter but should be evaluated together with density-dependent shielding parameters such as LAC, HVL, TVL, MFTP, RPE and lead equivalence to provide an accurate and physically meaningful assessment of radiation shielding performance.

4.7.2 Analysis of Linear Attenuation Coefficient (LAC) in Composite Materials

The LAC is a fundamental parameter in determining the radiation shielding effectiveness of a material which represents the probability of photon interaction per unit thickness of a material and is strongly dependent on photon energy and atomic number. A distinct pattern emerges from the examination of LAC values in different samples as they tend to fall as photon energy rises (Table 4.4 and Figure 4.9). The various photon interaction processes controlling gamma-ray attenuation account for this phenomenon. The photoelectric effect predominates at lower energies, producing large LAC values; at intermediate and high energies, Compton scattering takes over as the main interaction mechanism, causing LAC to gradually decrease [10].

There are notable variations in the attenuation capacities for the control samples. LAC values for the C range from 0.02 cm^{-1} at 1173.2 keV to 0.25 cm^{-1} at 356 keV, indicating the lowest attenuation capacity compared to other samples. As photon energy increases to higher values (1173.2 keV), the probability of interaction decreases significantly because high-energy photons have greater penetrating power and are less likely to interact with low-Z materials. At these energies, Compton scattering becomes the dominant interaction mechanism, and its cross-section decreases with increasing photon energy, leading to a reduced LAC value. In contrast, the CL sample exhibits a significant increase in attenuation, with a LAC of 2.70 cm^{-1} at 356 keV. Interestingly, the LAC values for CL are infinite (∞) at 122.1 keV, indicating full photon absorption at these energies as previously discussed in the section 4.7.1. This implies that the sample contains high-Z components, which lead to significant attenuation against gamma rays [10] .

With the highest value of 6.91 cm^{-1} at 122.1 keV, the CT sample shows even better attenuation performance than CL. However, LAC values significantly decrease with increasing photon energy, reaching 0.32 cm^{-1} at 1332.5 keV. The substantial number of high-Z elements, including tin, that are present in CT and efficiently absorb low-energy gamma rays is confirmed by the considerable attenuation at lower energies. CT is useful for low-energy gamma shielding, but its diminishing attenuation efficacy at higher energies indicates that it might not be as appropriate for applications that require attenuation of high-energy photons [8], [10], [121].

When compared to the C, the PT series (PT1 to PT6) exhibits better attenuation characteristics. The samples in this series with the greatest LAC values at low photon energy are PT4, PT5, and PT6; PT6's value is 3.77 cm^{-1} at 122.1 keV. The LAC values for PT6 and other PT samples range from 0.23 cm^{-1} to 0.44 cm^{-1} at higher energies, like 1332.5 keV, suggesting strong shielding efficiency against highly penetrating gamma radiation. Meanwhile, PT1 and PT2 exhibit lower attenuation coefficients, indicating that structural and compositional differences, particularly lower tin content, significantly reduce their radiation shielding efficiency. The trend observed in the PT series suggests that increasing the tin content or optimizing the composite compositions leads to enhanced attenuation efficiency.

The TA series (TA1 to TA6) exhibits modest attenuation performance. TA6 had the highest attenuation of all the TA samples, with a LAC of 1.53 cm^{-1} at 122.1 keV. These values, however, are slightly less than the reported values for PT4 to PT6. This is primarily due to the lower effective atomic number of the alloy, as copper (Z = 29) dominates the composition while tin (Z = 50) is present in small amounts. Since photoelectric absorption is highly dependent on atomic number, the lower Z reduces photon attenuation at low energy. Furthermore, the lower electron density in the copper-rich alloy also diminishes Compton scattering interactions at higher photon energies, resulting in overall reduced shielding efficiency. Among the TA samples, TA1 and TA2 exhibit the least amount of attenuation, particularly at higher photon energies, where their LAC values fall below 0.26 cm^{-1} at 1332.5 keV. This implies that these samples might not be appropriate for high-energy gamma radiation shielding applications if compared to the PT samples.

Table 4.4
LAC Values of All Composites Across Different Gamma Ray Energies

Sample	122.1 keV	356 keV	661.7 keV	834.8 keV	1173.2 keV	1332.5 keV
	LAC (cm^{1})					
C	0.11	0.25	0.06	0.04	0.02	0.21
CL	∞	2.70	1.16	0.96	0.73	0.74
CT	6.91	0.67	0.51	0.50	0.27	0.32
PT1	0.76	0.08	0.09	0.11	0.06	0.23
PT2	1.38	0.09	0.15	0.20	0.04	0.27
PT3	1.81	0.14	0.17	0.22	0.09	0.28
PT4	2.71	0.21	0.23	0.26	0.14	0.32
PT5	3.28	0.36	0.25	0.29	0.16	0.44
PT6	3.77	0.34	0.25	0.37	0.21	0.41
TA1	0.34	0.03	0.10	0.16	0.20	0.16
TA2	0.66	0.14	0.13	0.20	0.23	0.26
TA3	0.93	0.18	0.19	0.25	0.26	0.31
TA4	1.17	0.25	0.21	0.26	0.34	0.53
TA5	1.25	0.35	0.27	0.35	0.34	0.56
TA6	1.53	0.39	0.32	0.38	0.64	0.61
PA1	0.47	0.07	0.05	0.24	0.10	0.46
PA2	0.88	0.12	0.16	0.25	0.20	0.39
PA3	1.09	0.15	0.16	0.23	0.21	0.41
PA4	1.47	0.23	0.22	0.31	0.28	0.56
PA5	1.61	0.33	0.25	0.34	0.50	0.64
PA6	2.08	0.49	0.32	0.36	0.59	0.76

The PA series (PA1 to PA6) exhibits comparable trends, with PA6 showing the highest attenuation efficiency in its group. The LAC values are marginally below those found for PT4 to PT6, although they are higher than those found for the majority of TA samples. With the highest LAC of 0.76 cm^{-1} at 1332.5 keV from the overall fabricated samples, PA6 is among the best-performing samples at high energies. Based on these findings, PA6 is one of the samples that are able to fulfil the properties of the best radiation attenuation performance.

The research concludes that LAC values fall with increasing photon energy, with the photoelectric effect dominating at lower energies and causing the greatest attenuation. Overall, the most promising attenuation characteristics among the studied samples are shown by PT4 to PT6 and PA6, which makes them suitable options for radiation shielding applications at various energy ranges. These substances may be used as lead-

free substitutes for traditional shielding materials, especially those with excellent attenuation efficacy at lower photon energies. More research on their mechanical characteristics, structural soundness, and long-term durability is necessary to evaluate their viability. Furthermore, assessing these materials' suitability for usage in industrial, medical, and nuclear radiation protection applications would require optimizing composite formulations and testing them under actual radiation exposure.

The LAC values at 1332.5 keV revealed increased values, which are in contrast to the theoretical studies in section 2.6. These trends are due to the photons emitted being more likely to undergo Compton scattering rather than being fully absorbed through the photoelectric effect. In Compton scattering, a gamma photon transfers part of its energy to an electron and is deflected, which can result in scattered photons being detected at different energies as previously discussed in section 2.3.2. This phenomenon contributes to what is known as the Compton continuum, where a broad range of scattered photon energies can elevate the background signal, especially near the high-energy peak regions [120], [122], [123]. As a result, the 1332.5 keV peak may appear artificially high due to these additional scattered photon counts.

4.7.3 Comparative Assessment of Radiation Protection Efficiency (RPE) Across Samples

The graph in Figure 4.10 displays the radiation shielding efficiency of all composites against gamma ray energies ranging from 122.1 keV to 1332.5 keV. The results demonstrate the capability of each shielding material and the attenuation abilities of each composite across various energy levels.

At all photon energy, the PDMS control composite's radiation shielding efficacy is comparatively low (Table 4.5). With 100% at 122.1 keV, the CL exhibits exceptional radiation protection efficiency, especially at the lower photon energies. At lower energies, this composite outperforms other samples. It maintains a significant degree of attenuation at higher energies, with a radiation shielding efficiency of about 30.53% at

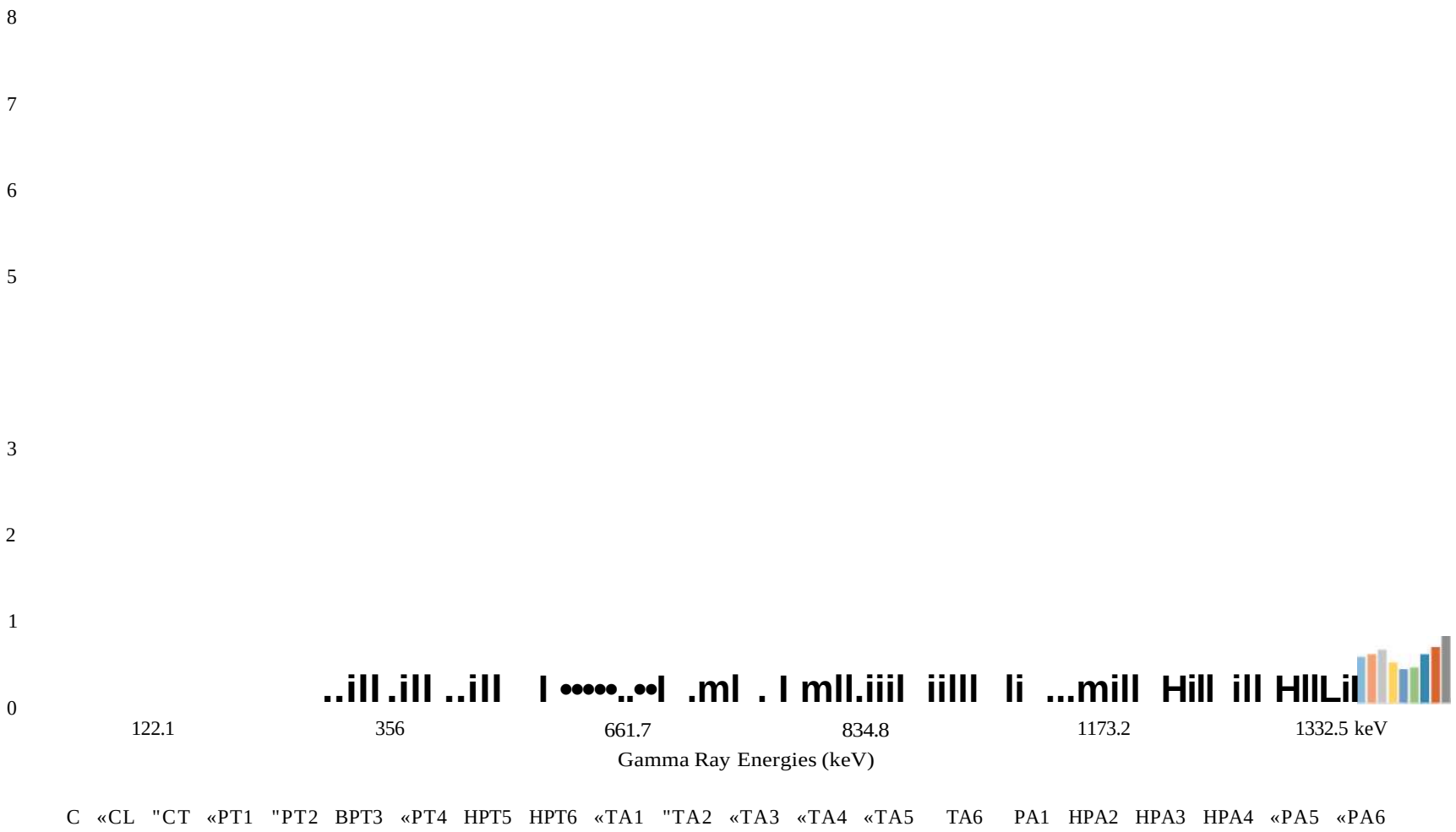

Figure 4.9 Bar Graph of LAC Values for Each Composite

1173.3 keV, however, the efficiency decreases as the energy increases. The CT composite shows good radiation shielding, particularly at lower energy (96.84%) at 122.1 keV), comparable to the CL sample. At 834.8 keV and 1332.5 keV, the protection efficiency drops to 22.47%> and 14.81%), respectively, as energy levels rise. The CT composite has a poorer attenuation at higher photon energy than the CL composite, but it is still effective at lower photon energies.

A variety of efficiencies are shown by the pure tin/PDMS composites with different compositions, such as PT1, PT2, PT3, and so forth. For instance, PT1 exhibits notable protection at lower energies, but at higher energy the efficiency sharply declines (2.54% at 1332.5 keV). At higher energies, however, PT6 exhibits better shielding. Among the pure tin/PDMS composites, it has the best radiation protection efficiency, reaching 19.64%) at 1332.5 keV. According to the trend for PT composites, the shielding efficiency is improved, especially at lower energies, by adding more tin or changing the composition reflecting the theories outlined in section 2.6.3.

The radiation shielding efficacy of the copper-based composites (TA1 to TA6) varies. As the tin content rises, TA1, which had lower efficiency (15.48%) at 122.1 keV), gets better. With values of 55.60% at 122.1 keV and 27.52% at 1332.5 keV, TA6 exhibits the highest radiation protection effectiveness in this group, indicating a good composite between material composition and shielding ability. Although they fall short of the CL and CT samples in terms of performance, these composites show good shielding properties at both low and high energies.

Next, the radiation protection efficacy of PA1 through PA6 has revealed an increasing pattern, with PA6 being the top performance. The efficiency of PA6 is 68.87% at 122.1 keV and 34.75% at 1332.5 keV, suggesting reliable shielding performance throughout the energy levels. At higher energies, PA1 and PA2 show less protection with 20.20 and 16.59%) at 1332.5 keV, respectively. The overall trend indicates that the addition of copper tin alloy greatly improves the shielding capabilities in comparison to the pure tin/PDMS composites. The PA6 composite has the highest overall radiation protection efficiency, attenuating y-ray radiation over the whole energy

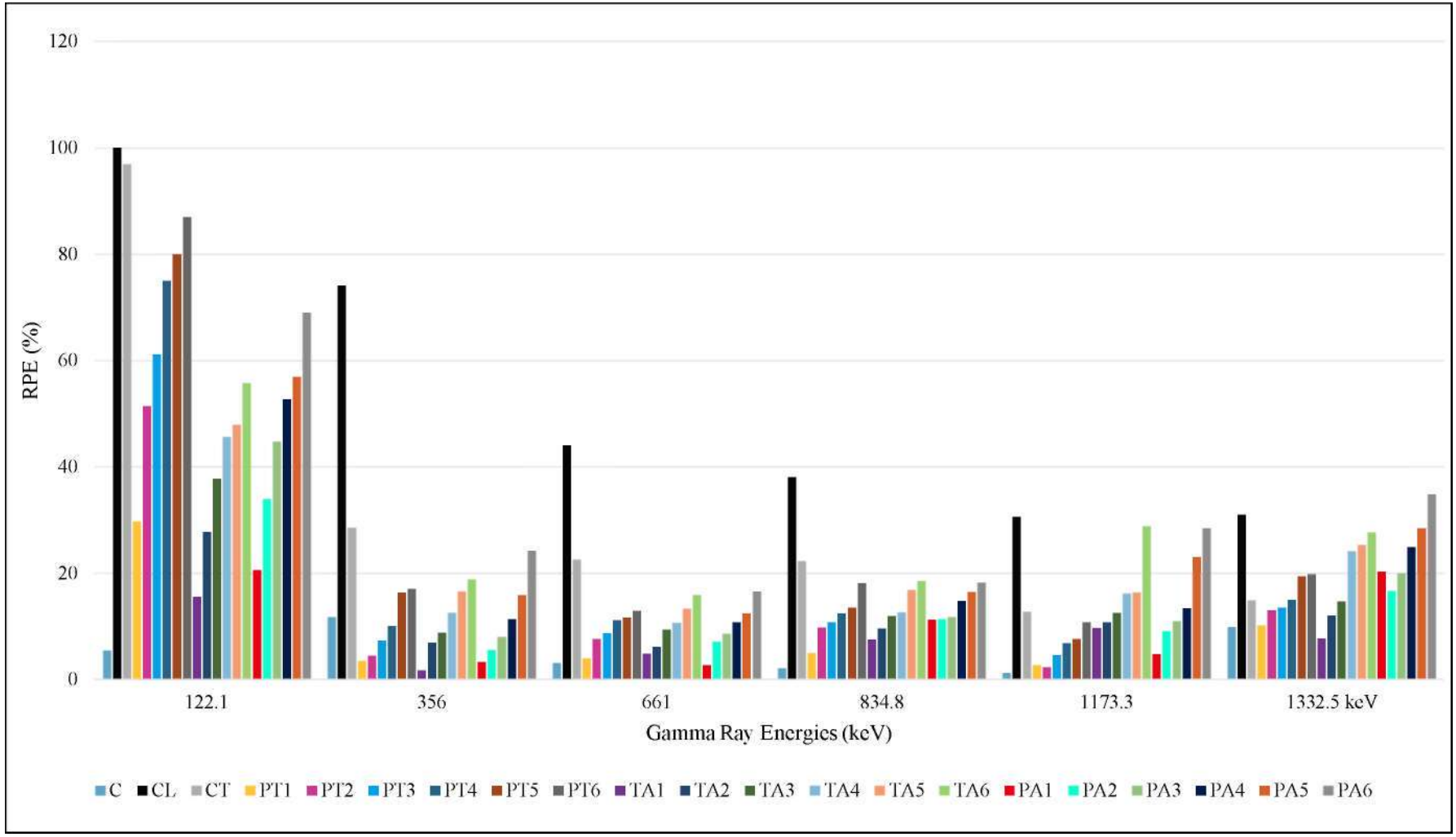

Figure 4.10 Bar Graph Comparison of RPE Results for Each Composite

Table 4.5
RPE Data Information of Each Prepared Composite

Sample	Radiation protection efficiency (%)					
	122.1 keV	**356 keV**	**661 keV**	**834.8 keV**	**1173.3 keV**	**1332.5 keV**
C	5.32	2.02	11.65	2.99	1.12	9.74
CL	100.00	37.98	74.01	43.99	30.53	30.85
CT	96.84	22.12	28.40	22.47	12.63	14.81
PT1	29.60	4.84	3.41	3.88	2.54	10.09
PT2	51.30	9.65	4.39	7.46	2.20	12.88
PT3	61.04	10.61	7.24	8.54	4.48	13.35
PT4	74.94	12.28	9.98	11.05	6.72	14.90
PT5	79.93	13.42	16.26	11.52	7.52	19.33
PT6	86.92	17.97	16.89	12.85	10.66	19.64
TA1	15.48	7.42	1.57	4.70	9.54	7.63
TA2	27.64	9.43	6.79	6.03	10.65	11.91
TA3	37.64	11.78	8.64	9.28	12.40	14.60
TA4	45.51	12.51	12.40	10.57	16.03	24.00
TA5	47.75	16.75	16.48	13.20	16.21	25.14
TA6	55.60	18.44	18.74	15.77	28.72	27.52
PA1	20.49	11.09	3.16	2.58	4.62	20.20
PA2	33.79	11.20	5.39	7.04	8.96	16.59
PA3	44.62	11.61	7.87	8.49	10.85	19.84
PA4	52.65	14.64	11.21	10.68	13.26	24.77
PA5	56.77	16.30	15.73	12.34	22.91	28.29
PA6	68.87	18.16	24.09	16.48	28.31	34.75

range, particularly at high energies like 1332.5 keV, with a radiation protection efficiency of 34.75%.

At moderate energy levels (356 keV, 661 keV, and 834.8 keV), attenuation becomes more difficult due to increased gamma ray penetration. TA6 performs slightly better with RPE values between 18.44% and 15.77%, while PT6 maintains its strong performance with values ranging from 17.97% to 12.85%. PA6, the most effective sample in the moderate energy range, outperforms both, achieving 18.16% at 356 keV, 24.09% at 661 keV, and 16.48% at 834.8 keV. The use of pure tin likely improves the shielding capacities of the PA composites. The PA composites show a little advantage over the TA and PT samples, despite the attenuation efficiency being significantly lower at lower energy levels. This drop suggests that these composites' overall density plays a major role in determining how effective they are at higher energies, and that further

tuning is necessary for higher energy shielding applications as described above in section 2.6.5 [124], [125].

At high energy levels such as 1173.3 keV and 1332.5 keV, shielding becomes even more difficult, and efficiency generally declines. TA6 improves with 28.72% and 27.52%, respectively, whereas PT6 records 10.66% at 1173.3 keV and 19.64% at 1332.5 keV. However, PA6 again leads with the highest efficiency, achieving 28.31% at 1173.3 keV and 34.75% at 1332.5 keV, confirming its superior performance in attenuating high-energy gamma radiation. Effective interactions with photon rays due to homogeneity of the pure tin filler and copper tin alloy within the PDMS matrix, result in reliable scattering and absorption processes that maximize radiation shielding. Therefore, multiple metals fabrication is a very useful method for radiation attenuation.

Across all sample series (PT, TA, and PA), the radiation protection efficiency exhibits slight increases and decreases with photon energy, rather than following a perfectly monotonic trend. This behavior arises from the energy-dependent dominance of photon interaction mechanisms: the photoelectric effect at low energies, which is highly sensitive to atomic number, and Compton scattering at higher energies, which depends on electron density and material thickness. Variations in filler content, particle distribution, and composite microstructure further influence attenuation efficiency, while minor experimental factors such as detector sensitivity and sample thickness tolerances can also contribute to fluctuations [28]. Despite these small deviations, the overall trend confirms that higher filler content and optimized compositions enhance shielding performance across the examined energy range.

In conclusion, PT6 is the most effective sample for low-energy radiation protection, while PA6 provides the best protection at both moderate and high energy levels. Among all tested samples, PA6 emerges as the most versatile and efficient composite for broad-spectrum gamma-ray shielding. According to the study, tin-based composites have the potential to replace lead as a radiation shielding material, particularly for low- to intermediate-energy photons. Even while lead is still the best option, PA composites show promising results and offer a safer, lighter, and more sustainable substitute. Future research should focus on improving high-energy photon attenuation, reducing porosity,

and optimizing filler content to further enhance the performance of these innovative composites.

4.7.4 Investigation of Half-Value Layer (HVL) and Tenth-Value Layer (TVL) for Radiation Attenuation Properties

The radiation shielding performance of tin/PDMS composites was assessed using HVL and TVL at different gamma-ray photon energies. It shows the compatibility of the composite to absorb energy by half or by 90%, respectively, with detailed analysis provided in Tables 4.6 and 4.7. In each sample, the HVL and TVL values show an increasing trend as photon energy rises (Figures 4.11 and 4.12). Since higher-energy gamma rays interact with the material less frequently, deeper penetration before noticeable attenuation takes place, this outcome is expected. Details of HVL and TVL are elaborated further in sections 4.6.3.1 until 4.6.3.3 accordingly.

The HVL and TVL results at certain energies (356 and 1332.5 keV) do not exhibit a strictly monotonic increase with photon energy. This behavior can be due to the energy-dependent transition of dominant photon interaction mechanisms and composite factors. At 356 keV, photon attenuation occurs within a transition region where both the photoelectric effect and Compton scattering contribute, making the attenuation coefficients highly sensitive to variations in effective atomic number, electron density, and filler dispersion [10]. Consequently, samples with lower metal content or less uniform microstructure may exhibit disproportionately high HVL and TVL values.

At 1332.5 keV, Compton scattering dominates and attenuation becomes primarily governed by electron density and material compactness rather than atomic number, allowing well-optimized composites to interact more effectively with high-energy photons [10]. This results in lower HVL and TVL values at 1332.5 keV compared to 356 keV despite the higher photon energy. Therefore, the observed non-linear trend reflects the complex interplay between photon energy, interaction mechanisms, and composite microstructure rather than experimental inconsistency. Compton scattering dominates and provides a more uniform interaction probability throughout the composite, especially for samples with high metal loading and good structural

continuity, resulting in higher measured attenuation coefficients and consequently lower HVL and TVL values [10], [115].

4.7.4.1 Tin/PDMS composites

The findings confirm that the tin/PDMS composites offer enhanced gamma-ray shielding performance compared to pure PDMS. The attenuation efficiency is particularly significant at lower photon energies, where the HVL and TVL values are minimized. However, at higher photon energies, a thicker composite is required to achieve effective shielding, as indicated by the increasing HVL and TVL values [7], [66], [126].

Table 4.6
Half Value Layer (HVL) of the Prepared Composite Samples at Different y-ray Photon Energies

Sample	122.1 keV	356 keV	661.7 keV	834.8 keV	1173.2 keV	1332.5 keV
	HVL (cm)					
C	6.34	2.80	11.41	17.00	30.80	3.38
CL	0.00	0.26	0.60	0.73	0.95	0.94
CT	0.10	1.04	1.36	1.39	2.57	2.16
PT1	0.91	9.19	8.07	6.42	12.37	3.00
PT2	0.50	8.02	4.65	3.55	16.17	2.61
PT3	0.38	4.80	4.04	3.21	7.87	2.52
PT4	0.26	3.36	3.02	2.70	5.08	2.19
PT5	0.21	1.91	2.77	2.36	4.34	1.58
PT6	0.18	2.02	2.72	1.89	3.32	1.71
TA1	2.02	21.41	7.06	4.40	3.39	4.28
TA2	1.05	4.83	5.46	3.43	3.02	2.68
TA3	0.75	3.91	3.63	2.82	2.67	2.24
TA4	0.59	2.72	3.23	2.70	2.06	1.31
TA5	0.56	2.00	2.55	1.97	2.04	1.24
TA6	0.45	1.77	2.14	1.80	1.09	1.14
PA1	1.48	10.56	12.98	2.89	7.19	1.51
PA2	0.79	5.87	4.46	2.74	3.47	1.80
PA3	0.63	4.57	4.22	3.03	3.26	1.69
PA4	0.47	2.97	3.13	2.23	2.48	1.24
PA5	0.43	2.11	2.74	2.03	1.39	1.08
PA6	0.33	1.41	2.16	1.94	1.17	0.91

When compared to the tin-reinforced composites, the C shows noticeably higher HVL and TVL values. For instance, the composite samples range from 2.72 cm (PT6) to 8.07 cm (PT1) at 661.7 keV, while the control sample has an HVL of 11.41 cm. The composites' lower HVL values indicate better attenuation related to the addition of tin, which has a greater Z and density and enhances photon interaction. Meanwhile, PT6 recorded 9.04 cm to reduce radiation intensity to 10% at 661.7 keV, this decrease demonstrates composite's efficiency in improving radiation shielding by adding tin filler into the PDMS.

Table 4.7
Tenth Value Layer (TVL) of the Prepared Composite Samples at Different y-ray Photon Energies

Sample	**122.1 keV**	**356 keV**	**661.7 keV**	**834.8 keV**	**1173.2 keV**	**1332.5 keV**
	TVL (cm)					
C	21.07	9.30	37.92	56.47	102.31	11.23
CL		0.85	1.99	2.41	3.16	3.12
CT	0.33	3.45	4.52	4.60	8.52	7.18
PT1	3.02	30.52	26.80	21.34	41.10	9.96
PT2	1.66	26.65	15.44	11.79	53.71	8.68
PT3	1.27	15.94	13.42	10.68	26.15	8.36
PT4	0.85	11.17	10.03	8.96	16.88	7.28
PT5	0.70	6.36	9.22	7.83	14.43	5.25
PT6	0.61	6.72	9.04	6.28	11.03	5.69
TA1	6.71	71.12	23.44	14.63	11.25	14.22
TA2	3.49	16.04	18.14	11.39	10.02	8.90
TA3	2.49	13.00	12.06	9.37	8.87	7.44
TA4	1.97	9.05	10.72	8.96	6.85	4.36
TA5	1.84	6.65	8.46	6.53	6.77	4.14
TA6	1.50	5.88	7.11	5.99	3.60	3.79
PA1	4.92	35.08	43.13	9.60	23.88	5.00
PA2	2.62	19.52	14.83	9.11	11.52	5.97
PA3	2.10	15.18	14.02	10.08	10.83	5.62
PA4	1.57	9.88	10.40	7.42	8.25	4.13
PA5	1.43	7.00	9.09	6.73	4.60	3.60
PA6	1.10	4.68	7.16	6.44	3.87	3.02

Superior shielding performance is indicated by samples with higher tin contents, like PT6, which have the lowest HVL and TVL values. Tin's increased density and Z, which increase the likelihood of photon interactions through Compton scattering and

photoelectric absorption, are responsible for this enhancement [10]. In contrast, samples like PT1 and PT2, which have less tin in them, have comparatively greater HVL and TVL values, indicating a lesser level of shielding effectiveness [61], [127], [128]. This result is consistent with earlier research that highlights the value of high Z elements in enhancing radiation shielding materials.

The effectiveness of the composite materials' shielding is greatly influenced by their composition. Tin's larger Z and density, which improve the material's capacity to interact with gamma rays, are responsible for the enhanced attenuation capabilities. Higher tin concentration improves gamma ray attenuation, particularly at lower photon energies, according to the pattern observed in the set of pure tin/PDMS composites. According to the results, tin/PDMS composites are excellent at protecting against y-rays, and their effectiveness improves with increasing tin content. The outcomes highlight these composites' potential as an alternative to conventional radiation shielding materials. The performance of the composite may be further improved for some applications by optimizing the tin content, especially in the application of low-energy gamma radiation. According to the findings, the tin/PDMS composites provide a versatile and effective way to defend against gamma radiation.

4.7.4.2 Copper Tin Alloy As a Filler

The HVL and TVL values of sample TA1 revealed notable improvements compared to C, particularly at higher energies such as 356 keV and 661.7 keV. This implies increased photon absorption, especially at higher energies, resulting from the addition of the copper tin alloy [10].

TA1 has an HVL of 2.02 cm at the lowest energy level of 122.1 keV, while TA6 displays a significantly lower HVL of 0.45 cm. Superior attenuation performance at low photon energy is indicated by this notable decrease in thickness for TA6. All TA samples show an increase in HVL values as the photon energy rises. TA1 requires an HVL of 21.41 cm at 356 keV, but TA6 only needs 1.77 cm. At intermediate energies, similar patterns are seen, with HVL values for TA2, TA3, TA4, and TA5 falling between those of TA1 and TA6.

These findings imply that the density or efficiency of the material's interaction with photons increases with the metal's composition [70]. TA1 exhibits a TVL of 6.71 cm at 122.1 keV, whereas TA6 reports a noticeably lower value of 1.50 cm, demonstrating TA6's superior performance once more. All samples exhibit higher TVL values as the photon energy increases, while TA6 consistently maintains the lowest TVL across the entire energy spectrum. TA1's TVL is 71.12 cm at 356 keV, while TA6's is only 5.88 cm. This noticeable difference demonstrates that TA6 continues to provide improved protection at higher energy while simultaneously attenuating radiation more efficiently at lower energies. To achieve effective gamma-ray attenuation, the findings show that the improved composition in TA6 leads to a more compact structure or a greater effective density.

In conclusion, it is evident from the analysis of the HVL and TVL data for the TA series that TA6 performs the best in terms of radiation shielding among the TA samples. In comparison to TA1 through TA5, it requires substantially less material thickness to produce effective attenuation, as evidenced by its significantly lower HVL and TVL values across the tested photon energies. According to these results, creating effective, lightweight, lead-free radiation shielding materials requires optimizing the composition, especially by raising the concentration or enhancing the dispersion of metal fillers. Even though the copper tin alloy/PDMS composites demonstrate encouraging radiation shielding properties, several parameters need to be taken into account for further research. The performance of these composites at varying filler concentrations of tin and copper should be explored further, as well as the impact of different curing temperatures and processing conditions. Moreover, the mechanical properties of these composites, which are crucial for practical applications, should be assessed to ensure that the composites remain stable and durable under radiation exposure.

4.7.4.3 Pure tin/Copper tin alloy/PDMS composites

While PA6 retains a comparatively lower HVL (0.33 cm), PA1 continues to show the largest HVL (1.48 cm) as photon energy rises to 122.1 keV. In contrast to PA1, which exhibits significantly higher HVL values of 10.56 cm at 356 keV and 1.51 cm at 1332.5 keV, PA6 continuously displays the lowest HVL values, such as 1.41 cm at

356 keV and 0.91 cm at 1332.5 keV. This tendency persists at higher energies. These findings demonstrate that PA6 provides excellent photon attenuation at every energy level examined. PA6 consistently exhibits the lowest TVL across all PA samples, and the TVL values follow the same trend as the HVL values. The difference is more noticeable as photon energy rises. For example, PA6 retains a significantly lower TVL of 4.68 cm at 356 keV, but PA1 displays a high TVL of 35.08 cm. At 1332.5 keV, PA6 exhibits better performance as well, recording a TVL of 3.02 cm as opposed to 5.00 cm for PA1.

The filler concentrations in each PA sample contribute to the observed variations in HVL and TVL values. With the maximum concentration of tin filler, PA6 efficiently lowers radiation penetration, which lowers HVL and TVL values. On the other hand, PA1, which has the lowest proportion of tin filler, offers less attenuation and necessitates a significantly larger thickness to produce the same degree of shielding. This indicates that by raising the material's density and interaction likelihood with incident photons, a higher tin concentration improves radiation attenuation [5], [10]. In summary, PA6 has the lowest HVL and TVL values across all photon energies, making it the most efficient shielding composite among the PA samples. This suggests that PA6 is an effective choice for radiation shielding applications, as it requires less material thickness to achieve the required attenuation. The results highlight the importance of filler concentration in maximizing the radiation protection of composite materials.

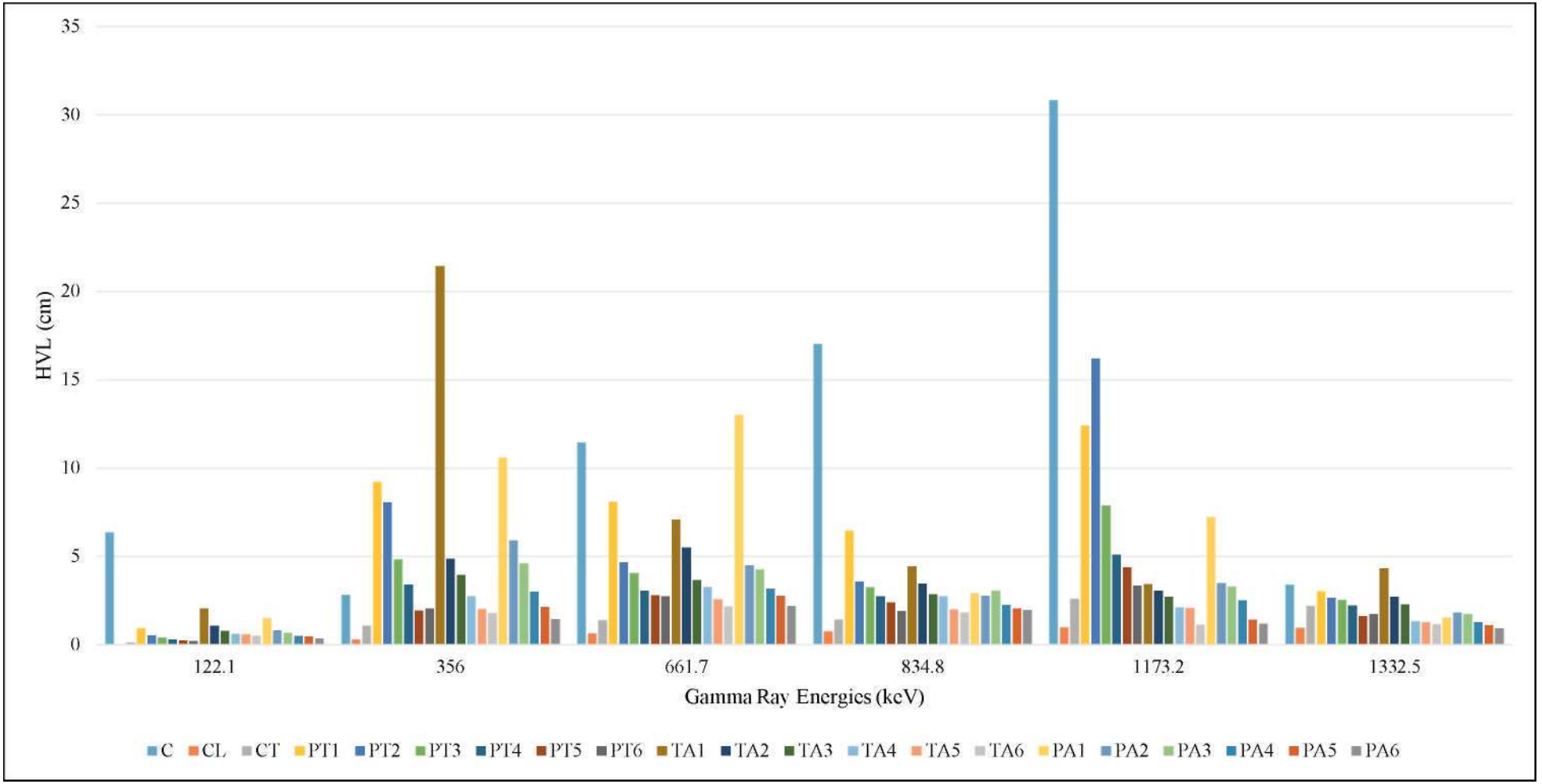

Figure 4.11 Bar Graph Comparison of HVL Results for Each Composite

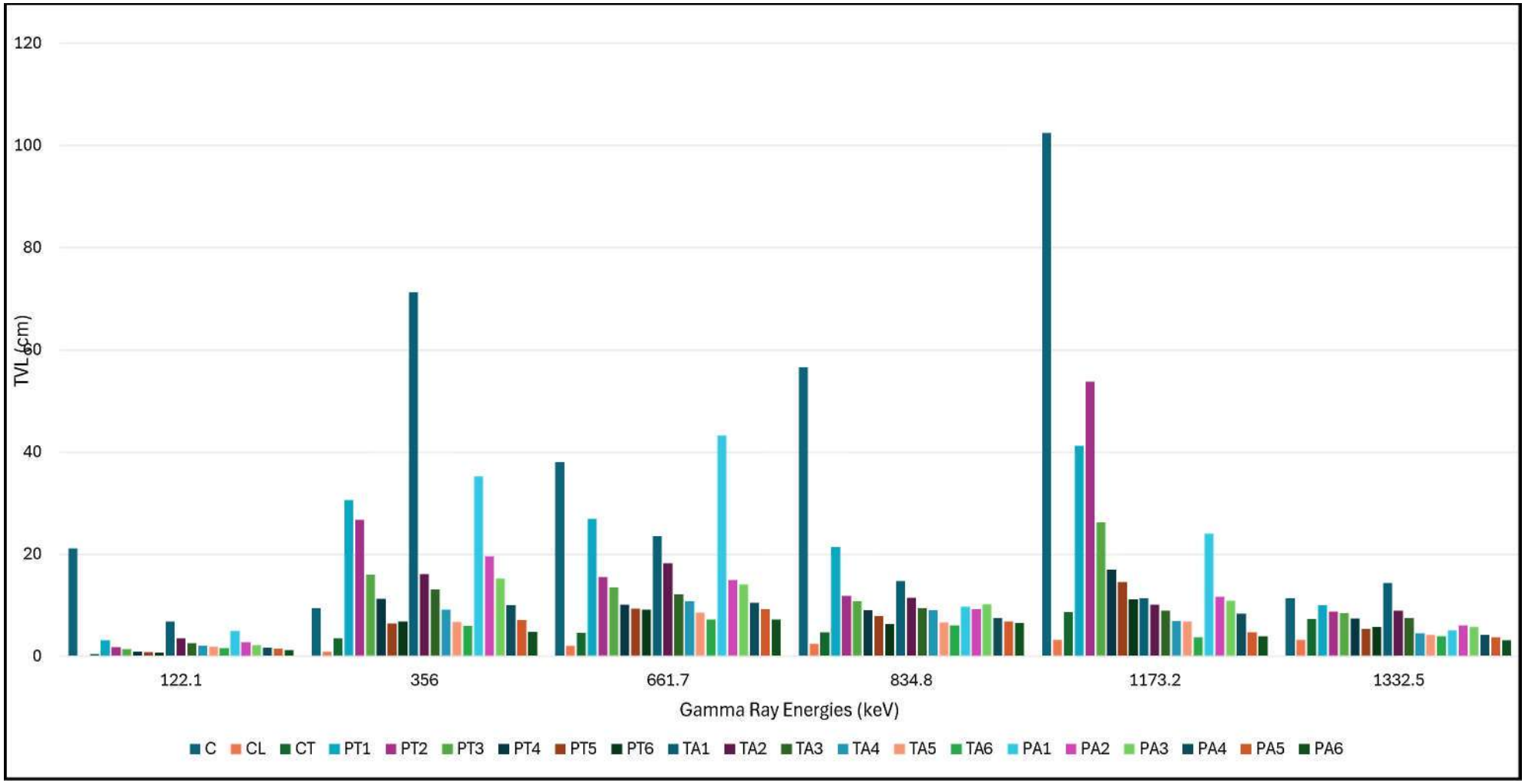

Figure 4.12 Bar Graph Comparison of TVL Results for Each Composite

4.7.5 Examination of Mean Free Path (MFP) in Relation to Composite Density and Shielding Capacity

The average distance a photon travels before encountering the shielding medium is known as the mean free path (MFP), and it is an essential metric for assessing a material's shielding capabilities. Stronger photon attenuation is indicated by a lower MFP value, which improves shielding effectiveness (Table 4.8 and Figure 4.13) [6], [8].

Despite being less dense than lead, tin exhibits intermediate performance, as evidenced by its shorter MFP compared to pure PDMS. The MFP for the tin-PDMS composites increases with photon energy because higher-energy photons are less likely to interact. PA samples show the shortest MFP among the composites, indicating better photon interaction, due to the combined effects of pure tin and copper tin alloy. This suggests that the addition of copper enhances the attenuation capability by improving filler dispersion and matrix interaction.

At every energy level, the C shows the largest MFP values, ranging from 9.15 cm at 122.1 keV to 44.43 cm at 1173.2 keV. Its weak attenuation qualities and reduced density prove its poor shielding capability. The improved shielding performance of the composite samples with higher tin filler concentrations, specifically PT6 (2.47 cm at 1332.5 keV), TA6 (1.65 cm at 1332.5 keV), and PA6 (1.31 cm at 1332.5 keV), is indicated by their much lower MFP values across all energy levels.

Because the photoelectric effect predominates at lower photon energies, MFP values stay relatively low. However, because of the Compton scattering interaction, the MFP values rise dramatically as photon energy rises above 356 keV, especially for composites with lower tin filler percentages. At higher photon energies, notably 2.47 cm at 1332.5 keV, PT6 exhibits the lowest MFP values of any investigated composite. PA6 and TA6 follow closely behind at 1.31 cm and 1.65 cm, respectively. This composite is the most promising option for radiation shielding applications due to its significant MFP decrease, which emphasizes its improved photon attenuation capabilities. Its enhanced attenuation performance is a result of a well-dispersed filler matrix and a high tin content.

Table 4.8
MFP Data Information for Each Composite

Sample	122.1 keV	356 keV	661.7 keV	834.8 keV	1173.2 keV	1332.5 keV
		MFP (cm)				
C	9.15	4.04	16.47	24.52	44.43	4.88
CL		0.37	0.86	1.05	1.37	1.36
CT	0.14	1.50	1.96	2.00	3.70	3.12
PT1	1.31	13.26	11.64	9.27	17.85	4.33
PT2	0.72	11.58	6.71	5.12	23.33	3.77
PT3	0.55	6.92	5.83	4.64	11.36	3.63
PT4	0.37	4.85	4.36	3.89	7.33	3.16
PT5	0.31	2.76	4.00	3.40	6.27	2.28
PT6	0.27	2.92	3.93	2.73	4.79	2.47
TA1	2.91	30.89	10.18	6.35	4.88	6.18
TA2	1.51	6.97	7.88	4.95	4.35	3.86
TA3	1.08	5.65	5.24	4.07	3.85	3.23
TA4	0.86	3.93	4.65	3.89	2.98	1.89
TA5	0.80	2.89	3.67	2.84	2.94	1.80
TA6	0.65	2.55	3.09	2.60	1.57	1.65
PA1	2.14	15.24	18.73	4.17	10.37	2.17
PA2	1.14	8.48	6.44	3.96	5.00	2.59
PA3	0.91	6.59	6.09	4.38	4.70	2.44
PA4	0.68	4.29	4.52	3.22	3.58	1.79
PA5	0.62	3.04	3.95	2.92	2.00	1.56
PA6	0.48	2.03	3.11	2.80	1.68	1.31

There are multiple reasons for the observed rise in attenuation levels at 1173.2 keV as compared to 1332.5 keV. Measurement variability and experimental uncertainty are two (2) potential explanations, where small data discrepancies may occur as a result of background noise, or device limits as explained earlier in section 2.6.2. Furthermore, as attenuation coefficients often decrease as photon energy increases, the energy-dependent behaviour of attenuation is significant. However, attenuation might not exhibit a strictly declining trend because of disruptions by some interactions, such as Compton scattering [10]. A combination of energy-dependent attenuation behaviour, material composition effects, detector response changes, and scattering processes is probably responsible for the attenuation values between 1173.2 keV and 1332.5 keV. This pattern may become clearer with a more thorough investigation, such as calibration studies or Monte Carlo simulations as highlighted in the section 2.6.1.

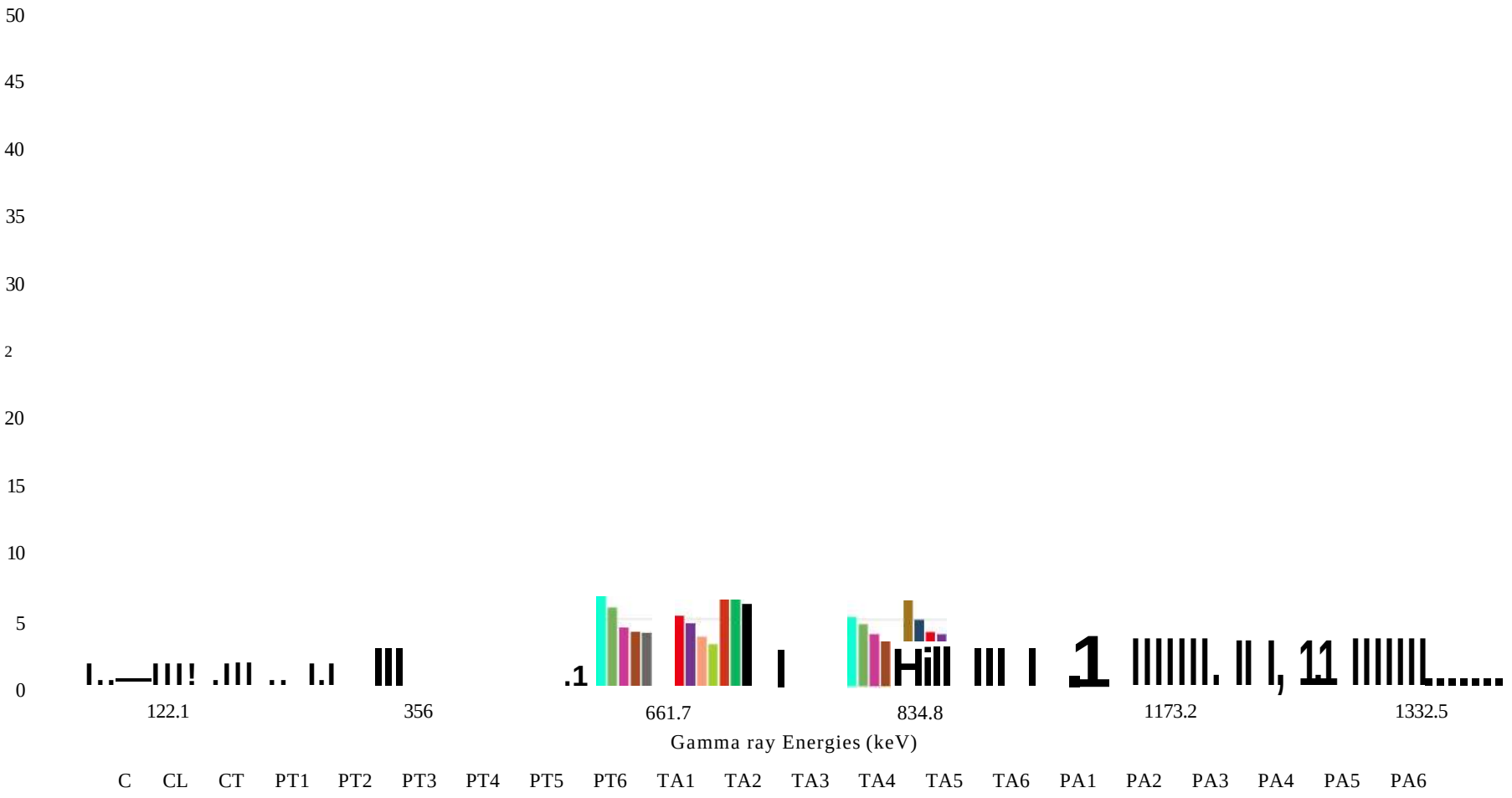

Figure 4.13 Bar Graph of MFP Values Against Different Energy Levels

In conclusion, the examination of MFP values shows that increasing filler concentrations enhances the shielding effectiveness of tin-PDMS composites. The top-performing composites are PT6, TA6, and PA6, with PT6 being the most efficient in reducing photon penetration. In order to create effective, lead-free radiation shielding materials appropriate for a wide range of photon energies, it is crucial to optimize the tin filler content inside polymer matrices.

4.7.6 Factors Influencing Radiation Shielding Efficiency

The finding that radiation intensities decrease in direct proportion to metal composition can be attributed to several material properties, interaction mechanisms, and laboratory settings. One of the primary causes is the composite materials' inhomogeneity. Uneven metal particle distribution in metal-polymer composites can lead to variations in density and shielding efficacy. Furthermore, a larger metal content may indirectly cause composites to become more porous. Increased porosity reduces the overall density of the material, countering the benefits of a higher metal content for radiation attenuation [129].

One important factor is the interaction between photons and materials. Radiation attenuation may depend on the photons' energy and the interaction mechanism, such as pair production, Compton scattering, or the photoelectric process. Experimental limitations and preparation conditions are additional factors that may be responsible for the non-proportional relationship. Background noise and detector sensitivity can affect variability, particularly at high attenuation levels where transmitted intensities are very low. Additionally, sample thickness or unequal exposure to radiation beams could affect the observed intensities as stated earlier in the section 2.6.2.

There are notable variations in the Z and density of the metals used in the composites, including tin and copper. Tin's better photon attenuation capabilities may dominate the shielding performance even at lower densities due to its bigger Z. However, copper's lower Z reduces its efficiency despite its higher content, resulting in different shielding attenuation capabilities. Furthermore, issues like as oxidation during preparation may alter the effective shielding contribution of the metals [102], [130]. To overcome these

challenges, steps including improving material homogeneity, standardizing sample thickness accurately, and conducting energy-dependent shielding tests are essential.

4.7.7 Identification of the Best Composite for Gamma Radiation Shielding

Several composite materials namely PT5, PT6, TA5, TA6, PA5, and PA6 were chosen as the best performers in attenuating radiation gamma ray. The effectiveness of these materials was assessed based on their MAC, LAC, RPE, HVL, TVL and MFP across gamma ray energies range from 122.1 keV to 1332.5 keV. Among these, PT5 and PT6 demonstrated the highest MAC and LAC values at low energies (Figures 4.14 and 4.15). However, the attenuation efficiency of these composites decreased significantly with increasing photon energy as expected.

In contrast, the PA5 and PA6 composites exhibited lower MAC and LAC values at low energies but showed a relatively stable or slightly increasing trend as photon energy increased. This suggests a superior performance in the medium to high energy range, making these composites suitable for shielding against industrial or therapeutic gamma sources. TA5 and TA6 showed moderate performance, with MAC and LAC values that were lower than those of the PT group but more stable than the PA group at lower energies.

Based on the analysis, PT6 emerges as the most effective composite material for shielding against low-energy gamma radiation due to its high MAC at 122.1 keV. Meanwhile, PA6 is identified as the most promising candidate for medium to high-energy radiation shielding, owing to its increasing MAC and LAC trends and stable performance across the evaluated energy range. These findings underscore the importance of selecting composite materials based on the energy spectrum of the intended radiation application.

In the plotted results (Figure 4.14), the "CL" sample shows an abnormally high or potentially infinite MAC at lower gamma ray energies (around 122.1 keV). This anomaly may be attributed to either experimental or computational factors. A likely explanation is that the thickness or density used in the MAC calculation was extremely

small or zero, which, according to the MAC formula in equation 2.2, would cause the MAC value to approach infinity as the denominator approaches zero.

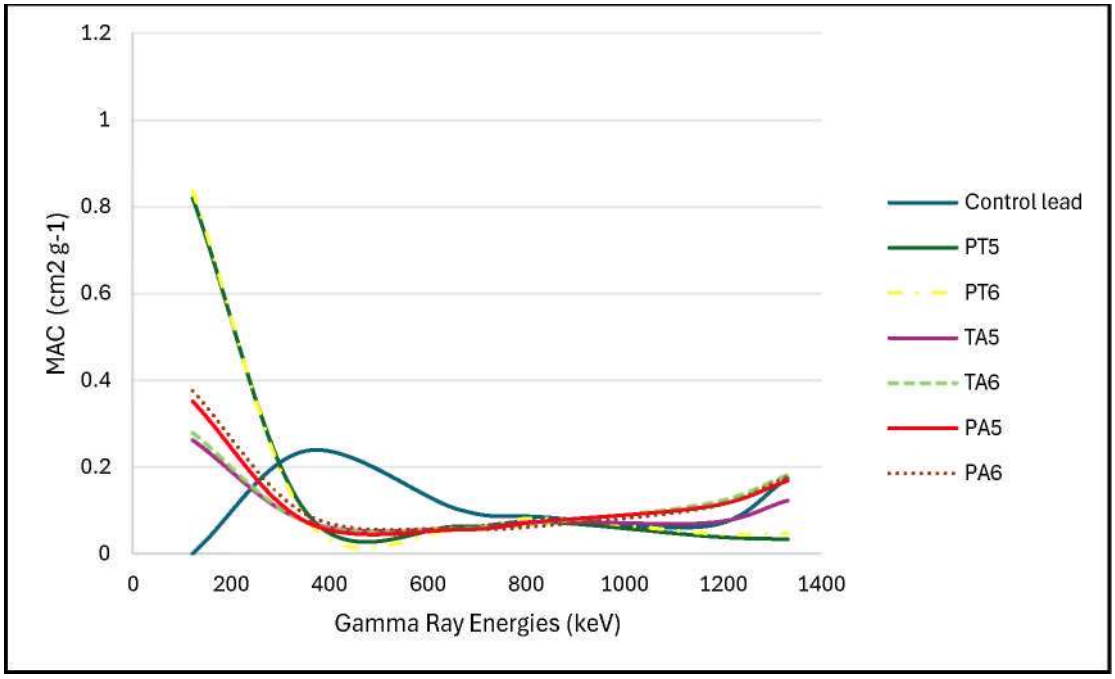

Figure 4.14 The Comparison of MAC Values Among Selected Composites

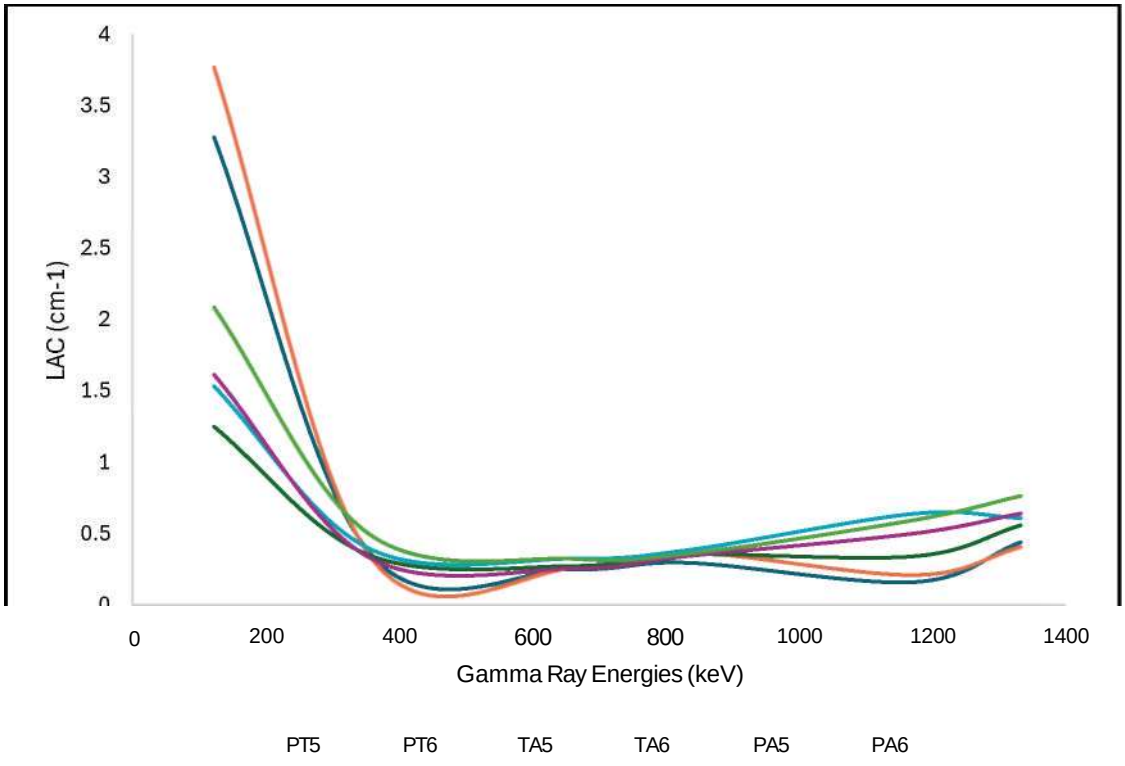

Figure 4.15 Comparison of LAC Values with Selected Composites

According to theoretical predictions, all samples show a declining trend in RPE as photon energy rises (Figure 4.16) reflecting the theoretical studies in section 2.6.4. This is because higher-energy gamma photons are more penetrating and thus more difficult to attenuate. The CL sample exhibits the largest RPE (100%) at 122.1 keV. This could be because of total attenuation or limitations during measurement or computation, which could be impacted by the thinner sample or higher density in the experimental apparatus as mentioned in the discussion in section 4.6.1.

All samples' RPE values drastically decrease as energy rises to 356 keV and 661.7 keV, with the majority falling to their lowest point near 661.7 keV. The energy area where Compton scattering takes over as the primary interaction process and lowers attenuation efficiency is reflected in this pattern [10]. A little rise in RPE is seen in a few of the samples after 661.7 keV, particularly in PA5, and PA6, indicating improved shielding effectiveness at higher energies. Increased homogeneity, ideal filler dispersion, or beneficial synergistic effects of the composite ingredients could be the cause of this improvement.

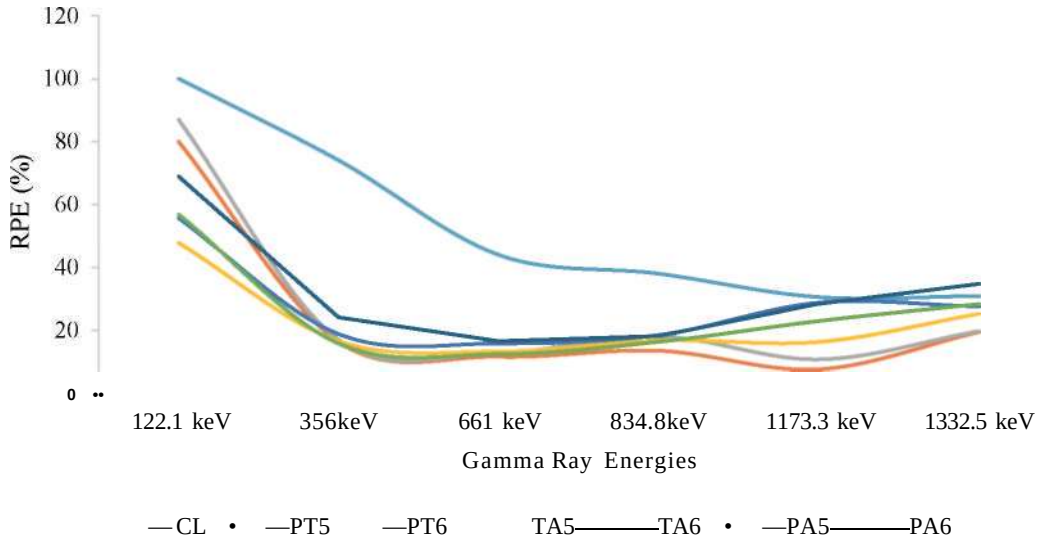

Figure 4.16 RPE Values of Selected Composites from Each Series

At medium to high energies (834.8-1332.5 keV), PA6 and TA6 consistently show reasonably constant and superior RPE performance compared to all evaluated samples, suggesting that these compositions may offer a more dependable shielding effect for high-energy gamma radiation. On the other hand, PT5 and PT6 exhibit comparatively

lower RPE values throughout the spectrum, particularly at intermediate and higher energies suggesting impairable characteristics for radiation shielding. This study consistent with the previous study, where the highest metal filler displayed the same pattern as this present research [131].

Therefore, from MAC, LAC and RPE results, PT and PA series were included for final evaluation to determine the best composite. An evaluation of HVL, TVL, and MFP offers more information on these composites' effectiveness (Figure 4.17). The lowest HVL, TVL, and MFP values are seen in PT6 and PA6, indicating that less material is needed to produce significant radiation attenuation. Higher energy photons require thicker shielding layers for effective attenuation, as indicated by the increasing values of HVL, TVL, and MFP with photon energy.

In general, the values of HVL, TVL, and MFP increase with photon energy, consistent with the fundamental principle that higher-energy gamma photons are more difficult to attenuate and thus require a thicker material for the same degree of shielding. For PT6, the shielding parameters (particularly TVL and MFP) rise sharply with energy, reaching their highest values at 1173.2 keV, where the TVL peaks at nearly 12 cm and the MFP exceeds 4 cm. This significant increase suggests that PT6 becomes less effective at attenuating high-energy gamma rays due to lower photon interaction probability at elevated energies.

In contrast, the PA6 sample demonstrates a more stable trend across the entire energy range. Its HVL, TVL, and MFP values increase more gradually and remain consistently lower than those of PT6 at high energies, indicating superior attenuation performance. Notably, the TVL of PA6 remains below 7 cm even at the highest energy of 1332.5 keV, while MFP stays under 3 cm, implying that this composite requires less material thickness to achieve effective radiation shielding. The more favorable performance of PA6 may be attributed to enhanced particle dispersion and the synergistic combination of copper tin alloy with pure tin, resulting in better density and structural uniformity [132].

The contrast in trends between PT6 and PA6 highlights the importance of material composition and microstructural integration in determining the shielding performance of composite materials. PA6's more efficient attenuation across a broad energy range supports its potential application as a promising lead-free shielding material, especially in environments exposed to medium- and high-energy gamma radiation.

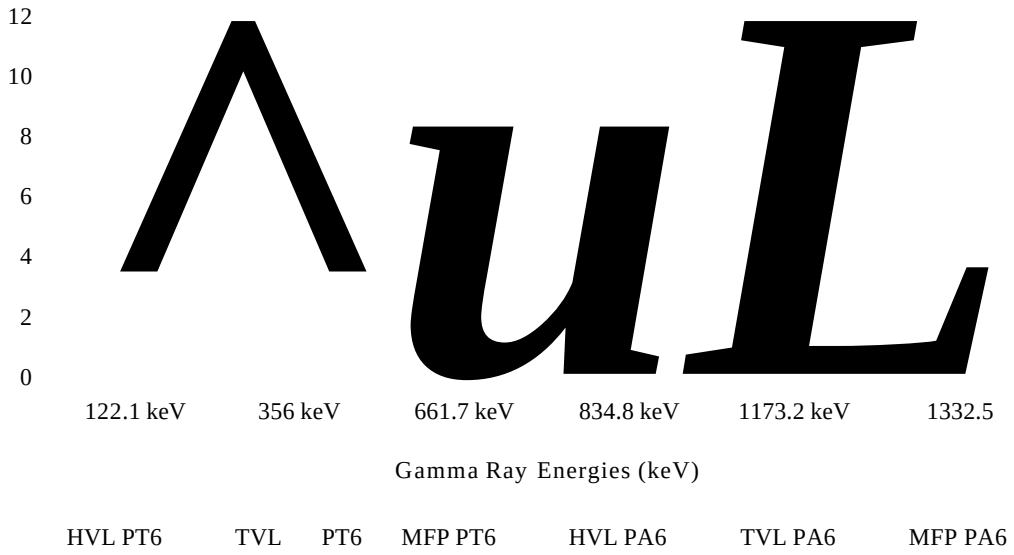

Figure 4.17 HVL, TVL and MFP of the Optimized Composites

In summary, PA6 is the best-performing composites for radiation shielding, according to a thorough investigation of RPE, MAC, LAC, HVL, TVL, and MFP. PA6 which consistently shows high RPE values across all photon energies, superior MAC and LAC values, and decreased HVL, TVL, and MFP values. These composites are ideal for applications needing small but efficient shielding because they have the best attenuation qualities and the lowest shielding thickness requirements. Excellent performance in attenuating high energies is demonstrated by PA6, which makes these composites promising options for lead-free radiation shielding.

While traditional lead-based PPE materials are effective at attenuating X-rays in the 30 to 70 keV range, their efficiency drops considerably at higher energies, similar to the observed trend in the tin-PDMS composites. However, the PA6 composite showed relatively stable attenuation properties across a broader energy spectrum, indicating better adaptability for medium- to high-energy gamma radiation applications. This makes PA6 especially promising for shielding settings where both flexibility and wide-

range energy protection are needed, such as interventional radiology, portable shielding equipment, or industrial radiography.

Beyond attenuation efficiency, lead-based PPE often imposes ergonomic constraints due to its rigidity and weight, which limit wearer mobility and long-term use comfort. In contrast, the flexibility and lightweight nature of the PDMS matrix allow the tin-based composites to be fabricated into various forms such as garments, panels, or equipment linings without sacrificing comfort or safety. The absence of lead also eliminates concerns regarding long-term toxicity and disposal, making these materials safer for repeated use in clinical, nuclear, or industrial environments.

The results of this work provide evidence for the fabrication of tin-reinforced PDMS composites with higher tin concentrations as an effective alternative to conventional lead-based shielding materials. To increase the suitability of these materials in industrial, medical, and nuclear shielding settings, further research should include enhancing mechanical strength, maximizing tin particle dispersion, and evaluating long-term stability under radiation exposure.

4.7.8 Lead Equivalent for Optimized Samples

Table 4.9 presents the lead equivalent thickness (Pb-eq, cm Pb) of PT6, and PA6 composites at photon energies ranging from 122.1 to 1332.5 keV, calculated based on their linear attenuation coefficients relative to lead using equation 2.9 stated in section 2.4. The Pb-eq values represent the thickness of lead required to provide equivalent gamma-ray attenuation as the fabricated composites at the same photon energy [53].

Table 4.9
Lead Equivalent for PT6 and PA6 Across Different Energy Levels

	Energy Levels (keV)					
Samples	122.1	356	661.	834.	1173.	1332.5
			Lead Equivalent (cm Pb)			
PT6	N/A	0.48	0.08	0.10	0.11	0.11
PA6	N/A	0.38	0.14	0.12	0.29	0.61

For all samples, the Pb-eq values decrease with increasing photon energy. This behaviour is expected due to the energy dependence of gamma-ray interaction mechanisms. At lower photon energies, attenuation is dominated by the photoelectric effect, which is highly dependent on atomic number, resulting in higher Pb-eq values. As photon energy increases, Compton scattering becomes the dominant interaction process, reducing the attenuation efficiency of the composites relative to lead and consequently lowering the Pb-eq values [10].

Among the investigated samples, PT6 exhibits the highest Pb-eq values across all measured energies proofing the promising shielding performance which is consistent with other radiation shielding parameter with RPE (86.92 to 19.64%), MAC (0.84 to 0.09 cm^2 g^1) and LAC (3.77 to 0.41 cm"^{1}), HVL (0.18 to 1.71 cm), TVL (0.61 to 5.69 cm), and MFP (0.27 cm) values. At 356 keV, PT6 records a Pb-eq of 0.48 cmPb, which gradually decreases to 0.11 cmPb at 1332.5 keV. The enhanced performance of PT6 is attributed to its high pure tin content, higher electron density, and better dispersion of tin particles within the PDMS matrix, as supported by FESEM observations. These factors contribute to more effective photon interaction and attenuation.

PA6 exhibits lower Pb-eq values compared to PT6 at all energies. The improved performance of PA6 compared to TA6 can be observed throughout out all the radiation shielding parameters, including Pb-eq, which is attributed to the synergistic effect of combining pure tin and alloy particles within the PDMS matrix. The increase in Pb-eq values for PA6 at 1173.2 keV (0.29 cmPb) and 1332.5 keV (0.61 cmPb) is attributed to the dominance of Compton scattering at high photon energies, where the heterogeneous polymer-metal structure enhances multiple scattering and effective attenuation relative to lead [87]. This hybrid composition enhances particle packing density and interaction probability with incident photons, resulting in higher Pb-eq values, particularly at higher photon energies.

The Pb-eq values at 122.1 keV are reported as not available (N/A) for all samples. This is likely due to near-complete attenuation or experimental limitations at low energy, which prevent accurate determination of the linear attenuation coefficient and subsequent Pb-eq calculation [113]. Such limitations are commonly reported in

radiation shielding studies and do not detract from the overall interpretation of shielding performance.

4.7.9 Comparison of Radiation Shielding Performance with Previous Studies

This present study introduces a novel approach to radiation shielding by integrating pure tin (Sn) and copper tin (Cu-Sn) alloy fillers into a PDMS (polydimethylsiloxane) matrix, to enhance X-ray and gamma-ray attenuation efficiency. Compared to previously reported metal-polymer composites such as PbO/PDMS, SnCh/PDMS, ZnO/PDMS, and E^Cb/PDMS, the current research stands out in several radiation attenuation characteristics (Table 4.10).

For instance, PbO/PDMS composites with 50 wt% filler reported by [30] exhibited high linear attenuation coefficients at low energies; however, a substantial reduction in LAC was observed as photon energy increased, reaching as low as 0.12 cm^{-1} at 1332.2 keV. This significant drop highlights the limitation of oxide-based fillers in shielding high-energy gamma radiation, where Compton scattering becomes dominant.

Similarly, Sn02/PDMS composites investigated by [9] demonstrated strong attenuation at 59.51 keV but showed a decrease in MAC values (0.05 cm^2 g^{-1}) at 1332 keV, indicating reduced shielding efficiency against high penetrating gamma photons. ZnO/PDMS composites reported by [31] required relatively thin sample thicknesses (0.10-0.20 cm) but exhibited large HVL and TVL values at 661.62 keV, reaching up to 7.40 cm and 24.54 cm, respectively. These results suggest that while ZnO-based composites may be effective for low-energy radiation protection, their performance becomes less practical for high-energy applications due to the need for greater shielding thickness. In contrast, Bi203/PDMS composites studied by [32] achieved high radiation protection efficiency (96.40%) under diagnostic X-ray conditions (100 kV), but the study was limited to low-energy photons and did not assess shielding performance in the MeV range.

Compared with these previous oxide-based systems, the present Sn/PDMS composite with 60% metallic tin demonstrates superior and more consistent shielding

performance across a broader photon energy range (122.1-1332.2 keV). The composite maintains relatively high LAC values even at 1332.2 keV (0.41 cm^{-1}), resulting in lower HVL (0.18-1.71 cm) and TVL (0.61-5.69 cm) values than those reported for ZnO- and SnCh-based PDMS composites. This improvement is attributed to the higher electron density of metallic tin compared to its oxide counterparts, which enhances Compton scattering interactions at high photon energies.

Importantly, the composites developed here show promising results without the use of toxic heavy metals like lead or bismuth, offering a safer and more environmentally friendly alternative. The ability of metallic pure tin and copper tin alloys to provide effective attenuation, particularly in the diagnostic and therapeutic energy ranges, emphasizes the novelty and practical relevance of the present research in developing lead-free, flexible, and efficient radiation shielding materials.

Table 4.10
Summary of Radiation Attenuation Characteristics of Selected Metal-PDMS Composites

References	Metal/Polymer	Metal (%)	Thickness (cm)	Radiation Energies (keV)	MAC (cm^2 g^1)	LAC (cm^1)	RPE (%)	HVL (cm)	TVL (cm)	MFP (cm)
[30]	PbO/PDMS	**50**	1.00	59.51-1332.20	~	4.71-0.12	~	~	~	-
[9]	$Sn0_2$/PDMS	**50**	0.50	59.51-1332.00	2.59-0.05		-			
[31]	ZnO/PDMS	**15**	0.10-0.20	22.16-661.62	**47.18-**0.08	5.40-0.09	~	0.13-7.40	0.19-24.54	0.43-10.67
[32]	Bi_20_3/PDMS	**40**	0.84	100 kV	-		96.40			-
Present	Sn/PDMS	60	0.50	122.10-1332.20	0.84-0.09	3.77-0.41	86.92-19.54	0.18-1.71	0.61-5.69	0.27-2.47
	Cu-Sn/PDMS				0.39-0.14	2.08-0.76	68.87-34.75	0.33-0.91	1.10-3.02	0.48-1.31

CHAPTER 5
CONCLUSION

5.1 Summary

This research successfully demonstrated the potential of PDMS-based composites reinforced with pure tin and copper tin alloy as promising alternatives to conventional lead-based materials for photon radiation shielding. Characterization methods like FESEM-EDX, XRD, FTIR spectroscopy, and gamma-ray spectroscopy were investigated to thoroughly assess the composites' functional, chemical, and physical characteristics.

The composite samples' microstructural morphologies differed noticeably, according to FESEM analysis. Tin particles were evenly dispersed and embedded within the PDMS matrix of the pure tin-filled PDMS composites, which demonstrated strong integration. Improved structural integrity, which is essential for mechanical stability and long-term shielding performance, has been improved by this homogeneity. The copper tin alloy particles in TA and PA composites, on the other hand, were spherical in shape and displayed proof of weak matrix adherence or dissociation. This suggested significantly poorer filler-matrix bonding, which could lead to decreased shielding effectiveness because of the development of micro-voids that let radiation pass through.

The XRD analysis confirmed structural and phase differences among the samples. The C sample showed an amorphous pattern, while the CT and PT6 samples exhibited sharp peaks corresponding to the P-Sn (tetragonal phase), indicating high crystallinity. The TA6 sample revealed weaker, broader peaks attributed to CueSns, reflecting lower crystallinity due to particle clustering and weaker bonding. The PA sample, combining pure tin and alloy in PDMS, showed a mix of P-Sn and CueSns phases, with better crystallinity than TA but less uniformity than PT. These results highlight how composition affects phase formation and structural integrity.

The absence of any notable chemical reactions between the metal fillings and the PDMS matrix was verified by FTIR spectroscopy. The lack of additional functional groups indicates physical interactions between the metal fillers and the polymer matrix. The results highlight the significance of particle form, dispersion, and mechanical integration in maintaining successful filler incorporation and preserving composite homogeneity. Measurements using gamma-ray spectroscopy gave important information about the fabricated composites' capacity to attenuate radiation. The findings showed that shielding performance and filler composition were positively correlated, with pure tin-reinforced PDMS outperforming the TA and PA groups. The PT6 composites showed higher MAC and LAC with lower HVL, TVL and MFP indicating superior photon absorption ability, particularly at low-energy gamma rays. These findings were also supported by higher RPE values in PT6, highlighting the dominant role of high-Z fillers like pure tin compared to copper tin alloy in attenuating ionizing radiation. However, for moderate and high energy gamma rays, PA6 displayed superior characteristics as it revealed stability in shielding radiation across moderate to high energies compared to PT6.

Overall, the research demonstrates that PDMS composites reinforced with pure tin have outstanding radiation shielding capabilities for low radiation energies while maintaining beneficial properties including flexibility, lightweight, and lead-free composition. The mixture of multiple metals reported better shielding efficiency for high energy gamma-ray. The study contributes to the development of composites in environmentally friendly and non-toxic radiation protection materials while effectively addressing the health and environmental issues related to conventional lead-based shields. Future research may further improve on these findings, especially in filler dispersion, composite formulation optimization, and structural modification for improved shielding at various energy levels. With additional research, these composites might find beneficial applications in nuclear installations, medical imaging centers, aircraft parts, and personal protective equipment.

5.2 Future works

Future study in a variety of fields is suggested in order to improve the performance and development of PDMS-based composites for radiation shielding

applications. First, the homogeneity and integration between the metallic particles and the PDMS matrix could be improved by optimizing the filler dispersion process, such as by utilizing coupling agents, surfactants, or ultrasonication. This is particularly applicable to alloys with poorer adhesion, such as copper-tin. Furthermore, adding additional high-Z nanoparticles, like tin oxide, zinc oxide or tungsten oxide, in hybrid or multi-layered concepts may increase attenuation efficiency even further while preserving flexibility and lightweight characteristics. The long-term stability, mechanical strength, and thermal resistance of these composites under various environmental circumstances may also be investigated in future research. Improved understanding of structural integrity and degradation behavior may be possible with the use of advanced characterization methods like mechanical testing, and thermogravimetric analysis. Additionally, testing across broader photon energy ranges and replicating the shielding performance under real-world circumstances could support the practical use of these materials in industrial, medical, or space-related settings. Lastly, increasing the fabrication process's capacity while maintaining its affordability and environmental safety is still a crucial step in achieving commercial viability.

REFERENCES

[1] F. R. Tang and K. Loganovsky, "Low dose or low dose rate ionizing radiation-induced health effect in the human," *J Environ Radioact*, vol. 192, pp. 32-47, 2018, doi: 10.1016/j.jenvrad.2018.05.018.

[2] A. Vaiserman, A. Koliada, O. Zabuga, and Y. Socol, "Health Impacts of Low-Dose Ionizing Radiation: Current Scientific Debates and Regulatory Issues," *Dose-Response*, vol. 16, no. 3, pp. 1-27, Jul. 2018, doi: 10.1177/1559325818796331.

[3] S. C. Kim, "Analysis of shielding performance of radiation-shielding materials according to particle size and clustering effects," *Applied Sciences (Switzerland)*, vol. 11, no. 9, 2021, doi: 10.3390/appl 1094010.

[4] M. Almurayshid *et al*, "Development of New Lead-Free Composite Materials as Potential Radiation Shields," *Materials*, vol. 14, no. 17, p. 4957, Aug. 2021, doi: 10.3390/mal4174957.

[5] W. Poltabtim, E. Wimolmala, and K. Saenboonruang, "Properties of lead-free gamma-ray shielding materials from metal oxide/EPDM rubber composites," *Radiation Physics and Chemistry*, vol. 153, pp. 1-9, 2018, doi: 10.1016/j.radphyschem.2018.08.036.

[6] A. H. Alsaab and S. Zeghib, "Study of prepared lead-free polymer nanocomposites for X- and gamma-ray shielding in healthcare applications," *Polymers (Basel)*, vol. 15, no. 9, May 2023, doi: 10.3390/polyml5092142.

[7] Z. Li, W. Zhou, X. Zhang, Y. Gao, and S. Guo, "High-efficiency, flexibility and lead-free X-ray shielding multilayered polymer composites: layered structure design and shielding mechanism," *Sci Rep*, vol. 11, no. 1, pp. 1-13, 2021, doi: 10.1038/s41598-021-83031-4.

[8] S. Jayakumar, T. Saravanan, and J. Philip, "A review on polymer nanocomposites as lead-free materials for diagnostic X-ray shielding: Recent advances, challenges and future perspectives," *Hybrid Advances*, vol. 4, p. 100100, Dec. 2023, doi: 10.1016/j.hybadv.2023.100100.

[9] M. M. Gouda, M. I. Abbas, S. I. Hammoury, K. Zard, and M. A. El-Khatib, "Nano tin oxide/dimethyl polysiloxane reinforced composite as a flexible radiation protecting material," *Sci Rep*, vol. 13, no. 1, pp. 1-13, 2023, doi: 10.1038/s41598-023-27464-z.

[10] A. Bijanu *et al,* "Metal-polymer composites for radiation protection: a review," Oct. 01, 2021, *Springer Science and Business Media B. V.* doi: 10.1007/s 10965-021-02751-3.

[11] A. Barabash, D. Barabash, V. Pertsev, and D. Panfilov, "Polymer-composite materials for radiation protection," *Advances in Intelligent Systems and Computing*, vol. 983, pp. 352-360, 2019, doi: 10.1007/978-3-030-19868-8_36.

[12] I. Blanco, "Silicon-containing polymeric materials," *Polymers (Basel)*, vol. 13, no. 2, p. 188, 2021, doi: 10.3390/polym.

[13] J. Wang *et al,* "The Characterization of Silicone-Tungsten-Based Composites as Flexible Gamma-Ray Shields," *Materials*, vol. 14, no. 20, p. 5970, Oct. 2021, doi: 10.3390/mal4205970.

[14] N. Nagaraja, H. C. Manjunatha, L. Seenappa, K. N. Sridhar, and H. B. Ramalingam, "Radiation shielding properties of silicon polymers," *Radiation Physics and Chemistry*, vol. 171, Jun. 2020, doi: 10.1016/j.radphyschem.2020.108723.

[15] M. P. Wolf, G. B. Salieb-Beugelaar, and P. Hunziker, "PDMS with designer functionalities—properties, modifications strategies, and applications," Aug. 01, 2018, *Elsevier Ltd.* doi: 10.1016/j.progpolymsci.2018.06.001.

[16] C. Jin, C. Ma, Z. Yang, and H. Lin, "A force measurement method based on flexible PDMS grating," *Applied Sciences (Switzerland)*, vol. 10, no. 7, Apr. 2020, doi: 10.3390/appl0072296.

[17] I. Miranda *et al*, "Properties and applications of PDMS for biomedical engineering: A review," Mar. 01, 2022, *MDPI.* doi: 10.3390/jfbl3010002.

[18] A. Romo-Uribe, K. Santiago-Santiago, A. Reyes-Mayer, and M. Aguilar-Franco, "Functional PDMS enhanced strain at fracture and toughness of DGEBA epoxy resin," *Eur Polym J*, vol. 89, pp. 101-118, Apr. 2017, doi: 10.1016/j.eurpolymj.2017.01.041.

[19] B. Ahmed, G. B. Shah, A. H. Malik, Aurangzeb, and M. Rizwan, "Gamma-ray shielding characteristics of flexible silicone tungsten composites," *Applied Radiation and Isotopes*, vol. 155, p. 108901, 2020, doi: 10.1016/j.apradiso.2019.108901.

[20] M. T. Alresheedi and M. Elsafi, "Effect of Waste Iron Filings (IF) on Radiation Shielding Feature of Poly epoxide Composites," *Crystals (Basel)*, vol. 13, no. 8, p. 1168, Jul. 2023, doi: 10.3390/crystl3081168.

[21] R. Mehrara, S. Malekie, S. M. S. Kotahi, and S. Kashian, "Introducing a novel low energy gamma ray shield utilizing Polycarbonate Bismuth Oxide composite," *Sci Rep*, vol. 11, no. 1, pp. 1-13, 2021, doi: 10.1038/s41598-021-89773-5.

[22] G. Chinangwa, J. K. Amoako, and J. J. Fletcher, "Radiation dose assessment for occupationally exposed workers in Malawi," *Malawi Medical Journal*, vol. 29, no. 3, pp. 254-258, 2022, Accessed: Feb. 15, 2024. [Online]. Available: https://doi.Org/10.4314/mmj.v29i3.5

[23] A. Engstrom, M. Isaksson, P. A. Larsson, C. Lundh, and M. Bath, "Lead aprons and thyroid collars: to be, or not to be?," *Journal of Radiological Protection*, vol. 43, no. 3, 2023, doi: 10.1088/1361-6498/acf76f.

[24] S. J. Hyun, K. J. Kim, T. A. Jahng, and H. J. Kim, "Efficiency of lead aprons in blocking radiation - how protective are they?," *Heliyon*, vol. 2, no. 5, p. eOOl 17, May 2016, doi: 10.1016/J.HELIYON.2016.E00117.

[25] A. Roguin *et al*, "Update on radiation safety in the cath lab - moving toward a 'lead-free' environment," Elsevier B.V., Jul. 2023. doi: 10.1016/j.jscai.2023.101040.

[26] H. M. Eyssa, R. F. Sadek, W. S. Mohamed, and W. Ramadan, "Structure-property behavior of polyethylene nanocomposites containing Bi203 and W03 as an eco-friendly additive for radiation shielding," *Ceram Int*, vol. 49, no. 11, pp. 18442-18454, 2023, doi: 10.1016/j.ceramint.2023.02.216.

[27] Y. Al-Hadeethi, M. I. Sayyed, A. Z. Barasheed, M. Ahmed, and M. Elsafi, "Fabrication of lead free borate glasses modified by bismuth oxide for gamma ray protection applications," *Materials*, vol. 15, no. 3, 2022, doi: 10.3390/mal5030789.

[28] N. J. Abualroos, K. A. Yaacob, and R. Zainon, "Radiation attenuation effectiveness of polymer-based radiation shielding materials for gamma radiation," *Radiation Physics and Chemistry*, vol. 212, no. May, p. 111070, 2023, doi: 10.1016/j.radphyschem.2023.111070.

[29] J. Abdullah, K. Zanudin, and M. A. Marzukhi, "Twelfth Malaysia plan:prospective impacts on urban and regional development," *Journal of the Malaysian Institute of Planners* , vol. 20, no. 4, pp. 331-345, 2022.

[30] M. T. Alresheedi *etal*, "Assessment of silicone rubber/Lead oxide composites," *Polymers (Basel)*, vol. 15, no. 9, 2023, doi:

https://doi.org/10.3390/polyml5092160.

[31] M. W. Aladailah *et ah,* "Exploration of physical and optical properties of ZnO nanopowders filled with polydimethylsiloxane (PDMS) for radiation shielding applications. Simulation and theoretical study," *Opt Mater (Amst),* vol. 134, p. 113197, Dec. 2022, doi: 10.1016/j.optmat.2022.113197.

[32] S. N. Yilmaz, A. Giingor, and T. Ozdemir, "The investigations of mechanical, thermal and rheological properties of polydimethylsiloxane/bismuth (III) oxide composite for X/Gamma ray shielding," *Radiation Physics and Chemistry,* vol. 170, p. 108649, May 2020, doi: 10.1016/J.RADPHYSCHEM.2019.108649.

[33] S. Jayakumar, T. Saravanan, and J. Philip, "A review on polymer nanocomposites as lead-free materials for diagnostic X-ray shielding: Recent advances, challenges and future perspectives," *Hybrid Advances,* vol. 4, p. 100100, Dec. 2023, doi: 10.1016/j.hybadv.2023.100100.

[34] E. T. Samara, D. Cester, M. Furlan, T. Pfammatter, T. Frauenfelder, and A. Stiissi, "Efficiency evaluation of leaded glasses and visors for eye lens dose reduction during fluoroscopy guided interventional procedures," *Physica Medica,* vol. 100, pp. 129-134, Aug. 2022, doi: 10.1016/J.EJMP.2022.06.021.

[35] Z. Shamsuddin, Z. Taat, and S. Mohamed Johar, "A study on effective dose to patients and workers during diagnostic X-ray procedure in UTFJJVI health centre," *Journal of Science and Technology,* vol. 10, no. 2, pp. 196-200, 2018, doi: 10.30880/jst.2018.10.02.027.

[36] Y. F. Ali, F. A. Cucinotta, L. Ning-Ang, and G. Zhou, "Cancer risk of low dose ionizing radiation," *Front Phys,* vol. 8, pp. 1-9, 2020, doi: 10.3389/fphy.2020.00234.

[37] H. Chartier *et ah,* "Occupational low-dose irradiation and cancer risk among medical radiation workers," *Occup Med (Chic III),* vol. 70, no. 7, pp. 476-484, 2020, doi: 10.1093/occmed/kqaal30.

[38] N. M. A. Mukhtar *et ah,* "The effects of education level on radiation professionals' knowledge and implementation of ALARA principles for occupational radiation protection," *Journal of Islamic, Social, Economics, and Development (JISED),* vol. 9, no. 60, pp. 82-92, 2024, [Online]. Available: 10.55573/JISED.096010

[39] J. A. Kamarolzeman and N. M. A. Mukhtar, "A review on the personal protective equipment (PPE) used in occupational radiation protection," 9th Virtual Science

Invention Innovation Conference (SIIC) 2020, 2020.

[40] I. J. Boniface and N. M. A. Mukhtar, "A study on the importance of personal protective equipment (PPE) in occupational radiation protection," 9th Virtual Science Invention Conference (SIIC) 2020, 2020.

[41] W. J. Lee, S. Ko, Y. J. Bang, S.-A. Choe, Y. Choi, and D. L. Preston, "Occupational radiation exposure and cancer incidence in a cohort of diagnostic medical radiation workers in South Korea," *Occup Environ Med*, vol. 78, no. 12, pp. 876-883, Dec. 2021, doi: 10.1136/oemed-2021-107452.

[42] S. M. Alkhateeb *et al*, "Effectiveness of protective thyroid shield in chest X-ray imaging," *Radiation Physics and Chemistry*, vol. 209, p. 110965, Aug. 2023, doi: 10.1016/J.RADPHYSCHEM.2023.110965.

[43] Y. J. Zhang, X. T. Guo, C. H. Wang, X. A. Lu, D. F. Wu, and M. Zhang, "Gadolinium- and lead-containing functional terpolymers for low energy X-ray protection," *Nuclear Engineering and Technology*, vol. 53, no. 12, pp. 4130-4136, 2021, doi: 10.1016/j.net.2021.06.021.

[44] A. Bijanu *et al*, "Metal-polymer composites for radiation protection: a review," Oct. 01, 2021, *Springer Science and Business Media B. V.* doi: 10.1007/s 10965-021-02751-3.

[45] T. Kaur, J. Sharma, and T. Singh, "Review on scope of metallic alloys in gamma rays shield designing," *Progress in Nuclear Energy*\ vol. 113, no. April 2018, pp. 95-113, 2019, doi: 10.1016/j.pnucene.2019.01.016.

[46] P. Aim-O, D. Wongsawaeng, P. Phruksarojanakun, and S. Tancharakorn, "Monte Carlo simulation of innovative neutron and photon shielding material composing of high density concrete, waste rubber, lead and boron carbide," *J PhysConfSer*, vol. 860, no. 1, 2017, doi: 10.1088/1742-6596/860/1/012043.

[47] T. Pianpanit and K. Saenboonruang, "High-energy photon attenuation properties of lead-free and self-healing poly (vinyl alcohol) (PVA) hydrogels: numerical determination and simulation," *Gels*, vol. 8, no. 4, 2022, doi: 10.3390/gels8040197.

[48] F. Ozel *et al*, "Production of microstructured BaZr03 and Ba2P207-based polymer shields for protection against ionizing photons," *Journal of Physics and Chemistry of Solids*, vol. 158, no. June, p. 110238, 2021, doi: 10.1016/j.jpcs.2021.110238.

[49] O. Kilicoglu *et al*, "Micro Pb filled polymer composites: Theoretical,

experimental and simulation results for y-ray shielding performance," *Radiation Physics and Chemistry*, vol. 194, p. 110039, May 2022, doi: 10.1016/j.radphyschem.2022.110039.

[50] N. A. Kawady, M. Elkattan, M. Salah, and A. A. Galhoum, "Fabrication, characterization, and gamma ray shielding properties of PVA-based polymer nanocomposite," *J Mater Sci*, vol. 57, no. 24, pp. 11046-11061, 2022, doi: 10.1007/sl0853-022-07213-9.

[51] S. Alshahri, M. Alsuhybani, E. Alosime, S. Alotaibi, M. Almurayshid, and A. Alrwais, "Ldpe/bismuth oxide nanocomposite: Preparation, characterization and application in x-ray shielding," *Polymers (Basel)*, vol. 13, no. 18, 2021, doi: 10.3390/polyml3183081.

[52] O. A. Ersoz, F. Y. Lambrecht, and H. M. Soylu, "Tungsten-ethylene vinyl acetate (EVA) composite as a gamma rays shielding material," *Indian Journal of Pure and Applied Physics*, vol. 54, no. 12, pp. 793-796, 2016.

[53] W. M. Al-Saleh, M. R. H. Dahi, M. I. Sayyed, H. M. Almutairi, I. H. Saleh, and M. Elsafi, "Comprehensive study of the radiation shielding feature of polyester polymers impregnated with iron filings," *E-Polymers*, vol. 23, no. 1, 2023, doi: 10.1515/epoly-2023-0096.

[54] M. Elsafi, A. H. Almuqrin, S. Yasmin, and M. I. Sayyed, "The affinity of bentonite and W03nanoparticles toward epoxy resin polymer for radiation shielding," *E-Polymers*, vol. 23, no. 1, 2023, doi: 10.1515/epoly-2023-0011.

[55] A. M. Konig, J. Verbe Zoum, M. Fiebich, P. W. Abissi, and A. H. Mahnken, "Comparison of the radiation protection effect of different radiation protection aprons made of different materials," *Eur J Radiol*, vol. 164, p. 110862, Jul. 2023, doi: 10.1016/J.EJRAD.2023.110862.

[56] M. Asgari, H. Afarideh, H. Ghafoorifard, and E. A. Amirabadi, "Comparison of nano/micro lead, bismuth and tungsten on the gamma shielding properties of the flexible composites against photon in wide energy range (40 keV-662 keV)," *Nuclear Engineering and Technology*, vol. 53, no. 12, pp. 4142-4149, 2021, doi: 10.1016/j.net.2021.06.022.

[57] M. Zehtabvar, K. Taghandiki, N. Madani, D. Sardari, and B. Bashiri, "A review on the application of machine learning in gamma spectroscopy: challenges and opportunities," *Spectroscopy Journal 2024, Vol. 2, Pages 123-144*, vol. 2, no. 3, pp. 123-144, Jul. 2024, doi: 10.3390/SPECTROSCJ2030008.

[58] N. Reinhardt and L. Herrmann, "Gamma-ray spectrometry as versatile tool in soil science: A critical review," *Journal of Plant Nutrition and Soil Science*, vol. 182, no. 1, pp. 9-27, Feb. 2019, doi: 10.1002/JPLN.201700447.

[59] C. L. Kim, H. C. Jeong, and J. H. Kim, "Radiation shielding effects of lead equivalent thickness of a radiation protective apron and distance during C-arm fluoroscopy-guided pain interventions: A randomized trial," *Medicine (United States)*, vol. 102, no. 48, p. E36447, Dec. 2023, doi: 10.1097/MD.0000000000036447.

[60] C. M. Hayre, H. Bungay, and C. Jeffery, "How effective are lead-rubber aprons in protecting radiosensitive organs from secondary ionizing radiation?," *Radiography*, vol. 26, no. 4, pp. e264-e269, Nov. 2020, doi: 10.1016/J.RADI.2020.03.013.

[61] M. E. Mahmoud, A. M. El-Khatib, M. S. Badawi, A. R. Rashad, R. M. El-Sharkawy, and A. A. Thabet, "Fabrication, characterization and gamma rays shielding properties of nano and micro lead oxide-dispersed-high density polyethylene composites," *Radiation Physics and Chemistry*, vol. 145, no. 2017, pp. 160-173, 2018, doi: 10.1016/j.radphyschem.2017.10.017.

[62] T. Ozdemir, A. Giingor, I. K. Akbay, H. Uzun, and Y. Babuccuoglu, "Nano lead oxide and epdm composite for development of polymer based radiation shielding material: Gamma irradiation and attenuation tests," *Radiation Physics and Chemistry*, vol. 144, pp. 248-255, 2018, doi: 10.1016/j.radphyschem.2017.08.021.

[63] M. Elsafi, N. Almousa, F. I. Almasoud, M. Almurayshid, A. R. Alyahyawi, and M. I. Sayyed, "A Novel Epoxy Resin-Based Composite with Zirconium and Boron Oxides: An Investigation of Photon Attenuation," *Crystals (Basel)*, vol. 12, no. 10, p. 1370, Sep. 2022, doi: 10.3390/crystl2101370.

[64] N. J. Abualroos and R. Zainon, "Fabrication of new non-hazardous tungsten carbide epoxy resin bricks for low energy gamma shielding in nuclear medicine," *JPhys Commun*, vol. 5, no. 9, 2021, doi: 10.1088/2399-6528/AC26DE.

[65] B. Korpinar, B. C. Oztiirk, N. F. Cam, and H. Akat, "Investigations on thermal and radiation shielding properties of the poly(hydroxyethyl methacrylate-co-styrene)/tungsten(VI) oxide composites," *Progress in Nuclear Energy*, vol. 126, p. 103424, Aug. 2020, doi: 10.1016/j.pnucene.2020.103424.

[66] L. Chang *et ah*, "Preparation and characterization of tungsten/epoxy composites

for y-rays radiation shielding," *Nucl Instrum Methods Phys Res B*, vol. 356-357, pp. 88-93, 2015, doi: 10.1016/j.nimb.2015.04.062.

[67] A. M. El-Khatib *et al*, "Gamma attenuation coefficients of nano cadmium oxide/high density polyethylene composites," *Sci Rep*, vol. 9, no. 1, pp. 1-11, 2019, doi: 10.1038/s41598-019-52220-7.

[68] M. Elsafi *et al*, "Optimizing the gamma-ray shielding behaviors for polypropylene using lead oxide: A detailed examination," *Journal of Materials Research and Technology*, vol. 19, pp. 1862-1872, 2022, doi: 10.1016/j.jmrt.2022.05.128.

[69] R. M. El-Sharkawy, F. S. Abdou, M. A. Gizawy, E. A. Allam, and M. E. Mahmoud, "Bismuth oxide nanoparticles (Bi203 NPs) embedded into recycled-poly(vinyl chloride) plastic sheets as a promising shielding material for gamma radiation," *Radiation Physics and Chemistry*, vol. 208, p. 110838, 2023, doi: 10.1016/j.radphyschem.2023.110838.

[70] A. M. El-Khatib, M. I. Abbas, S. I. Hammoury, M. M. Gouda, K. Zard, and M. Elsafi, "Effect of PbO-nanoparticles on dimethyl polysiloxane for use in radiation shielding applications," *Sci Rep*, vol. 12, no. 1, pp. 1-13, 2022, doi: 10.103 8/s41598-022-20103-z.

[71] H. Ogul *et al*, "A comparative neutron and gamma-ray radiation shielding investigation of molybdenum and boron filled polymer composites," *Applied Radiation and Isotopes*, vol. 194, Apr. 2023, doi: 10.1016/j.apradiso.2023.110731.

[72] O. P. Lakhwani, V. Dalai, M. Jindal, and A. Nagala, "Radiation protection and standardization," *J Clin Orthop Trauma*, vol. 10, no. 4, p. 738, Jul. 2018, doi: 10.1016/JJCOT.2018.08.010.

[73] E. Emiliani *et al*, "Radiation exposure using leaded versus regular latex surgical gloves in endourological procedures: a prospective comparative study," *Urolithiasis*, vol. 53, no. 1, pp. 1-6, Dec. 2025, doi: 10.1007/S00240-024-01676-Y/METRICS.

[74] L. Gilys, E. Griskonis, P. Griskevicius, and D. Adliene, "Lead free multilayered polymer composites for radiation shielding," *Polymers (Basel)*, vol. 14, no. 9, pp. 1-15, 2022, doi: https://doi.org/10.3390/polyml4091696.

[75] M. Mirzaei, M. Zarrebini, A. Shirani, M. Shanbeh, and S. Borhani, "X-ray shielding by a novel garment woven with melt-spun monofilament weft yarn

containing lead and tin particles," *Textile Research Journal,* vol. 89, no. 1, pp. 63-75, 2019, doi: 10.1177/0040517517736475.

[76] A. Saleh, H. Almohiy, R. M. Shalaby, and M. Saad, "Comprehensive investigation on physical, structural, mechanical and nuclear shielding features against X/gamma-rays, neutron, proton and alpha particles of various binary alloys," *Radiation Physics and Chemistry,* vol. 216, Mar. 2024, doi: 10.1016/j.radphyschem.2023.111443.

[77] M. Zarei, S. Sina, and S. A. Hashemi, "Superior X-ray radiation shielding of biocompatible platform based on reinforced polyaniline by decorated graphene oxide with interconnected tungsten-bismuth-tin complex," *Radiation Physics and Chemistry,* vol. 188, Nov. 2021, doi: 10.1016/j.radphyschem.2021.109588.

[78] Y. Zhan, R. Grottenmuller, W. Li, F. Javaid, and R. Riedel, "Evaluation of mechanical properties and hydrophobicity of room-temperature, moisture-curable polysilazane coatings," *JAppl Polym Sci,* vol. 138, no. 21, Jun. 2021, doi: 10.1002/app. 50469.

[79] I. Teixeira *et al,* "Polydimethylsiloxane mechanical properties: A systematic review," *AIMS Mater Sci,* vol. 8, no. 6, pp. 952-973, 2021, doi: 10.3934/matersci.2021058.

[80] Y. H. Kang *et al,* "Proton conducting perhydropolysilazane-derived gate dielectric for solution-processed metal oxide-based thin-film transistors," *ACS Appl Mater Interfaces,* vol. 12, no. 13, pp. 15396-15405, Apr. 2020, doi: 10.1021/acsami.0c01274.

[81] K. Akutsu-Suyama *et al,* "Fine-structure analysis of perhydropolysilazane-derived nano layers in deep-buried condition using polarized neutron reflectometry," *Polymers (Basel),* vol. 12, no. 10, Oct. 2020, doi: 10.3390/POLYM12102180.

[82] P. Pospiech, J. Chojnowski, U. Mizerska, and G. Cempura, "Platinum catalyst on polysiloxane microspheres with N-chelating groups," *JMol Catal A Chem,* vol. 424, pp. 402-411, Dec. 2016, doi: 10.1016/j.molcata.2016.09.016.

[83] Z. M. Cinan, B. Erol, T. Baskan, S. Mutlu, S. S. Yilmaz, and A. H. Yilmaz, "Gamma irradiation and the radiation shielding characteristics: For the lead oxide doped the crosslinked polystyrene-b-polyethyleneglycol block copolymers and the polystyrene-b-polyethyleneglycol-boron nitride nanocomposites," 2021. doi: 10.3390/polyml3193246.

[84] S. Alshahri, M. Alsuhybani, E. Alosime, S. Alotaibi, M. Almurayshid, and A. Alrwais, "LDPE/bismuth oxide nanocomposite: Preparation, characterization and application in x-ray shielding," *Polymers (Basel)*, vol. 13, no. 18, 2021, doi: 10.3390/polyml3183081.

[85] H. Zainal Abidin *et ah*, "Effect of tin filler composition on porosity in tin-polydimethylsiloxane composites," *Pure and Applied Chemistry*, Apr. 2025, doi: 10.1515/PAC-2024-0347.

[86] S. N. Yilmaz, A. Giingor, and T. Ozdemir, "The investigations of mechanical, thermal and rheological properties of polydimethylsiloxane/bismuth (III) oxide composite for X/Gamma ray shielding," *Radiation Physics and Chemistry*, vol. 170, p. 108649, May 2020, doi: 10.1016/J.RADPHYSCHEM.2019.108649.

[87] N. J. Abualroos, M. I. Idris, H. Ibrahim, M. I. Kamaruzaman, and R. Zainon, "Physical, mechanical, and microstructural characterisation of tungsten carbide-based polymeric composites for radiation shielding application," *Sci Rep*, vol. 14, no. 1, Dec. 2024, doi: 10.1038/s41598-023-49842-3.

[88] R. Ariati, F. Sales, A. Souza, R. A. Lima, and J. Ribeiro, "Polydimethylsiloxane composites characterization and its applications: A review," Dec. 01, 2021, *MDPI*. doi: 10.3390/polyml3234258.

[89] B. Ahm, "A comprehensive study on radiation shielding characteristics of Tin-Silver, Manganin-R, Hastelloy-B, Hastelloy-X and Dilver-P alloys," *Appl Phys A Mater Sci Process*, vol. 126, no. 4, Apr. 2020, doi: 10.1007/s00339-020-3442-7.

[90] M. Ramli, A. A. Tabassi, and K. W. Hoe, "Porosity, pore structure and water absorption of polymer-modified mortars: An experimental study under different curing conditions," *Compos B Eng*, vol. 55, pp. 221-233, 2013, doi: 10.1016/j.compositesb.2013.06.022.

[91] H. Zainal Abidin *et al*, "Porosity and Structural Integrity of Tin-Polydimethylsiloxane (PDMS) Composites for Radiation Shielding Application," *Baghdad Science Journal*, vol. 23, no. 1, pp. 121-137, Jan. 2026, doi: 10.21123/2411-7986.5143.

[92] S. Prabhu, S. G. Bubbly, and S. B. Gudennavar, "X-Ray and y-Ray Shielding Efficiency of Polymer Composites: Choice of Fillers, Effect of Loading and Filler Size, Photon Energy and Multifunctionality," *Polymer Reviews*, vol. 63, no. 1, pp. 246-288, 2023, doi: 10.1080/15583724.2022.2067867.

[93] T. Sekiguchi *et al,* "UV-curable polydimethylsiloxane photolithography and its application to flexible mechanical metamaterials," *Sensors and Materials,* vol. 35, no. 2-6, pp. 1995-2011, 2023, doi: 10.18494/SAM4351.

[94] H. Song, N. A. Rodriguez, J. S. Oakdale, E. B. Duoss, R. H. Crawford, and C. C. Seepersad, "Aging of UV curable PDMS developed for large-scale, high viscosity stereolithography," *Polym Degrad Stab,* vol. 207, Jan. 2023, doi: 10.1016/j.polymdegradstab.2022.110227.

[95] M. S. Gharissah *et al,* "Composites cement/BaS04/Fe304/CuO for improving X-ray absorption characteristics and structural properties," *Sci Rep,* vol. 12, no. 1, pp. 1-9, 2022, doi: 10.1038/s41598-022-23908-0.

[96] M. A. Al-Balushi *et al.,* "Ionization radiation shielding effectiveness of lead acetate, lead nitrate, and bismuth nitrate-doped zinc oxide nanorods thin films: A comparative evaluation," *Materials,* vol. 15, no. 1, Jan. 2022, doi: 10.3390/mal5010003.

[97] A. Fisli *etal,* "Some metal oxide-natural rubber composites for gamma and low-energy X-Ray radiation shielding," *Atom Indonesia,* vol. 49, no. 1, pp. 45-52, 2023, doi: 10.55981/aij.2023.1213.

[98] Y. Jia, J. Chen, H. Asahara, T. A. Asoh, and H. Uyama, "Polymer surface oxidation by light-activated chlorine dioxide radical for metal-plastics adhesion," *ACS Appl Polym Mater,* vol. 1, no. 12, pp. 3452-3458, Dec. 2019, doi: 10.1021/acsapm.9b00871.

[99] R. M. Town, H. P. van Leeuwen, and J. F. L. Duval, "Effect of polymer aging on uptake/release kinetics of metal ions and organic molecules by micro- and nanoplastics: implications for the bioavailability of the associated compounds," *Environ Sci Technol,* vol. 57, no. 43, pp. 16552-16563, Oct. 2023, doi: 10.1021/ACS.EST.3C05148/ASSET/IMAGES/LARGE/ES3C05148_0008.JPEG.

[100] M. Dawoud and I. Taha, "Effects of contamination with selected polymers on the mechanical properties of post-industrial recycled polypropylene," *Polymers 2024, Vol. 16, Page 2301,* vol. 16, no. 16, p. 2301, Aug. 2024, doi: 10.3390/POLYM16162301.

[101] M. Kadleckova *et al,* "Release of contaminants from polymer surfaces under condition of organized fluid flows," *Water Res X,* vol. 24, p. 100248, Sep. 2024, doi: 10.1016/J.WROA.2024.100248.

[102] S. Kozdra *et ah,* "Suppression of iron oxidation problem into PVDF/PMMA composites with ceramic additives: Si02 vs. Ti02," *Polymer (Guildf),* vol. 320, p. 128100, Feb. 2025, doi: 10.1016/J.POLYMER.2025.128100.

[103] P. K. Roy, P. Surekha, R. Raman, and C. Rajagopal, "Investigating the role of metal oxidation state on the degradation behaviour of LDPE," *Polym Degrad Stab,* vol. 94, no. 7, pp. 1033-1039, Jul. 2009, doi: 10.1016/J.POLYMDEGRADSTAB.2009.04.025.

[104] D. Mardiansyah *et ah,* "Effect of temperature on the oxidation of Cu nanowires and development of an easy to produce, oxidation-resistant transparent conducting electrode using a PEDOT:PSS coating," *Sci Rep,* vol. 8, no. 1, Dec. 2018, doi: 10.1038/S41598-018-28744-9.

[105] Z. S. Khalifa and S. H. Mohamed, "Effect of Sn concentration on the structural and thermal properties of SnxSb20Se80-x glasses," *J Electron Mater,* vol. 52, no. 12, pp. 7920-7930, Dec. 2023, doi: 10.1007/S11664-023-10709-Y/FIGURES/10.

[106] R. Hu, W. Sun, M. Zeng, and M. Zhu, "Dispersing Sn02 nanocrystals in amorphous carbon as a cyclic durable anode material for lithium ion batteries," *Journal of Energy Chemistry,* vol. 23, no. 3, pp. 338-345, 2014, doi: 10.1016/S2095-4956(14)60156-X.

[107] S. Zhou, L. Zhou, Y. Su, X. Yang, and H. He, "Synthesis of Sn-Beta Zeolite via Quasi-Solid-Phase Route with Low Amount of Organic Template," *Eur JInorg Chem,* vol. 2022, no. 16, Jun. 2022, doi: 10.1002/EJIC.202200130.

[108] T. Malik, P. Cifligu, C. Park, andE. Evlyukhin, "X-ray induced synthesis of beta tin (P-Sn)," *Journal of Physics and Chemistry of Solids,* vol. 196, p. 112351, Jan. 2025, doi: 10.1016/J.JPCS.2024.112351.

[109] J. S. Oh *et ah,* "Electrochemical performances of the Sn-Cu alloy negative electrode materials through simple chemical reduction method," *Journal of Electrochemical Science and Technology,* vol. 10, no. 3, pp. 329-334, Sep. 2019, doi: 10.33961/JECST.2019.00024.

[110] J. Feng *et ah,* "Electrolyte-assisted structure reconstruction optimization of Sn-Zn hybrid oxide boosts the electrochemical C02-to-HCOO- conversion," *Advanced Science,* vol. 11, no. 39, p. 2407019, Oct. 2024, doi: 10.1002/ADVS .202407019; WGROUP: STRING:PUBLIC ATION.

[Ill] Y. T. Prabhu, K. Venkateswara Rao, V. Sesha Sai, and T. Pavani, "A facile

biosynthesis of copper nanoparticles: A micro-structural and antibacterial activity investigation," *Journal of Saudi Chemical Society*, vol. 21, no. 2, pp. 180-185, Feb. 2017, doi: 10.1016/J.JSCS.2015.04.002.

[112] M. Yilmaz, M. E. Pekdemir, and E. Ozen Oner, "Evaluation of Pb doped Poly(lactic acid) (PLA) / Poly(ethylene glycol) (PEG) blend composites regarding physicochemical and radiation shielding properties," *Radiation Physics and Chemistry*, vol. 202, 2023, doi: 10.1016/j.radphyschem.2022.110509.

[113] H. Zainal Abidin, N. M. A. Mukhtar, A. Mahmood, N. A. Abdul Wahab, R. Zainon, and N. S. Roslan, "Radiation shielding properties of tin-poly dimethylsiloxane (PDMS) composites against gamma ray at 356 keV," *International Journal ofInnovation and Industrial Revolution*, vol. 7, no. 20, pp. 352-369, Mar. 2025, doi: 10.35631/IJIREV.720023.

[114] C. V. More, Z. Alsayed, M. S. Badawi, A. A. Thabet, and P. P. Pawar, "Polymeric composite materials for radiation shielding: a review," Jun. 01, 2021, *Springer Science and Business Media Deutschland GmbH*. doi: 10.1007/sl0311-021-01189-9.

[115] H. Zainal Abidin, N. maizatul A. Mukhtar, A. Mahmood, and R. Zainon, "A Systematic Review on the Radiation Shielding Performance of Metal-Polymer Composites," *MALAYSIAN JOURNAL OF APPLIED SCIENCES*, vol. 10, no. 2, pp. 63-93, 2025, doi: 10.3723l/myjas.2025.10.2.455.

[116] B. Korpinar, B. Canbaz Oztiirk, N. F. Cam, and H. Akat, "Radiation shielding properties of poly(hydroxylethyl methacrylate)/tungsten(VI) oxide composites," *Mater ChemPhys*, vol. 239, 2020, doi: 10.1016/j.matchemphys.2019.121986.

[117] N. Hesham *et al*, "Development of PMMA composites with tungsten tri oxide for improved gamma radiation shielding in microsatellites," *Scientific Reports 2025 15:1*, vol. 15, no. 1, pp. 1-15, Apr. 2025, doi: 10.1038/s41598-025-94120-z.

[118] K. G. Mahmoud, M. I. Sayyed, A. H. Almuqrin, J. Arayro, and Y. Maghrbi, "Monte Carlo investigation of gamma radiation shielding features for Bi203/epoxy composites," *Applied Sciences (Switzerland)*, vol. 13, no. 3, 2023, doi: 10.3390/appl3031757.

[119] M. Kazempour, M. Saeedimoghadam, F. Shekoohi Shooli, and N. Shokrpour, "Assessment of the radiation attenuation properties of several lead free

composites by monte carlo simulation," *J Biomed Phys Eng*, vol. 5, no. 2, pp. 67-76, 2015.

[120] S. C. Sanchez El Ryfaie and M. Heredia Conde, "Breaking the Limits of Gamma-Ray Spectrometry by Exploiting Sparsity of Photon Arrivals," in *2020 28th European Signal Processing Conference (EUSIPCO)*, IEEE, Jan. 2021, pp. 2075-2079. doi: 10.23919/Eusipco47968.2020.9287728.

[121] M. Lopresti *et ah*, "Light weight, easy formable and non-toxic polymer-based composites for hard x-ray shielding: A theoretical and experimental study," *IntJ MolSci*, vol. 21, no. 3, 2020, doi: 10.3390/ijms21030833.

[122] M. Blaauw, "Detection limits should be a thing of the past in gamma-ray spectrometry in general as well as in neutron activation analysis," *J Radioanal NuclChem*, vol. 309, no. 1, p. 39, Jul. 2016, doi: 10.1007/S10967-016-4843-0.

[123] Y. Y. Ji, J. M. Lim, H. Kim, C. J. Kim, C. S. Lim, and K. H. Chung, "Limitations of gamma-ray spectrometry in the quantification of 238U and 232Th in raw materials and by-products," *J Radioanal Nucl Chem*, vol. 311, no. 2, pp. 1163-1168, Feb. 2017, doi: 10.1007/S 10967-016-4978-Z/METRICS.

[124] A. Almuqrin, S. A. Tijani, A. Al-Ghamdi, T. Alhuzaymi, and M. F. Alotiby, "Radiation shielding properties of high-density polyethylene (C2H4)/molybdenum III oxide (Mo03) polymer composites for dental diagnostic applications," *JRadiat Res Appl Sci*, vol. 16, no. 4, p. 100681, 2023, doi: 10.1016/j.jrras.2023.100681.

[125] M. I. A. Abdel Maksoud, S. M. Kassem, A. H. Ashour, and A. S. Awed, "Recycled high-density polyethylene plastic reinforced with ilmenite as a sustainable radiation shielding material," *RSC Adv*, vol. 13, no. 30, pp. 20698-20708, 2023, doi: 10.1039/d3ra03757f

[126] F. Wahyuni, S. P. Sakti, D. J. D. Herry Santjojo, and U. P. Juswono, "Bismuth oxide filled polyester composites for X-ray radiation shielding applications," *Pol J Environ Stud*, vol. 31, no. 4, pp. 3985-3990, 2022, doi: 10.15244/pjoes/146935.

[127] C. Li, Y. Sun, M. Cheng, S. Sun, and S. Hu, "Fabrication and characterization of a Ti02/polysiloxane resin composite coating with full-thickness super-hydrophobicity," *Chemical Engineering Journal*, vol. 333, pp. 361-369, Feb. 2018, doi: 10.1016/j.cej.2017.09.165.

[128] M. E. Mahmoud, R. M.El-Sharkawy, E. A. Allam, R. Elsaman, and A. El-Taher, "Fabrication and characterization of phosphotungstic acid - Copper oxide

nanoparticles - Plastic waste nanocomposites for enhanced radiation-shielding," *J Alloys Compd*, vol. 803, pp. 768-777, 2019, doi: 10.1016/j.jallcom.2019.06.290.

[129] L. M. Anovitz and D. R. Cole, "Characterization and analysis of porosity and pore structures," in *Pore Scale Geochemical Processes*, De Gruyter, 2015, pp. 61-164. doi: 10.2138/rmg.2015.80.04.

[130] N. I. Egorenkov, D. G. Lin, and V. A. Bely, "Effect of metals on melt oxidation of polyethylene," *Journal of Polymer Science: Polymer Chemistry Edition*, vol. 13, no. 7, pp. 1493-1498, Jul. 1975, doi: 10.1002/POL.1975.170130701.

[131] M. T. Alresheedi *et ah*, "Assessment of silicone rubber/lead oxide composites enriched with Bi203, W03, BaO, and Sn02 nanoparticles for radiation shielding applications," *Polymers (Basel)*, vol. 15, no. 9, May 2023, doi: 10.3390/polyml5092160.

[132] M. Asgari, H. Afarideh, H. Ghafoorifard, and E. A. Amirabadi, "Effects of particle size and weight percentage of heavy metal elements on photon shielding efficiency of reinforced polymer composites," *International Journal of Radiation Research*, vol. 19, no. 1, pp. 55-61, 2021, doi: 10.29252/IJRR.19.1.55.

AUTHOR'S PROFILE

Hanisah Zainal Abidin obtained a Foundation in Science in 2019 from Universiti Teknologi MARA, Dengkil, Bachelor of Medical Laboratory Technology (Hons.) in 2023 from Universiti Teknologi MARA, Puncak Alam and currently doing a Master of Science (Applied Physics). Her master's research focuses on the development and characterization of tin (Sn)-reinforced polydimethylsiloxane (PDMS) composites for radiation shielding applications. Her work involves various analytical techniques, including Field Emission Scanning Electron Microscopy-Energy Dispersive X-ray (FESEM-EDX), Fourier Transform Infrared Spectroscopy (FTIR), X-Ray Diffraction (XRD) and gamma-ray spectroscopy, to evaluate the structural, chemical, and shielding properties of the composites. She investigates key parameters such as mass attenuation coefficient (MAC), linear attenuation coefficient (LAC), radiation protection efficiency (RPE), half-value layer (HVL), tenth-value layer (TVL), mean free path (MFP) and lead equivalent to determine the effectiveness of the composites in photon attenuation. Her study aims to provide a lead-free alternative for radiation shielding, optimizing fabrication conditions and material compositions to achieve superior shielding performance.

LIST OF PUBLICATION:

Zainal Abidin, H.., Mukhtar, N. M. A., Mahmood, A., Abdul Wahab, N. A., Zainon, R., Roslan, N. S., Nor Izaham, N. I., & Shah, A. Z. (2026). Porosity and Structural Integrity of Tin-Polydimethylsiloxane (PDMS) Composites for

Radiation Shielding Application. Baghdad Science Journal, 23(1), 121-137. https://doi.org/10.21123/2411-7986.5143

Zainal Abidin, H., Mukhtar, N. M. A., Mahmood, A., Abdul Wahab, N. A., Zainon, R., Roslan, N. S., Nor Izaham, N. I., & Zarzali Shah, A. (2025). Effect of tin filler composition on porosity in tin-polydimethylsiloxane composites. Pure and Applied Chemistry. https://doi.org/10.1515/PAC-2024-0347

Zainal Abidin, H., Mukhtar, N. M. A., Mahmood, A., Abdul Wahab, N. A., Zainon, R., & Roslan, N. S. (2025). Radiation shielding properties of tin-polydimethylsiloxane (PDMS) composites against gamma ray at 356 keV. International Journal of Innovation and Industrial Revolution, 7(20), 352-369. https://doi.org/10.35631/IJIREV.720023

Zainal Abidin, H., Mukhtar, N. M. A., Mahmood, A., Abdul Wahab, N. A., & Roslan, N. S. (2024). Tin-PDMS composite: innovative structure as a shield against ionizing radiation. International Journal of Allied Health Sciences, 8(3), 23. https://doi.org/10.31436/ijahs.v8i3.928

Roslan, N. S., Mukhtar, N. M. A., Mahmood, A., Abdul Wahab, N. A., & Zainal Abidin, H. (2024). Double layer of PDMS-based composite as an alternative method in radiation shielding. International Journal of Allied Health Sciences, 8(3), 22. https://doi.org/10.31436/ijahs.v8i3.928

Roslan, N. S., Maizatul, N., Mukhtar, A., Zainal Abidin, H., Mahmood, A., Aimi, N., Wahab, A., Shah, A. Z., & Zainon, R. (2025). Radiation shielding performance of double-layered tin-pdms against 661.7 kev gamma rays. 7(22), 497-510. https://doi.org/10.35631/IJIREV.722028

Roslan, N. S., Mukhtar, N. M. A., Mahmood, A., Wahab, N. A. A., Zainon, R., Abidin, H. Z., Shah, A. Z., & Izaham, N. I. N. (2026). Double-Layered Tin-Polydimethylsiloxane (PDMS) Composites: Evaluation of Porosity and Structural Morphology of Polymeric Composites. *Baghdad Science Journal,* 23(1), 138-150. https://doi.org/10.21123/2411-7986.5141

Table of contribution and involvement

No	Involvement	Description	Title	Awards/Copyright
1	Conference	International Conference Young Chemists (ICYC 2024)	Effect of tin filler composition on porosity in tin-polydimethylsiloxane composites	
		International Conference on Discoveries in Applied Sciences & Advanced Technology (DASAT 2025)	Porosity and structural integrity of tin-poly di methyl siloxane (PDMS) composites for radiation shielding applications	-
2	Innovation	HUM Research & Innovation Day (IRID 2024)	Tin-PDMS composite: innovative structure as a shield against ionising radiation	-Gold Award -Copyright no: CRLY2024P03668
			Fabrication and analysis of tin-polydimethylsiloxane (PDMS) composite layers for enhance radiation shielding: an alternative to lead (Pb) material	-Bronze Award -Copyright no: CRLY2024P03669
		6th Malaysia-Japan International Conference on Nanoscience, Nanotechnology, and Nanoengineering 2025 (MJIC 2025)	Tin-reinforced polydimethylsiloxane composites: a lead-free innovation for superior gamma radiation shielding	-Gold Award -Copyright no: CRLY2025P00379
			An innovation of the double layer polymeric composites enriched with tin fillers as radiation shielding material at low energy gamma rays	-Gold Award -Copyright no: CRLY2025P00378
		International Teaching Aid Competition (iTAC 2024)	TiPhAny: innovative teaching aids for engaging learning on thermodynamics topics	-Silver Award -Copyright no: CRLY2024P03665
		INNOMed: Innovation Pitching Powered by PERANTIM 2024	NMaM method: an innovative mix-mixing method of nano-microparticle tin-PDMS-based composites to block radiation penetration	-Gold award -Copyright no: CRLY2024P07806

		Postgraduate Research Image Competition UiTM Penang 2025	FESEM microstructural analysis of tin-poly di methyl siloxane (PDMS) composite: a lead-free alternative for radiation shielding	
		International Invention, Innovation and Design Expo (INoDEx 2025)	Lead-free tin-PDMS-based composite: a novel metal-polymeric material for radiation shielding	-Gold Award -Copyright no: CRLY2025P06217
			Double-layer tin-PDMS composites: a novel shielding absorber for radiation protection against gamma ray	-Diamond and Gold Award -Copyright no: CRLY2025P06218
5	Community service	Kami Prihatin 7.0 Ahli Jawatan Kuasa		
6	Others	Graduate Research Assistant October 2023 - September 2025		
		UiTM Postgraduate Assistance March 2025 - August 2025		